

UNCLASSIFIED

AD NUMBER
AD822593
NEW LIMITATION CHANGE
TO Approved for public release, distribution unlimited
FROM Distribution authorized to U.S. Gov't. agencies and their contractors; Critical Technology; SEP 1967. Other requests shall be referred to Air Force Rocket Propulsion Laboratory, ATTN: RPPR/STINFO, Edwards AFB, CA 93523.
AUTHORITY
AFRPL ltr dtd 27 Oct 1971

THIS PAGE IS UNCLASSIFIED

AD822593

Unclassified TR

AFRPL-TR-67-202

ELECTRIC ARC DISCHARGE IN SUPERSONIC FLOW
FOR THRUST VECTOR CONTROL

Jain-Ming Wu and Shen Ching Lee
The University of Tennessee Space Institute

TECHNICAL REPORT AFRPL-TR-67-202

September 1967

Air Force Rocket Propulsion Laboratory
Research and Technology Division
Air Force Systems Command, United States Air Force
Edwards Air Force Base, California

This document is subject to special export controls and each transmittal to foreign governments or foreign nationals may be made only with prior approval of AFRPL (RPPR/STINFO), Edwards, California 93523.

AD822593

When U. S. Government drawings, specifications, or other data are used for any purpose other than a definitely related Government procurement operation, the Government thereby incurs no responsibility nor any obligation whatsoever, and the fact that the Government may have formulated, furnished, or in any way supplied the said drawings, specifications, or other data, is not to be regarded by implication or otherwise, or in any manner licensing the holder or any other person or corporation, or conveying any rights or permission to manufacture, use, or sell any patented invention that may in any way be related thereto.

Unclassified

ELECTRIC ARC DISCHARGE IN SUPERSONIC FLOW
FOR THRUST VECTOR CONTROL

Jain-Ming Wu and Shen Ching Lee

This document is subject to special export controls and each transmittal to foreign governments or foreign nationals may be made only with prior approval of AFRPL (RPPR/STINFO), Edwards, California 93523.

FOREWORD

This research program was conducted by The University of Tennessee Space Institute, Tullahoma, Tennessee. The work covered by this report was sponsored by the Air Force Rocket Propulsion Laboratory, Research and Technology Division, Edwards, California under Air Force Contract AF 04(611)-11388. The experimental phase was carried out at the Arnold Engineering Development Center, Arnold Air Force Station, Tennessee with assistance of Arnold Center personnel.

The University of Tennessee Space Institute personnel who participated in this study were as follows:

- L. G. Hunter: Especially, on the first nozzle design and power source study
- W. Bergt: on the influence parameter and the characteristic of arc discharge study
- L. C. Chow: on the evaluation of side force
- T. C. Powell: on the calculation of plane flame theory
- T. D. Buchanan: on the design of the rectangular nozzle.

Technical assistance was also received from: T. A. Tell, M. McIlveen, M. P. Smith, R. E. Taylor and J. W. Tipps; and Ruth Binkley typed the final report.

ARO, Inc. personnel who contributed greatly to the accomplishment of this work were: L. E. Rittenhouse and J. M. Whoric of PWT; and G. H. Pope and D. Miller of ESF.

The work was monitored by Captain D. Stump, AFRPL/RPMCH; Captain H. Shock and Captain D. Pilkington. The research reported herein was conducted from February 15, 1966 through May 31, 1967. This report was submitted by the authors on September 30, 1967.

This technical report has been reviewed and approved.

Captain D. Stump
AFRPL/RPMCH

ABSTRACT

The phenomenon of disturbances caused by electric arc discharge in a supersonic flow was studied both analytically and experimentally. The purpose was to study the feasibility of using this concept for attitude control of space vehicles. A possible application for rocket propelled vehicles was selected for the test condition of an experimental program. Fair agreement was obtained between the test results and the analytical solutions. It was found that:

1. A local static pressure rise can be created by the electric discharge in a supersonic stream.
2. The electric field to initiate discharge was about 2×10^3 volts/in for nitrogen stream at Mach number 2.5 with static pressure of 2 psia and stagnation temperature of 4000°R .
3. The arc discharge, without a magnetic field, in a supersonic flow of Mach number 2.5 can be maintained and is stable.
4. The affected area is small which resulted in small side force.
5. The generated side force per unit electric power input is small in view of the available electric power supply.

The use of an electric discharge for practical thrust vector control of rocket motors is only feasible if the power supply can be improved. This concept, however, proved to be physically sound and may be very important for applications in nuclear rockets where electrical energy is already available on board, or to the space mission re-entry vehicles which the needed power has been generated and stored before re-entry.

TABLE OF CONTENTS

List of Tables	vii
List of Figures	vii
List of Symbols	x
I. Introduction	1
II. Analytical Investigation	3
2.1 Theoretical Models	3
2.1.1 Blast Wave Analogy	3
2.1.2 Supersonic Small Disturbance Theory	7
2.1.3 Plane Flame Analogy	10
2.1.4 Summary of Theoretical Studies	15
2.1.5 Comparison of Heat Addition and Mass Injection in Generating Side Force	16
2.1.5.1 Blast Wave Theory	18
2.1.5.2 Linearized Small Disturbance Theory	19
2.2 Electric Arc Characteristics	20
III. Experimental Program	21
3.1 Test Facility	21
3.2 Test Nozzles	22
3.2.1 Axisymmetric Copper Nozzle	22
3.2.2 Rectangular Copper Nozzle	23
3.2.3 Axisymmetric Silicon Phenolic Nozzle	24
3.3 Test Procedure	24
3.4 Results and Discussion	25
3.4.1 Breakdown Voltage in a Supersonic Stream	25
3.4.2 Operating Characteristics of an Electric Arc	27
3.4.3 Pressure Distributions	27
3.4.3.1 Axisymmetric Copper Nozzle	27
3.4.3.2 Rectangular Copper Nozzle	29
3.4.3.3 Silicon Phenolic Axisymmetric Nozzle	30
3.5 Comparison of Pressure Rise in Main Stream due to Electric Discharge and the Presence of Solid Body	30
3.6 Side Force Evaluation	31

TABLE OF CONTENTS (Continued)

IV. Conclusions	33
4.1 Static Pressure Rise can be Produced by Electric Discharge	33
4.2 Side Force Generated by an Arc Discharge may be Predicted with Simplified Theory	33
4.3 Arc can be Established and Maintained in the Supersonic Stream	33
4.4 The Breakdown Voltage is within the Practical Range	33
4.5 The Side Force Specific Impulse of Arc Discharge Depends on the Specific Energy of Power Source	34
4.6 Material Problems Associated with Electric Arc Discharge in Supersonic Flow	34
V. Recommendations	35
5.1 Arc Discharge for Rocket Applications	35
5.2 Arc Discharge for Re-Entry Applications	35
5.3 A Combined Application of Secondary Mass Injection and Arc Discharge	35
5.4 Arc Applications for Supersonic Combustion	35
Appendix I - Discussion on "Analysis of the Fluid Mechanics of Secondary Injection for Thrust Vector Control," by Broadwell	79
Appendix II - Willmarth's Heat and Mass Analogy	81
Appendix III - Survey on Chemical Battery Power Sources	84
Appendix IV - Influence Parameters on the Arc Discharge	86
Appendix V - Analytical Determination of the Arc Characteristic	90
Appendix VI - Difficulties of the Experiment	102
Appendix VII - An Example of the Side Force Calculation	109
References	116

LIST OF TABLES

	Page
I. Flow Patterns	12
II. Arc Establishment Parameters (Mach No. of Gas Stream = 2.5)	26
III. Comparison of Measured and Predicted Side Force	32

LIST OF FIGURES

1. Flight Direction Control by Electric Discharge	37
2. Schematic Drawing of Generated Shock Wave Due to Arc Discharge	38
3. Generated Side Force vs. Free Stream Mach Number by Blast Wave Theory	39
4. Small Disturbance Due to Uniformly Distributed Source	40
5. Generated Side Force vs. Free Stream Mach Number by Linearized Theory	41
6. Schematic Drawing of Plane Flame and Shock Wave	42
7. Theoretical Performance of Side Force Specific Impulse	43
8. Schematic Diagram of the Test Set-up	44
9. Photograph of the Test Facility	45
10. Axisymmetrical Water-Cooled Copper Nozzle	46
11. Side-View of the Axisymmetric Water-Cooled Copper Nozzle	47
12. End-View of the Axisymmetric Water-Cooled Copper Nozzle	48
13. Modified Axisymmetric Water-Cooled Copper Nozzle	49
14. Assembly of the Modified Axisymmetric Water-Cooled Copper Nozzle	50
15. End-View of the Modified Axisymmetric Water-Cooled Copper Nozzle	51
16. Drawing of Rectangular Test Nozzle	52

17.	Photograph of the Rectangular Nozzle Throat (looking downstream)	53
18.	Parts of the Rectangular Nozzle with Silicon Phenolic Plate (looking upstream)	54
19.	End-View of the Rectangular Nozzle Assembly with Silicon Phenolic Plate	55
20.	Side-View of the Rectangular Nozzle Assembly with Silicon Phenolic Plate	56
21.	Drawing of Axisymmetric Silicon Phenolic Nozzle	57
22.	Side-View of the Axisymmetric Silicon Phenolic Nozzle	58
23.	End-View of the Axisymmetric Silicon Phenolic Nozzle	59
24.	Electrode Electrical System Schematic	60
25.	Measured Arc Characteristic	61
26.	Pressure Distributions along Nozzle Center Line (Axisym. Copper Nozzle Cross-Flow Electrodes, 0.25 in. apart)	62
27.	Pressure Distributions along Nozzle Center Line (Axisym. Copper Nozzle Cross-Flow Electrodes, 0.125 in. apart)	63
28.	Pressure Distributions along Nozzle Center Line (Axisym. Copper Nozzle Parallel-Flow Electrodes, 0.25 in. apart)	64
29.	Post-Discharge of the Axisymmetric Copper Nozzle	65
30.	Pressure Distributions along Nozzle Center Line (Axisymmetric Nozzle; 0.25 in. apart with K ₂ CO ₃ Seedings and Boron Nitride Insulations)	66
31.	Variations of Pressure Rise and Power Input as a Function of Time	67
32.	Pressure Distributions along Nozzle Center Line (Modified Axisymmetric Copper Nozzle, Cross-Flow, 0.25 inches apart)	68
33.	Pressure Distributions along Nozzle Center Line (Rectangular Nozzle with Silicon Phenolic Plate, Cross-Flow, 0.25 in. apart)	69
34.	Flow Field Disturbance Visualization	70

35.	Post-Discharge of the Rectangular Nozzle (Cross-Flow, Silicon Phenolic Plate)	71
36.	Pressure Distributions along Nozzle Center Line (Rectangular Nozzle with Copper Plate, Cross- Flow Electrodes, 0.25 in. apart)	72
37.	Post-Discharge of the Rectangular Nozzle (Cross-Flow, Copper Plate)	73
38.	Post-Discharge of the Rectangular Nozzle (Parallel-Flow, Copper Plate)	74
39.	Pressure Distributions along Center Line of the Axisymmetric Silicon Phenolic Nozzle	75
40.	Post-Discharge of the Axisymmetric Silicon Phenolic Nozzle	76
41.	Pressure Rise due to Different Methods of Flow Disturbances	77
IV-1.	Breakdown Voltage between Cylindrical Rods at Atmospheric Pressure	89
V-1.	Principal Circuit Diagram	98
V-2.	Graphical Approximation of Material Function	99
V-3.	Predicted and Measured Arc Power	100
V-4.	Calculated and Measured Arc Characteristics	101
VI-1.	Pressure Distributions Affected by Electrode Protrusion	107
VI-2.	Pressure Response History	108
VII-1.	The Axisymmetric Silicon Phenolic Nozzle with 0.5 in. Electrode Distance in Cross-Flow	111
VII-2.	Pressure Readings along Center Line of the Axisymmetric Silicon Phenolic Nozzle	112
VII-3.	Pressure Readings along X_1 -Section ($y = 0$ is the projection of Y_0 -Section)	113
VII-4.	Pressure Readings along X_2 -Section	114
VII-5.	Pressure Change over all the Affected Area	115

LIST OF SYMBOLS

A	Area
a	Speed of sound
C_p	Specific heat at constant pressure
C_v	Specific heat at constant volume
E	Line energy source per unit length
E'	Electric field strength
E'_a	Electric field of the arc
E_{sp}	Specific energy of power source, Watt-hr/lb
F_0	Rocket main thrust
F_s	Side force exerted on the wall
F_x	X-component total body force
f, f_1	Filling factors
f	Body force volume
f_x	X-component of the body force per unit volume
g	Gravity constant
$g(\gamma)$	Non-dimensional pressure
I	Current, amp
i_x	Unit vector in x-direction
$J_0(x)$	Bessel function of zero order
$J_1(x)$	Bessel function of 1st order
$j_0(\gamma)$	A function of γ
k	Thermal conductivity

L	An arbitrary length toward downstream from injection port
L'	Arc length
M	Flow Mach number
\dot{m}	Total rate of mass addition
\dot{m}_i	Secondary mass flow rate
\dot{n}	Mass source per unit volume per unit time
P_a	Arc power
P_{in}	Total power input
P_{before}	Pressure before discharge
P_{during}	Pressure during discharge
P_{after}	Pressure after discharge
$p_{1,2,3}$	Pressure at region 1, 2 and 3 respectively
p	Static pressure
$p_t = p_0$	Total pressure
$\dot{Q} = \dot{p}_{in}$	Total rate of heat addition
\dot{Q}	Heat addition per unit mass of gas
\dot{q}	Heat source per unit volume per unit time
R	Radius of shock wave, or gas constant
R_0	$= E^{1/2} (2\pi p_0)^{-1/2}$
R_2	Resistance of the arc
R_c	Resistance of the outer circuit
r	Radial distance
r_2	Arc radius

S	Entropy of the flow, or the heat conduction function
S_0	Entropy constant, or heat conduction function at center of arc
S_2	Heat conduction function at edge of arc
T	Static temperature
T_0	Total temperature
$T_{1,2,3}$	Temperature at region 1, 2 and 3 respectively
$T_t = T_0$	Total temperature
T_2	Temperature of arc at its edge
T_c	Arc center temperature
t	Time
u	Shock speed = dr/dt , or x-component velocity
u_∞	Free stream velocity
$u_{1,2,3}$	Velocity at region 1, 2 and 3 respectively
V	Voltage
V_0	Power source voltage
V_2	Arc voltage
v	Y-component of velocity vector \vec{W}
v_u	Equivalent upwash velocity
\vec{W}	Velocity vector
\vec{W}_1	Disturbed velocity = $u\vec{i}_x - v\vec{i}_y - w\vec{i}_z$
\dot{W}	Flow rate
\dot{W}_e	Power source consumption rate
w	Z-component of velocity vector \vec{W}
\dot{w}	Flow rate of secondary injectant
λ_0	= 2.405

Greek Symbols

α	Angle between plane flame and plate, or slope of approximated $\sigma(s)$ line segment, see Fig. V-2
β	Oblique shock wave angle
γ	Ratio of specific heats = C_p/C_v
θ	Deflection angle across the shock wave
ϵ	Angle of deflection of rocket exhaust jet
$\tau(\gamma)$	A constant depending on γ
$\sigma(T)$	Electrical conductivity
σ^*	Approximated electric conductivity, see Fig. V-2
σ_0	Material function at center of arc
τ	= r/R
ρ	Local gas density
$\rho_{1,2,3}$	Gas Density at region 1, 2 and 3 respectively

Subscripts

∞	For free stream condition
b	By blast wave theory
e	By electric arc discharge
l	By linearized disturbance theory
m	By mass injection

SECTION I

INTRODUCTION

Attitude control is needed for both rocket propelled and re-entry vehicles. The first device to achieve this purpose was to control the jet vanes or to gimble the rocket exhaust nozzles by mechanical means. The scheme of secondary fluid injection was introduced in 1952 (Ref. 1) by using mass addition into the rocket exhaust nozzle to create the desired side force for thrust vector control. Analytical studies made in early 1950's (Refs. 2, 3, and 4) provided several different approaches for predicting the generated side force, and also revealed the possible applications for re-entry vehicles. Kaufman (Ref. 5) in 1957 showed his experimental results in hypersonic regime. The equivalence principle between heat and mass sources in high speed flows was noticed by Hicks (Ref. 6) in 1950 and by Chu (Ref. 7) in 1955, and further developed by Willmarth (Ref. 8) in 1957. This concept leads to the present investigation of using electric arc discharge to produce the heat source for vehicle attitude control.

Compared with the existing techniques, the electric discharge concept promises the following inherent advantages:

- i) It has no moving parts.
- ii) Plumbing system is not required.
- iii) Instantaneous response rate appears possible.
- iv) Since the system is electrical, it may be more compatible with the guidance and control systems.

The possible disadvantages may be as follows:

- i) It may result in a heavier system compared to that of the secondary injection scheme.
- ii) There may be material problems associated with high arc temperatures.

This report is a study of the feasibility of using the new method to steer a vehicle during its flight. The proposed technique is an attempt to obtain a positive and instantaneous control of the system by means of discharging electric energy locally into the supersonic stream as shown in Fig. 1.

For rocket applications, the electric discharge is accomplished by an arc located at one side of the nozzle wall, which causes a static pressure rise in the vicinity of the

discharge. This asymmetric pressure rise inside the nozzle exit cone results in a side force exerted against the nozzle wall. A similar phenomenon has been observed in the secondary fluid injection scheme for thrust vector control of rockets. The same concept may also be applicable to the re-entry vehicles.

In order to gain some insight of the phenomenological aspects of this concept, a feasibility study has been conducted both theoretically and experimentally. The magnitude of the side force was predicted by three different analytical models as discussed in Section II. The electric discharge and its corresponding pressure rises were investigated by a limited experimental program as discussed in Section III.

SECTION II

ANALYTICAL INVESTIGATION

2.1 THEORETICAL MODELS

The phenomena associated with electric discharge in supersonic flow (Refs 9, 10, and 11) are very complex. The flow field is affected by the electric discharge, which in turn will be influenced by the flow. The side force, produced by the interaction of the flow field and the electric discharge, can only be analyzed based on simplified models at the present time. The validity of these simplifications, however, will be verified by experimental investigation.

From experience in secondary fluid injection into a supersonic flow, it was found that both the "Blast Wave Analogy," (Ref. 4), and the "Linearized Small Disturbance Theory" (Ref. 2) gave a fairly good agreement with the measured side force. In addition to the above two models, a "Plane Flame Analogy" was also employed to predict the magnitude of the generated side force. All three models gave the same order of magnitude results and are discussed as follows.

2.1.1 Blast Wave Analogy

The flow field induced by a blast wave in a quiescent atmosphere was studied extensively by various authors (Refs. 12, 13, 14, and 15). Lees (Ref. 16) observed that the bow shock wave formation due to blunt nosed bodies in a hypersonic flow is equivalent to a constant energy supply in the form of a body drag. He successfully related the unsteady phenomenon of a sudden energy release into a quiescent flow to the steady phenomenon of an aerodynamic body in hypersonic flow. The electric arc discharge in a supersonic flow can be considered as a high thermal energy release into a high velocity gas stream.

The combined effects of both the thermal energy and the free stream velocity makes it possible to apply the concept of the blast wave analogy for analyzing electric discharge and flow field interactions. It is obvious that the accuracy obtained from this analogy can be improved as the thermal energy or the free stream velocity increases. Roman (Ref. 17) also observed that an electric arc confined by a magnetic field behaves like a heated solid body in a flow field. This observation lends a strong support of the validity of the blast wave

analogy applying to electric arc discharge into a supersonic flow field.

In order to see the nature of the problem and to determine the equivalent energy source strength, it is assumed that a large amount of heat is released on a flat plate which has a zero angle of attack in a uniform supersonic stream. The energy dissipation in the viscous boundary layer is small compared to the energy release due to the blast and was ignored. The net result of interaction between the flow field and the released energy can then be adequately treated by the blast wave theory.

If the energy is released at a point at a constant rate, the pressure wave will be spherically symmetric. This corresponds to a point-blast case. A uniform flow of velocity u_∞ superimposed on the point energy source will result in an axially symmetrical steady flow. In other words, the phenomenon is equivalent to that of the point energy source moving with a speed of u_∞ in the upstream direction with respect to a quiescent flow.[∞] This constitutes the strength of the line energy source per unit length, E , and can be expressed as

$$E = \frac{P_{in}}{u_\infty} \quad (1)$$

where P_{in} is the total energy input per unit time, or the power input. The above relation may be understood in a different manner; the total power input to the flow has to be equal to the strength of a line source carried with the characteristic velocity in question, namely, the free stream velocity u_∞ .

The above equation is derived without considering the wall effect. If the source is on the wall, and without considering the boundary layer, this means that only the half-space is affected by the above energy release; that is, half of the strength will produce the same net result in the half-space. Hence, in the flat plate case, the energy per unit length is given by

$$E = \frac{2P_{in}}{u_\infty} \quad (2)$$

The first order similarity solution, from blast wave theory, for a strong shock wave is given by Sakurai (Ref. 13) and Sedov (Ref. 14) for the effected area as

$$\left(\frac{a_\infty}{u}\right)^2 \left(\frac{R_0}{R}\right)^2 = j_0(\gamma) \quad (3)$$

and for the magnitude of pressure as,

$$\left(\frac{p}{p_\infty}\right) \left(\frac{a_\infty}{u}\right)^2 = g(\eta) \quad (4)$$

where R_0 is defined as,

$$R_0 = \left(\frac{E}{2\pi p_\infty}\right)^{\frac{1}{2}} \quad (5)$$

and a_∞ is the free stream speed of sound, R is the shock radius $u = dR/dt$ is the shock speed, j_0 is a constant depending on the ratio of specific heats γ , p is the pressure, $\eta = r/R$, with r the distance from the center of explosion, and $g(\eta)$ is a non-dimensional pressure given as:

$$g(\eta) = \frac{2\gamma}{\gamma+1} \left[\frac{\gamma+1-\eta}{\gamma} \frac{2\gamma^2+4\gamma-1}{\gamma^2-1} \right]^{-(\gamma^2+2\gamma-1)} \quad (6)$$

If the energy is released adjacent to a wall, the force exerted on the wall can be obtained by integrating the pressure rises over the effective area as (Fig. 2),

$$F_s = 2 \int_0^L \int_0^R (p - p_\infty) dr dx \quad (7)$$

where L is an arbitrary length toward downstream, and R is to the shock position. Broadwell (Ref. 4) successfully showed that Equation (7) can be integrated for the maximum side force by employing the relations of Equations (3), (4), (5), and (6), and resulted in:

$$F_{\max} = \frac{1}{2} \sigma(\gamma) E M_\infty^2 \quad (8)$$

where M_∞ is free stream Mach number and $\sigma(\gamma)$ is a constant depending on the value of γ ,

$$\begin{aligned} \sigma(\gamma) &= 0.10 & \text{for } \gamma &= 1.2 \\ \sigma(\gamma) &= 0.14 & \text{for } \gamma &= 1.3 \\ \sigma(\gamma) &= 0.17 & \text{for } \gamma &= 1.4 \end{aligned} \quad (9)$$

The side force F_s exerted on the plate due to a certain power input P_{in} , in the present problem, then becomes

$$F_s = \frac{\sigma(\gamma) P_{in}}{a_\infty} \quad (10a)$$

or, the side force per unit power input is

$$\frac{F_s}{P_{in}} = \frac{c(\gamma)}{a_\infty} = \frac{\sigma(\gamma)M_\infty}{u_\infty} \quad (10b)$$

In terms of the line energy strength,

$$\left(\frac{F_s}{E/2}\right) = \sigma(\gamma)M_\infty \quad (10c)$$

Equation (10c) indicates that the side force generated is linearly proportional to the free stream Mach number for the same line energy strength. Hence, it will be more beneficial to have the energy released to a higher Mach number stream than the lower Mach number supersonic stream. A plot of the generated side force vs. free stream Mach number is shown in Fig. 3.

2.1.2 Supersonic Small Disturbance Theory

The present problem of heat release to a supersonic flow, if viewed from the other angle, namely, the entire flow field, may be said to only be a local phenomenon. The energy addition only constitutes a perturbation to the main flow, hence linearized theory can be used.

Linearized supersonic small disturbance theory has been employed in Wu, Chapkis and Mager's (Ref. 2) analysis and showed a good agreement in predicting the order of magnitude of side force generation by fluid injection. Broadwell (Ref. 4) also pointed out that the linearized theory should give the right order of magnitude of the side force. However, Broadwell added one additional term to the side force equation proposed by Wu, et al. He argued that the supersonic small disturbance theory implicitly included the mass source entered to the free stream with an x-component velocity of the same magnitude of the free stream. The addition of that term made the result of the equation by an order of magnitude greater than the original

one. The disturbance created by the plane source flow in a supersonic stream is caused only by the "interaction" of the main and the source streams. There is no need to add another term to take care of the artificial x-component of the velocity since the disturbance created by the plane source flow is a net interaction phenomenon. A detailed discussion of Broadwell's additional term is included in Appendix I.

The analysis of a plane mass injection into a supersonic stream on a flat plate was performed by Wu, et al. The pressure coefficient C_p due to the mass injection disturbance is analogous to the disturbance created by the half-wedge angle δ (Fig. 4)

$$\delta = \frac{v_u}{u_\infty} \quad (11)$$

where v_u is the vertical disturbance velocity. If the secondary mass flow rate \dot{m}_i , over the area A , is small as compared to the mainstream mass flow rate, then the vertical disturbance velocity can be related to the injected mass flow rate as follows:

$$\frac{v_u}{u_\infty} = \frac{\dot{m}_i}{\rho_\infty u_\infty A} \quad (12)$$

Hence, the pressure disturbance by the mass injection can be written as

$$p - p_\infty = \frac{\rho_\infty u_\infty^2}{\sqrt{M_\infty^2 - 1}} \left(\frac{v_u}{u_\infty} \right) = \frac{\dot{m}_i u_\infty}{A \sqrt{M_\infty^2 - 1}} \quad (13)$$

The side force exerted on the flat plate is therefore

$$F_S = \iint_A (p - p_\infty) dA = \frac{\dot{m}_1 u_\infty}{\sqrt{M_\infty^2 - 1}} \quad (14)$$

Assuming that the disturbances were created by a mass source, a heat source and a body force, Willmarth (Ref. 8) derived the governing flow equation of the x-component as follows (Appendix II),

$$(1 - M_\infty^2) \frac{\partial u}{\partial x} + \frac{\partial v}{\partial y} + \frac{\partial w}{\partial z} = \frac{\dot{m}}{\rho_\infty} + \frac{\gamma - 1}{\rho_\infty a_\infty^2} \dot{q} - \frac{u_\infty}{\rho_\infty a_\infty^2} f_x \quad (15)$$

where \dot{m} is the mass source per unit volume, \dot{q} is the heat source per unit volume, and f_x is the x-component of the body force per unit volume. It can be seen that the mass source and heat source can be related as

$$\dot{m} = \frac{\gamma - 1}{a_\infty^2} \dot{Q} \quad (16)$$

where \dot{m} and \dot{Q} are the total quantities of the rate of mass and heat additions respectively. This analogy was also observed by Hicks (Ref. 6) and Chu (Ref. 7).

Employing Equation (16), the generated side force on the wall as expressed in Equation (14) can be written as

$$F_S = \frac{(\gamma - 1) M_\infty^2}{\sqrt{M_\infty^2 - 1}} \frac{\dot{Q}}{u_\infty} \quad (17a)$$

Since $\dot{Q} = P_{in}$, the side force per unit power input can be expressed as

$$\frac{F_S}{P_{in}} = \frac{(\gamma - 1)M_\infty}{a_\infty \sqrt{M_\infty^2 - 1}} \quad (17b)$$

It is surprising to find out that the asymptotic form of the above equation for large M_∞ is similar to that of the blast wave theory, although linearized assumption should not apply to high Mach number flows. Nevertheless, both theories give the relation that

$$\left(\frac{F_S}{E/2}\right) \sim M_\infty \text{ for } M_\infty \gg 1 \quad (18)$$

The plot of generated side force vs. free stream Mach number is shown in Fig. 5.

2.1.3 Plane Flame Analogy

There is another possible way to calculate the magnitude of the side force by a simple plane flame analogy. It is assumed that the heat is added into an inviscid supersonic stream through a plane thin flame as shown in Fig. 6. This approach is similar to Willmarth's (Ref. 8) flame method except that the solutions of the flow parameters can be uniquely determined.

The analysis of the flow field resulting from the heat addition through a plane flame can be greatly simplified by making the following assumptions:

- i) The gas is thermally and calorically perfect.
- ii) Gas properties do not change across the flame.
- iii) Plane flame has a negligible thickness, standing at an angle α to the plate (Fig. 6).
- iv) Heat transfer occurs only when the flow passes this flame.

Across a flame sheet, the normal component of the flow velocity may either increase or decrease depending on whether the flame is undergoing a deflagration or detonation process. In either case, the velocity component parallel to the flame is unaffected. Therefore, a deflagration flame will turn the flow toward the plate, while a detonation flame will turn the flow away from the plate. However, the boundary condition requires that the flow must be parallel to the plate, therefore the presence of a second wave is necessary. There are two possible waves that may be present, namely, a shock wave which always decelerates the normal (to shock wave) component of the velocity, hence turns the flow away from the plate, or expansion waves which always turns the flow toward the plate, in the configuration as shown in Fig. 6. Therefore, we may have eight possible flow patterns, as listed in Table I.

There are four cases where the boundary conditions are satisfied. Case (1) (a shock wave followed by a deflagration flame) does not violate any basic physical or mathematical laws, therefore its existence is possible. Case (4) (an expansion wave followed by a detonation flame) is ruled out because of the following consideration. In supersonic flow (here only the velocity component normal to these waves are considered, the parallel component may be eliminated if the observer moves with that speed), all disturbances propagate downstream only. The existence of an expansion wave upstream of the detonation flame requires the signals propagate upstream. Therefore, Case (4) can not occur. Case (5) is a deflagration flame followed by a shock. However, there is no deflagration flame in supersonic flow, this rules out the possibility of Case (5). Finally, we shall consider Case (8) (detonation followed by an expansion). Expansion waves can only occur in supersonic flow. In the present case it requires the flow be supersonic (the normal component) after the detonation flame. This type of flame is called weak detonation which has not been observed in reality. Therefore, Case (8) does not exist. The only condition, which both satisfies the boundary condition and is physically possible, is a shock wave followed by a deflagration flame (Case (1)). Therefore, the solution is uniquely determined.

TABLE I - FLOW PATTERNS

<u>Case</u>	<u>First Wave</u>	<u>Second Wave</u>	<u>Flow Configuration</u>	<u>Boundary Condition Satisfied</u>
(1)	Shock	Deflagration		yes
(2)	Shock	Detonation		no ¹
(3)	Expansion	Deflagration		no
(4)	Expansion	Detonation		yes
(5)	Deflagration	Shock		yes
(6)	Deflagration	Expansion		no
(7)	Detonation	Shock		no ¹
(8)	Detonation	Expansion		yes

¹The viscous effect is neglected here.

The continuity, momentum and energy equations, together with the equation of state, for the flow normal to the shock wave are:

$$\rho_1 u_1 \sin \beta = \rho_2 u_2 \sin(\beta - \delta) \quad (19)$$

$$p_1 + \rho_1 u_1^2 \sin^2 \beta = p_2 + \rho_2 u_2^2 \sin^2(\beta - \delta) \quad (20)$$

$$C_p T_1 + \frac{1}{2} u_1^2 = C_p T_2 + \frac{1}{2} u_2^2 \quad (21)$$

and

$$p_1 / \rho_1 T_1 = p_2 / \rho_2 T_2 \quad (22)$$

Those equations for the flow normal to the flame are:

$$\rho_2 u_2 \sin(\alpha - \delta) = \rho_3 u_3 \sin \alpha \quad (23)$$

$$p_2 + \rho_2 u_2^2 \sin^2(\alpha - \delta) = p_3 + \rho_3 u_3^2 \sin^2 \alpha \quad (24)$$

$$C_p T_2 + \frac{1}{2} u_2^2 + \Delta Q = C_p T_3 + \frac{1}{2} u_3^2 \quad (25)$$

$$\frac{p_2}{\rho_2} T_2 = \frac{p_3}{\rho_3} T_3 \quad (26)$$

The Chapman-Jouguet deflagration process across the flame is:

$$u_3 \sin \alpha = (\gamma R T_3)^{1/2} \quad (27)$$

In addition, two equations expressing the fact that the tangential velocity does not change across the shock and the flame may be written as:

$$u_1 \cos \beta = u_2 \cos (\beta - \delta) \quad (28)$$

$$u_2 \cos (\alpha - \delta) = u_3 \sin \alpha \quad (29)$$

where ρ is the density, u the velocity, T the temperature, p the pressure, ΔQ the heat addition per unit mass of gas, β the oblique shock wave angle, α the flame angle, δ the deflection angle across the shock wave and the subscripts, $1, 2, 3$, are indicating the regions respectively, as shown in Fig. 6. Now we have eleven equations with eleven unknowns. This problem is solveable. However, due to the complexity of algebra involved in simplifying the above equations, it is felt that the best method is to solve numerically and iterate the results with the help of tabulated numerical tables for the static temperatures and pressures of one-dimensional heat addition.

The generated side force per unit power input can be calculated by considering the geometrical relationships as shown in Fig. 6. The total power input through the flame is $\rho_1 u_1 \Delta Q$,

hence the side force per unit power input is

$$\frac{F_S}{P_{in}} = \frac{(p_2 - p_1) \left(\frac{\cos \beta}{\cos \alpha} \right) [\cos(\beta - \alpha) + \sin(\beta - \alpha) \cot(\alpha - \delta)]}{\rho_1 u_1 \Delta Q} \quad (30)$$

The side force per unit power input calculated according to Equation (30) is in agreement with the order of magnitude to that of the blast wave theory. Side forces evaluated by both the blast wave theory and the flame theory appeared to be less than that of the linearized theory. This is to be expected because the linearized theory implicitly assumed reversible heat addition and should give the minimum loss. However, in reality, the blast wave theory and the flame theory should give better results due to the non-linear effect caused by the large amount of heat addition.

2.1.4 Summary of Theoretical Studies

From the above-mentioned three approaches, one can predict the magnitude of the side force generated by heat addition from a side wall to the main stream. For a special case which is investigated later experimentally, the following conditions are used:

$$p_t \approx 50 \text{ psia}$$

$$T_t \approx 6000^\circ \text{R}$$

$$M_\infty \approx 2.5$$

$$\gamma = \frac{C_p}{C_v} \approx 1.3$$

the specific side force per unit power input F_s/P_{in} for the three approaches are as follows:

	Blast Wave	Linearized	Plane Flame
F_s/P_{in}	~ .05	~ .10	~ .035

where F_s/P_{in} has the unit of lbs/kw, or approximately, lbs/BTU/sec. All of the three different approaches predict the side forces of the same order of magnitude. Blast wave and linearized theories give the solution explicitly, while the plane flame theory needs iteration. As expected, the blast wave theory gives the better agreement than the linearized theory as compared to our experimental results which will be presented in Section III.

The linearized theory predicts the highest specific side force per unit power input. This is so because the small disturbance theory represents the condition of minimum loss. Therefore, the value may be considered as the upper limit of side force obtainable by the arc discharge in a low supersonic flow. For a high supersonic flow or large energy addition, the linearized theory breaks down due to its inherent assumption which we made in the derivation of the governing equations.

The blast wave theory, on the other hand, can not extrapolate to the low Mach number flow or low energy addition case. This is due to the assumption of a strong shock wave boundary condition employed in its original derivation.

2.1.5 Comparison of Heat Addition and Mass Injection in Generating Side Force

From the above discussions, it is clear that both mass injection and electrical energy addition are capable to generate side force locally in a supersonic stream. Purely from a theoretical point of view, it is difficult to determine which method

is superior. Depending on the quantities of injection, both schemes may yield comparable magnitudes of side force. Therefore, the selection of either method for a specific mission, depends very much on the conditions such as the state of the art on power source, the material capability, the hardware designs, etc. In some cases, there is electrical power available on board such as nuclear propelled vehicles, the electrical energy addition through the arc discharge technique appears to be superior, because there is no need to carry the redundant auxiliary tank for the mass injection. On the other hand, the arc discharge method depends on the specific energy of the power source if the power source needs to be carried on board. The specific energy of the power source is defined as the ratio of the energy of the source to its weight.

From the airborne weight penalty point of view, the performance of arc discharge may be best analyzed by using the parameter of side force specific impulses, I_{sps} . This parameter is defined as the side force generated per unit weight consumption.

For the mass injection case,

$$(I_{sps})_m = \frac{F_s}{\dot{w}} \quad (31)$$

and for the electric discharge case,

$$(I_{sps})_e = \frac{F_s}{\dot{W}_e} \quad (32)$$

where \dot{w} = flow rate of secondary injectant, \dot{W}_e = battery, or electric power source, consumption rate defined as

$$\dot{W}_e = \frac{P_{in}}{E_{sp}} \quad (33)$$

and E_{sp} = battery specific energy, usually is given by watt-hr/lb. Hence,

$$(I_{sps})_e = \frac{F_s E_{sp}}{F_{in}} \quad (34)$$

The side force specific impulse can be evaluated by the blast wave theory and the linearized theory, respectively.

2.1.5.1 Blast Wave Theory

The side force generated by the thermal energy release has been derived as

$$F_{seb} = \sigma(\gamma) M_\infty \frac{P_{in}}{u_\infty} \quad (35)$$

Hence, the specific impulse may be written as

$$\begin{aligned} (I_{sps})_{eb} &= \frac{F_{sb}}{W_e} \\ &= \sigma(\gamma) M_\infty \frac{E_{sp}}{u_\infty} \end{aligned} \quad (36a)$$

by employing the conventional unit, i.e., E_{sp} in watt-hr/lb, u_∞ in ft/sec, I_{sps} in sec, the above equation becomes

$$(I_{sps})_{eb} = 2655 \sigma(\gamma) M_\infty \frac{E_{sp}}{u_\infty} \quad (36b)$$

2.1.5.2 Linearized Small Disturbance Theory

The same argument may be also applied to the linearized theory. The expression for specific impulse of electric discharge based on linearized theory is as follows:

$$(I_{\text{sps}})_{\text{el}} = 2655 \frac{M_{\infty}^2}{\sqrt{M_{\infty}^2 - 1}} \frac{E_{\text{sp}}}{u_{\infty}} \quad (37)$$

The theoretical performance of employing electric discharge in generating side force by the above two theories are shown in Fig. 7. The side force specific impulse is linearly related to the specific energy of the power source. At the present state, the specific impulse of using electric discharge, by carrying chemical batteries on board, is significantly lower than that of the secondary mass injection because of the low specific energy values. However, the electric discharge technique will appear to be superior than the secondary fluid injection scheme, if

- i) the electrical source is available on board, such as nuclear rockets,
- ii) storage of solar energy is possible during the long time space mission vehicles in its re-entry phase,²
- iii) further improvement and development of chemical batteries are possible,³ and
- iv) development of new type power source like MHD generators⁴ becomes available.

²At the present capability, a round trip to outer planets takes several years in space. In addition, according to Cheng (Ref. 21) the arc discharge applied to a high Mach number low density flow may result in some other effects which will help in generating side force.

³It is felt, with the present technology on chemical batteries, that the limit of specific energy required from this system is below that required to make thrust vector control by electric arc discharge competitive.

⁴Airborne type MHD generators are in the development stage at the J. B. Dicks and Associates, Tullahoma, Tennessee (see detail in Appendix III).

2.2 ELECTRIC ARC CHARACTERISTICS

An analytical method is not available for predicting either the breakdown voltage or the operating characteristic of an electric arc with sufficient confidence. For the configurations that the electrodes are mounted flush on the same surface without facing at each other, there is no information available even to serve as a guide for an intelligent guess. It is felt that there is a need to collect the existing information on electric arcs for defining an operation range in order to investigate the aerodynamic aspect of the flow field phenomenon caused by electric discharge.

The breakdown voltage as indicated by Cobine (Ref. 18) and explained in Appendix IV could be as high as 23,000 volts for the present problem. Of course, this is not practical for any possible aerospace applications. Experimental methods for establishing an arc with reasonable breakdown voltage are available for different electrode configurations. A literature survey of the available information under various conditions is discussed in detail in Appendix IV and revealed the possibility of establishing an arc at a breakdown voltage at about 400 volts. The value is encouraging but the information curves are not directly comparable with the present problem. Nevertheless, the range of investigation can be considered as a guide for the purpose of preparing experimental investigations.

The operating characteristics for a cylindrical arc were analyzed by Maecker (Ref. 19) with the assistance of some experimental results. Following Maecker's approach, the voltage-current variations of an arc operating characteristic at a nitrogen stream of 5000°R was evaluated in Appendix V. There the consideration of thermal-chemical effect concerning ionization for an arc discharge at various temperatures and pressures was based on the results of Cambel (Ref. 20).

SECTION III

EXPERIMENTAL PROGRAM

Electric arc studies have relied on experimental programs because of the complex emission processes caused by various parameters, such as the electrode surfaces and the surrounding conditions. Available theories can only provide qualitative guidance for designing the experimental apparatus. The desired configuration with the electrodes embedded in the same surface without facing each other has not been examined in the literature. Preliminary study of Appendix IV indicated that

- i) the breakdown voltage could be as high as 23,000 volts for a pair of electrodes separated by one quarter of an inch between the shortest distance, and
- ii) the arc might not be stable without the confinement of a strong magnetic field.

Consideration for apparatus design further revealed that the material problem could be very serious especially in the vicinity of the electric arc. In order to study the aerodynamic phenomena on pressure rises caused by electric discharge, all the related problems need to be investigated. Three different types of testing nozzles were designed and tested. The difficulties encountered during the testing processes are presented in Appendix VI.

3.1 TEST FACILITY

The experimental program was conducted at the Arnold Engineering Development Center, Arnold Air Force Station, Tennessee. The two-megawatt arc heater located in the Propulsion Wind Tunnel was selected because it provides i) the high temperature gas stream for simulating the rocket exhaust and ii) the required d-c power supply for starting and maintaining the electric arc. Since the facility has been scheduled for other higher priority tests at the same time, the apparatus and instrumentation were so designed that a minimum alteration of the standard set-up was needed.

The arc heater supplied heated nitrogen at a stagnation temperature range between 3000°R and 6000°R, and a stagnation pressure of about 50 psia. With a vacuum system to provide an ambient pressure approximately 2 psia, at a continuous flow rate of .3 lb/sec, the high temperature environment of a rocket

nozzle was able to be simulated at an exhaust Mach number approximately 3. Due to the high temperature environment of a cooling system at 400 psia with a maximum water flow rate approximately 300 gallons per minute was used to maintain the test apparatus within the allowable stress limit. A schematic diagram of the test facility is shown in Fig. 8 and a photograph of this facility is shown in Fig. 9.

In order to provide the electric energy for establishing and maintaining an electric arc, a d-c power supply up to 1200 volts was used at a maximum possible current of 800 amperes. The d-c voltage can only be applied at an increment of 75 volt interval; the voltage and current were registered on standard meters and recorded photographically at three frames per second.

The stagnation temperature of the arc heated nitrogen was determined by using the relation obtained from thermal energy balance between the cooling water and the heated nitrogen. No temperature measurement was attempted in the test section because the arc temperature generally is out of the range of conventional temperature measurement technique such as thermocouples. Optical systems for temperature measurements were studied, but the reliability and accuracy could not be proven to justify the effort.

The stagnation pressure of the heated nitrogen was measured directly from the stilling chamber. The static pressures in the gas stream was measured through wall pressure taps by transducers and manometers, and recorded by an oscillograph and cameras respectively. Due to the distance between the test apparatus and the instrumentation panel, a minimum time of 0.8 seconds for the transducer readings and 3.0 seconds for the manometer readings were required to give the steady state response. The detailed study of the response time is discussed in Appendix VI. The standard set-up of the test facility is described in the AEDC Test Facilities Handbook (Ref. 22).

3.2 TEST NOZZLES

Three test nozzles were designed for adapting to the two-megawatt heater for rocket nozzle simulation. Due to the high temperature requirement, only water-cooled copper and ablative composite material were chosen for this study.

3.2.1 Axisymmetric Copper Nozzle

A water-cooled axisymmetric copper nozzle was built for the purpose of studying: i) arc establishment, ii) insulation materials, and iii) electrode configuration investigations. Preliminary information on arc establishment was obtained by surveying

the available literature as outlined in Appendix IV. The heat transfer analysis was made by considering the conductive and convective heat transfer at the test conditions. The insulation materials were determined by trial and error method as outlined in Appendix VI. Two pairs of electrodes were installed for obtaining the information on breakdown voltages affected by electrode arrangements. However, the available space for pressure measurements was limited by the number of electrode configuration possibilities. A schematic diagram of the axisymmetric copper nozzle is shown in Fig. 10; the photographs of the side and end views are shown in Figs. 11 and 12, respectively, to indicate the pressure tap and electrode arrangements. The water-cooled axisymmetric nozzle was modified for studying pressure distributions. A schematic diagram of the modified axisymmetric copper nozzle is shown in Fig. 13 to illustrate the pressure tap locations with respect to the tested electrode configuration. The photographs of Figs. 14 and 15 show the assembly and the exit of this nozzle.

3.2.2 Rectangular Copper Nozzle

The rectangular copper nozzle was designed for the following purposes:

- i) Visualization of electric arc and flow field interaction.
- ii) Electrode configuration variations, and
- iii) Material selections for electrodes, insulators, and plastic nozzle parts.

In order to meet these requirements, three nozzle sections were used, namely, the throat section, the top and side wall sections and the bottom wall section. Water-cooled copper was used for the first two sections with quartz windows installed at the downstream portion of the side walls for flow visualization. Various materials were used for the third section which was simply a flat plate with electrodes and pressure taps. This third section can be easily replaced for investigating electrode configurations. A drawing of the rectangular nozzle is shown in Fig. 16, photographs of Figs. 17 and 18 show the three main sections of the rectangular nozzle; Figs. 19 and 20 show the assembly and the side views, respectively.

3.2.3 Axisymmetric Silicon Phenolic Nozzle

The water-cooled copper nozzle was inherently accompanied with a cold boundary layer which may affect the electric discharge characteristics. In order to investigate the possible effect on the flow field, an axisymmetric silicon phenolic nozzle was built identical with the axisymmetric water-cooled copper nozzle. Due to the high ablation rate of this material, a graphite throat insert was used for better duration. A design drawing of the axisymmetric silicon phenolic nozzle is shown in Fig. 21. Photographs of Figs. 22 and 23 show the pressure tap locations and overall assembly of the nozzle.

3.3 TEST PROCEDURE

After all instruments were properly calibrated, the test was started for any predetermined test conditions. The standard procedure for each test run was as follows:

The vacuum system was started first to establish the desired back pressure at the nozzle exit. The cooling water was then started to circulate. The water flow rates of all cooling sections were recorded and inspected to insure sufficient amount of cooling for preventing any possible overheating of any parts. Since the test was conducted at very high temperature and low pressure environment, the cooling water flow rate could be very critical in order to keep the apparatus within the allowable stress limit.

When the cooling water system was functioning properly, the cold nitrogen flow was then started. Simultaneously, all the cameras and oscillograph were turned on to record time dependence variations of all pressures and temperatures.

The arc heater was then started to heat the nitrogen at the stilling chamber. As soon as steady state was reached (generally, it required 3 to 5 seconds), the d-c power for electric discharge was applied. A high frequency starter was connected in the circuit and could be used if necessary.

The operating characteristics could be established by decreasing the circuit resistance or increasing the circuit voltage. The variations of both current and voltage were continuously recorded by photographing the ammeter and voltmeter readings. The voltage for electric discharge was discontinued after a period of time which was considered long enough for steady response of all the pressure measurements. The nitrogen flow, instrumentation recorders, cooling water

and the vacuum system were then turned off in sequence. In some cases, the static pressure after discharge did not return to the before-discharge readings as discussed in Appendix VI. Cautions were taken to allow at least 3 seconds between the voltage off and instrumentation off in order to check the possible cause of pressure rise other than the electric discharge. The actual pressure rise caused by electric discharge was determined by using the pressure difference between the pressure reading during and after discharge. This method of determining pressure rise caused by electric arc is being considered as conservative because the material is deforming continuously even shortly after the electric discharge.

3.4 RESULTS AND DISCUSSION

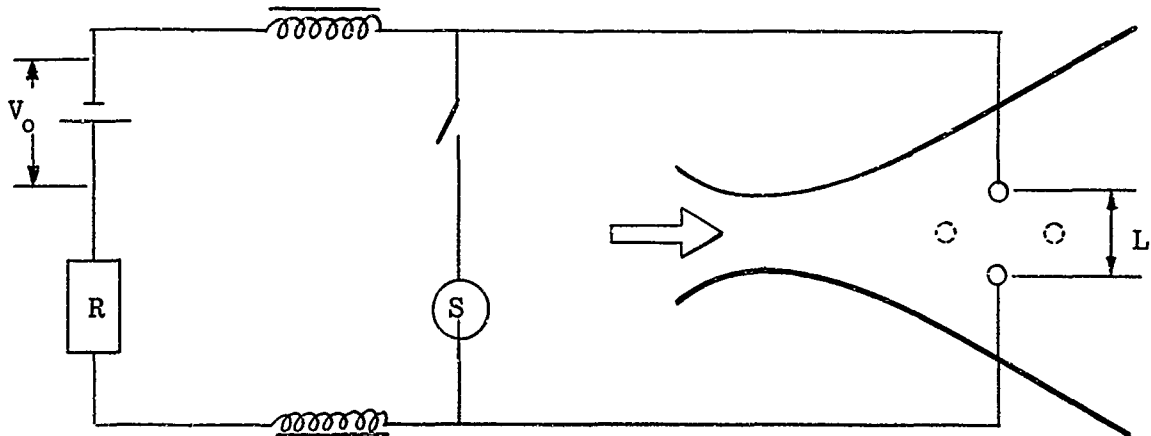
3.4.1 Breakdown Voltage in a Supersonic Stream

No information is available concerning the breakdown voltage between two parallel electrodes embedded flush in the same surface in a supersonic stream. Various sources as discussed in Appendix IV indicated the possible breakdown voltage ranges from 400 to 23,000 volts for the desired configurations. This uncertainty caused a great deal of difficulty in selecting an appropriate test facility for the experimental investigation. A compromise had to be made in order to cover the reasonable ranges for the flow Mach numbers, the stream temperatures, and the d-c power availability. The two-megawatt heater provided the conditions closest to the desired range with the disadvantages that the flow Mach number was limited to 3 and the side force could not be directly measured.

The axisymmetrical water-cooled copper nozzle was used for investigating the breakdown voltage. A 75 volt increment was applied for testing at various design parameters. The experimental results are tabulated in Table II. It can be seen that a breakdown voltage of 375 volts was needed to start an arc between a pair of electrodes of one-quarter inch apart mounted flush on the same surface over which a Mach 2.5 nitrogen stream flowing at a static pressure of 2 psia and a stagnation temperature of 4000°R. The breakdown voltage was substantially reduced by increasing the stream temperature, decreasing the distance between the electrodes, arranging the electrodes parallel instead of perpendicular to the flow direction, or seeding the stream with low ionization potential material. It is to be emphasized that the tabulated results in Table II are only qualitative nature because of the d-c power supply was limited to 75 volt increments. Nevertheless, the possibility of successfully establishing an electric arc in a supersonic stream is proved to be within the practical voltage range;

TABLE II - ARC ESTABLISHMENT PARAMETERS
(MACH NO. OF GAS STREAM = 2.5)

Investigated Parameters						Circuit Voltage (Vo)
Total Temp. (T _t)	High Freq. Starter (S)	Dist. (d) Between Electrode	Electrode Arrg't	Polarity	Seeding (K ₂ CO ₃)	
°R	—	in.	—	—	%	volt
4200	w/o	.25	⊥	—	0	375
6000						300
4200	w/o	.25	—	—	0	375
	w					300
4200	w	.25	⊥	—	0	300
		.125				225
4200	w	.125	⊥	—	0	300
		.20				150
4200	w	.20		—	0	150
				Reverse		225
4200	w	.20		Reverse	0	225
					.25	150
5700	w	.20		—	.28	75



namely, the electric field required to initiate discharge was about 2×10^3 volts per inch at the studied condition. Moreover, the use of high frequency starter was found to be very effective in assistance to establish the arc.

3.4.2 Operating Characteristics of an Electric Arc

The operating characteristics of an electric arc can only be analyzed for highly simplified models as discussed in Appendix V. Configurations for the proposed scheme have not yet been studied. The experiment for establishing a voltage-current curve was conducted by

- i) increasing the circuit voltage, V_0 , as shown in Figure 24 and,
- ii) reducing the circuit resistance, R_c .

The operating characteristics are shown in Figure 25 for the electrode arrangements perpendicular and parallel to the flow direction.

3.4.3 Pressure Distributions

The pressure distributions in the vicinity of the electrodes were measured. However, due to the high temperature environment (approximately $10,000^\circ\text{K}$ arc temperature), and the high velocity (about 5000 ft/sec) flow field, the material problem became so severe that the pressure distributions could not be obtained without any interference from the material deformation. Three test nozzle designs were used for investigating the static pressure distributions:

3.4.3.1 Axisymmetric Copper Nozzle

The pressure distribution along the nozzle centerline is shown in Figs. 26, 27, and 28 for the electrode configurations, A, B, and C, respectively. Configuration A was for electrodes one-quarter inch apart perpendicular to the flow direction. Configuration B was for electrodes one-eighth inch apart perpendicular to the flow direction. Configuration C was for electrode one-quarter inch apart parallel to the flow direction. The area affected by pressure rise in configuration A is comparatively larger than those of configurations B and C. However, the pressure taps were not dense enough to provide the detailed distribution especially in the vicinity of the electrodes. Furthermore, the deformation of the insulation material destroyed the

smooth contour of the nozzle surface, which caused the static pressures after discharge to differ from that before discharge. The insulation damage can be seen from a photograph for electrode after discharge in Fig. 29. By examining the post discharged test nozzle the different colors on the wall downstream of the electrodes indicated a very similar pattern as observed downstream of the injection part of the secondary fluid injection cases (Ref. 23). These color changes were considered as an evidence of the presence of a shock wave caused by the mass addition in the secondary fluid injection case and by the electric arc discharge in the present case.

The insulation material created a serious problem, as discussed in Appendix VI. Among all the tested materials, boron nitride appeared to be the only one possible to provide the desired performance and was used for electrode insulators for all the remaining experiments. The electrode configuration C was tested for measuring pressure distributions at various power inputs. The arc was established at a breakdown voltage of 75 volts, with the assistance of a high frequency starter under the flow conditions of a Mach 2.5 nitrogen stream seeded with K_2CO_3 (approximately 0.28% of potassium) at 5700°R stagnation temperature and 2 psia static pressure. The pressure distributions are shown in Fig. 30. The history of the pressure variations corresponding to the power variations is shown in Fig. 31. It can be seen that the pressure rise is a function of power input. Moreover, the static pressure after discharge returned to the values of before discharge which proved that the boron nitride could be used as insulators between the electrodes and the copper wall.

It is necessary to point out that the static pressure at the nozzle exit was not following the isentropic expansion curve even without electric discharge. This was caused by flow separations resulting from the leaking problem of the vacuum system which prevented the test facility from reaching the designed nozzle back pressure. The axisymmetric copper nozzle was modified by changing the exit area to the attainable back pressure of the facility and installing more pressure taps in the vicinity of the electrodes. The problems of flow separations and insulation damages appeared to be considerably improved. The static pressure distributions are shown in Fig. 32. The static pressure rise due to electric arc discharge seemed to affect only a very small area.

3.4.3.2 Rectangular Copper Nozzle

The pressure distribution of the rectangular copper nozzle was measured using several types of material as the bottom nozzle wall. The purpose of eliminating the cold boundary layer effect was the main reason for using a non-metallic material as the bottom nozzle wall. However, several problems were encountered during the testing. Boron nitride was the first material selected because of its high thermal shock resistance, but the difficulty of preventing leaks between the pressure taps and the boron nitride plate made this material impractical from the cost standpoint. The leak prevention effort for using boron nitride is discussed briefly in Appendix VI.

Silicon phenolic material was used with fair success when the electrodes were insulated with boron nitride. The insulation is necessary because charred silicon phenolic is a good electric conductor. The pressure distributions are shown in Fig. 33 for electrode arrangement perpendicular to the flow direction. The flow field disturbances caused by electric arc were recorded with high speed movie cameras for visualization purposes (available on request). Fig. 34 shows a typical movie frame of the flow field disturbance due to electric discharge which is very similar to the picture for secondary fluid injection as shown in Ref. 3. It was observed that the extensive heat of the arc caused the plate to ablate and deform and prevented the pressure reading from returning to the original value after discharge. Moreover, the highest peak of the pressure rise was not detected because the insulation occupied the space where the pressure tap was located in the axisymmetric nozzle. The phenolic plate after discharge is shown in Fig. 35. A water-cooled copper plate was also used for the configuration of electrodes perpendicular to the flow direction. The electric discharge was established through the copper plate. Ceramic coating on the surface of the water-cooled copper plate was used. The pressure distribution is shown in Fig. 36. The static pressure returned to the original values after discharge. The ceramic coated copper plate seemed to be a better approach to prevent erosion as well as to maintain the arc between electrodes. However, the ceramic coating could not remain effective for sufficient time to give steady state manometer readings and the effective pressure rise area appeared to be very small. The picture in Fig. 37 shows the copper plate after discharge.

It is noted that the supplied electric energy partially went to ablate the material as in the silicon phenolic plate case and to heat the cooling water as the ceramic coated copper

plate. In any event, the phenomenon that electric discharge can cause pressure rise in a supersonic flow field is confirmed. The effective area, however, is very small for free stream Mach numbers near 3.

An electrode configuration arranged parallel to the flow direction was also tested. No substantial pressure rise was measured during discharge for all the pressure taps. The ceramic coated copper plate after discharge is shown in Fig. 38.

3.4.3.3 Silicon Phenolic Axisymmetric Nozzle

The pressure distributions obtained from the silicon phenolic axisymmetric nozzle are shown in Fig. 39. The static pressure after discharge failed to return to the before discharge values because of the severe damage of the surface of phenolic material. The information on pressure rise was obtained by using the pressure differences between, during and after discharges. The actual pressure rise caused by electric discharge could be higher than the used value because of the continuous deformation of the phenolic material. Nevertheless, this method provided the quantitative results on the most conservative side. Thus, the concept that the electric discharge can cause sudden pressure rise is confirmed. Fig. 40 shows the picture of the phenolic nozzle taken after discharge. By examining the post discharged test nozzle, the color changes on the wall downstream of the electrodes indicates the shock wave pattern caused by the electric arc.

3.5 COMPARISON OF PRESSURE RISE IN MAIN STREAM DUE TO ELECTRIC DISCHARGE AND THE PRESENCE OF SOLID BODY

It has been reported by Roman (Ref. 17) that a magnetic confined arc in a cross flow behaves like a heated solid body as has been mentioned in Section II. In the present experiment, the arc discharge is not magnetically confined. However, it has been observed that the same arc - solid body analogy still exists. Once the discharge is established, energy is continuously being fed in. The discharge takes a curved path rather than a straight one (as in the magnetically confined arc) because of the blowing effect of the main stream.

Figure 41 shows the pressure rise caused by the protrusion of electrodes above the nozzle wall about 0.06 in. without discharge and caused by electric discharge with flush mounted electrodes. It is clear that the pressure rise caused by these two effects are

quite similar. The pressure rise was shifted downstream in the discharge cases (Fig. 41). This was caused by the curved shape of the discharge due to the blowing effect. Vas and Bogdonoff (Ref. 24) reported that the pressure just upstream of a forward facing step increases linearly with step height as long as the step height is less than the boundary layer thickness. Since the distance of protrusion of electrodes were less than the boundary layer thickness (about 0.2 in. in our test case), it may be able for us to estimate the equivalent step height corresponding to a similar pressure rise by an arc discharge.

3.6 SIDE FORCE EVALUATION

The side force was evaluated by integrating the pressure differences during and after discharge over the affected areas. The detailed evaluation procedures are discussed in Appendix VII. Due to the limited experimental data available, this evaluation only gives the order of magnitude of the generated side force. The evaluated results are compared with theoretical calculations and presented in Table III. The experimental level for the parameter F_s/P_{in} is low but comparable to that of the theoretical calculations. The energy lost in ablating electrodes, insulators, and conduction to the cooled walls has not been considered.

TABLE III. COMPARISON OF MEASURED AND PREDICTED SIDE FORCE

Type of Nozzle and Flow Conditions	Experimental F_S/P_{in} , lb/kw	Blast Wave Theory F_S/P_{in} , lb/kw	Linearized Theory \bar{F}_S/P_{in} , lb/kw
Modified Axisymmetric Copper Nozzle $P_0 = 55$ psia, $T_0 = 5850^\circ R$	~ 0.02	~ 0.03	~ 0.06
Rectangular Nozzle with Copper Plate $P_0 = 55.1$ psia, $T_0 = 6300^\circ R$	~ 0.03	~ 0.05	~ 0.14
Axisymmetric Silicon Phenolic Nozzle $P_0 = 59$ psia, $T_0 = 6480^\circ R$	~ 0.04	~ 0.04	~ 0.10
Rectangular Nozzle with Silicon Phenolic Plate $P_0 = 54.2$ psia, $T_0 = 5680^\circ R$	~ 0.03	~ 0.06	~ 0.14

SECTION IV

CONCLUSIONS

Analytical and experimental investigations were conducted for the electric discharge in a supersonic stream. The following conclusions were reached.

4.1 STATIC PRESSURE RISE CAN BE PRODUCED BY ELECTRIC DISCHARGE

A static pressure rise occurred in the vicinity downstream of the electrodes when an arc discharge was applied in a supersonic flow field. This type of static pressure distribution was also observed in secondary fluid injection case, especially when gas was used as the injectant. The pressure peak caused by arc discharge agreed with the trend predicted by the blast wave theory.

4.2 SIDE FORCE GENERATED BY AN ARC DISCHARGE MAY BE PREDICTED WITH SIMPLIFIED THEORY

The blast wave analogy, linearized small disturbance theory, and plane flame theory all predicted with the same order of magnitude of the experimental result. The blast wave analogy appeared to be more advantageous because it considered the nonlinear interaction phenomena of the energy source with the flow and also resulted in a simple mathematical expression.

4.3 ARC CAN BE ESTABLISHED AND MAINTAINED IN THE SUPERSONIC STREAM

There is no report available on the arc discharge to a pair of electrodes which are embedded flush on the wall and are not directly facing each other. From this study, it was found that the arc can be established and maintained in a supersonic flow without magnetic confinement.

4.4 THE BREAKDOWN VOLTAGE IS WITHIN THE PRACTICAL RANGE

The electric field, to initiate arc discharges, was about 2×10^3 volts/in. for nitrogen stream at Mach number 2.5 with static pressure of 2 psia and stagnation temperature of 4000°R . The required electric field can be reduced to approximately 3×10^2 volts/in., if the gas stream stagnation temperature is about 6000°R with 0.28% of potassium seeds and favorable electrodes orientation.

4.5 THE SIDE FORCE SPECIFIC IMPULSE OF ARC DISCHARGE DEPENDS ON THE SPECIFIC ENERGY OF POWER SOURCE

Comparing the specific impulse of arc discharge scheme to that of the secondary fluid injection method, it was found that the arc discharge technique only becomes competitive when

- i) high specific energy power source is available for rocket type vehicles, or
- ii) sufficient power source is available on board for re-entry type vehicles.

4.6 MATERIAL PROBLEMS ASSOCIATED WITH ELECTRIC ARC DISCHARGE IN SUPERSONIC FLOW

It was found in the experiments that the available material can only sustain a very short duration without serious deformation. In order to obtain accurate measurements, highly sensitive instrumentation must be used. The experimental program was discontinued because the development of high temperature material at the present is not adequate for system applications.

SECTION V
RECOMMENDATIONS

Based on the results of this investigation, the following recommendations can be made:

5.1 ARC DISCHARGE FOR ROCKET APPLICATIONS

The most attractive place to use the arc discharge technique is for nuclear energy propelled rockets where energy consumption for auxiliary power does not result in significant weight and cost penalties. For chemical rockets, however, the only possibility of making the electric arc discharge for thrust vector control to be feasible is to employ high specific energy power source which may be available in the future.

5.2 ARC DISCHARGE FOR RE-ENTRY APPLICATIONS

For the long time mission space vehicles, the solar energy may be stored and used for the re-entry trajectory control purpose. The phenomena of arc discharge in a very high Mach number case needs further investigation.

5.3 A COMBINED APPLICATION OF SECONDARY MASS INJECTION AND ARC DISCHARGE

From the side force specific impulse point of view, it is found that the arc discharge alone, or purely by the thermal energy addition, under the present available power source is not as effective as the secondary injection. A new device may be developed by combining the two methods. The arc discharge could be designed, such as the arc jet device, to provide thermal energy for the secondary injection gas rather than directly delivered to the main gas stream. By this means, the secondary gas flow will receive an additional energy or to increase its momentum as it leaves the injection port, and resulted in a more effective side force generation than by either gas injection or arc discharge alone.

5.4 ARC APPLICATIONS FOR SUPERSONIC COMBUSTION

The electric arc discharge proved to be a very practical means for energy addition at low pressure environment. This phenomenon may assist to overcome the difficulties for diffusional mixing in supersonic combustion at low pressure. There, in general, the long relaxation time results in a combustor being too long for practical purposes. Arc discharge in the fuel and air mixing region may accelerate the mixing and combustion

processes. Moreover, the required power source can be obtained through a MHD generator which may be located at the downstream portion of the system.

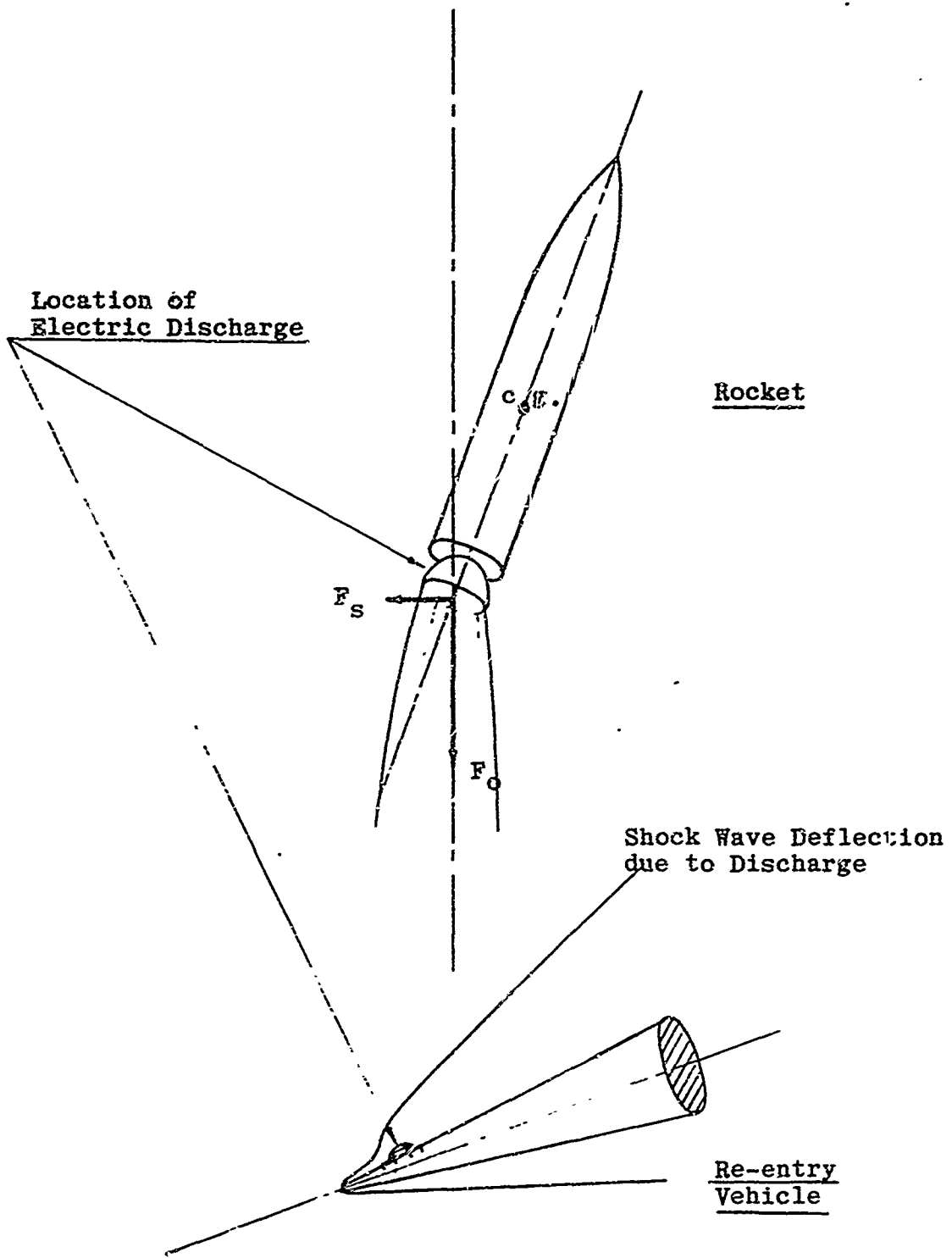


Figure 1 . Flight Direction Control By Electric Discharge

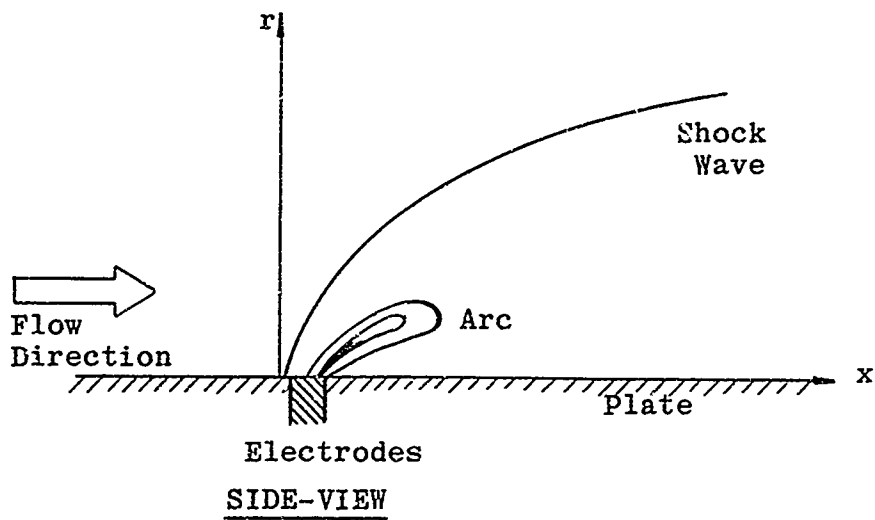
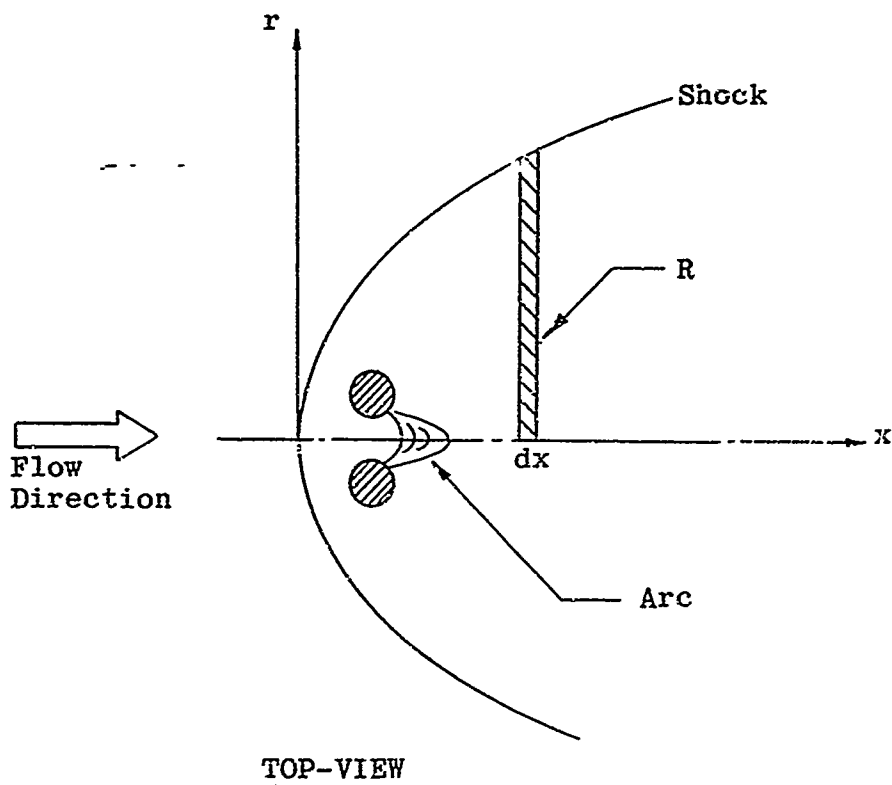


Figure 2. Schematic Drawing of Generated Shock Wave Due to Arc Discharge

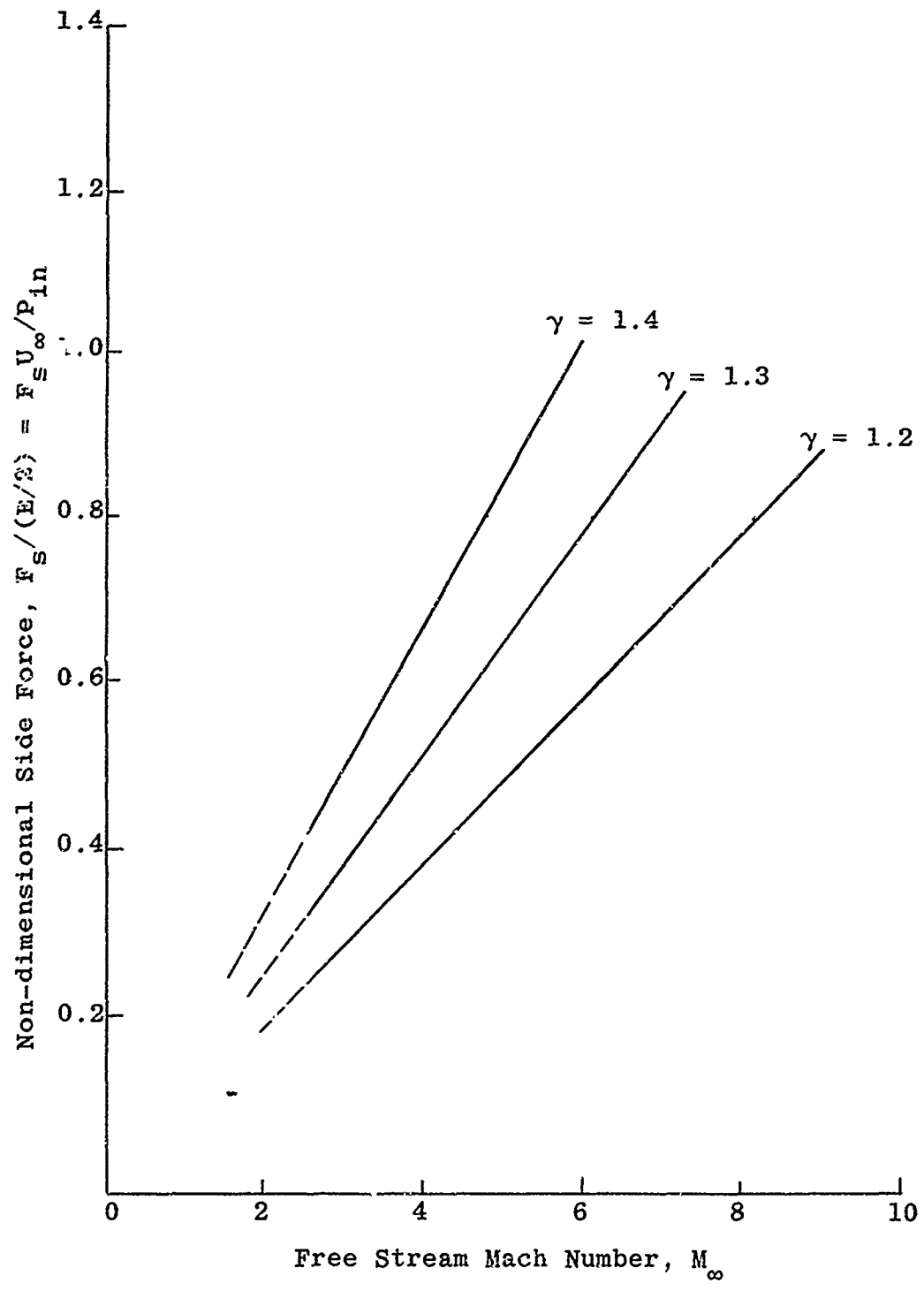


Figure 3. Generated Side Force vs. Free Stream Mach Number by Blast Wave Theory

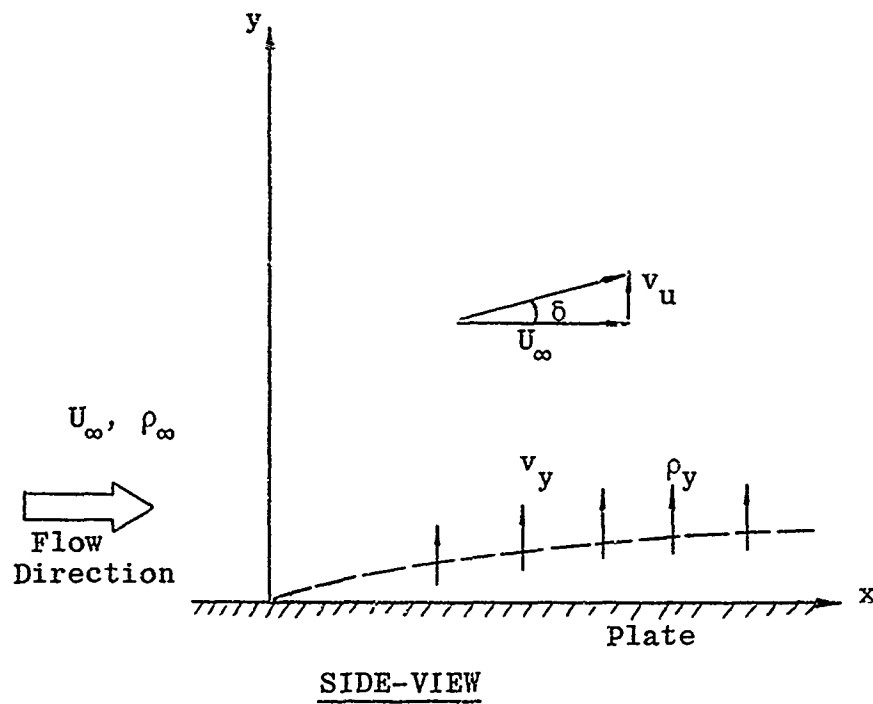


Figure 4. Small Disturbance Due to Uniformly Distributed Source

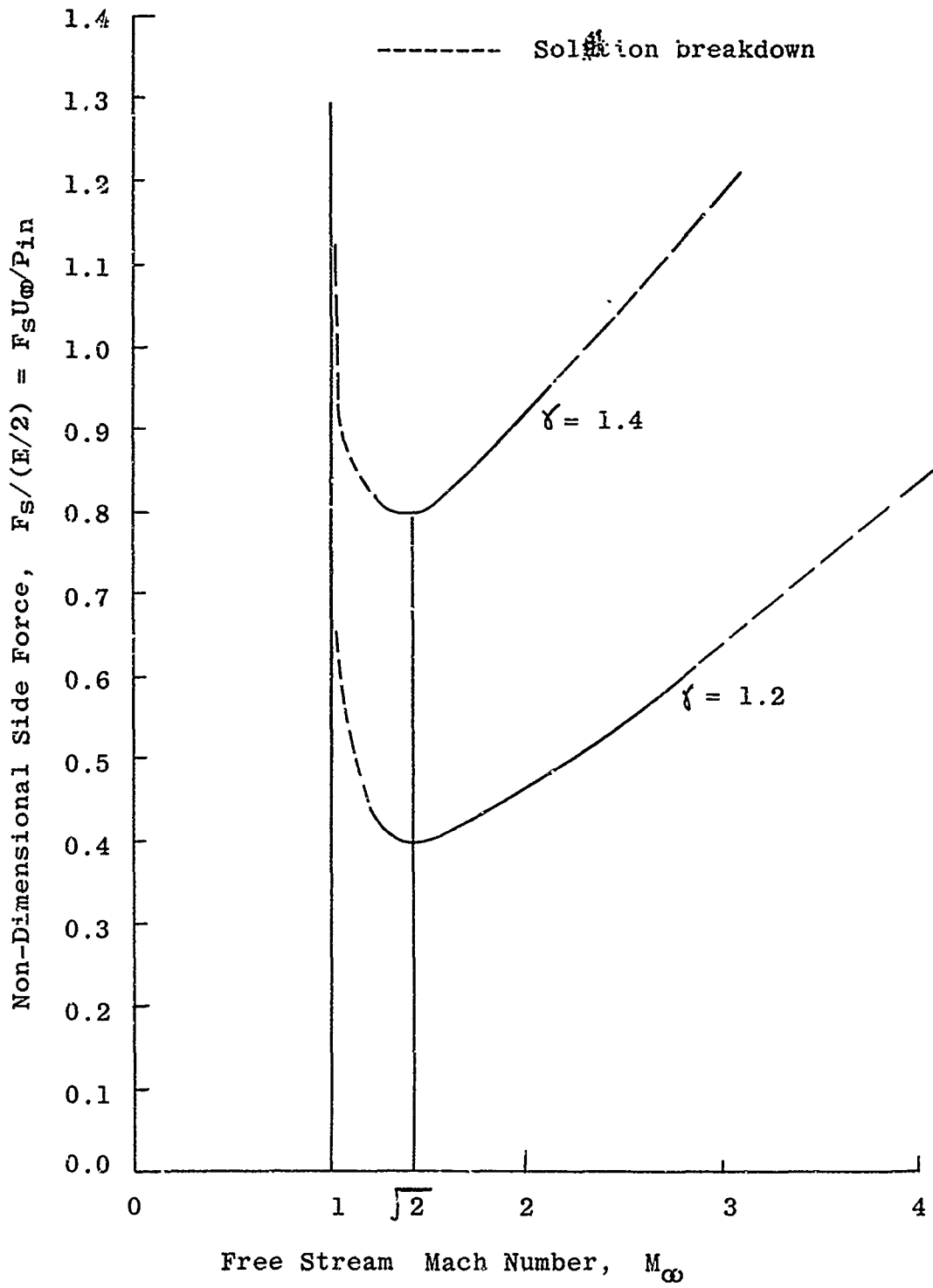


Figure 5. Generated Side Force vs. Free Stream Mach Number by Linearized Theory

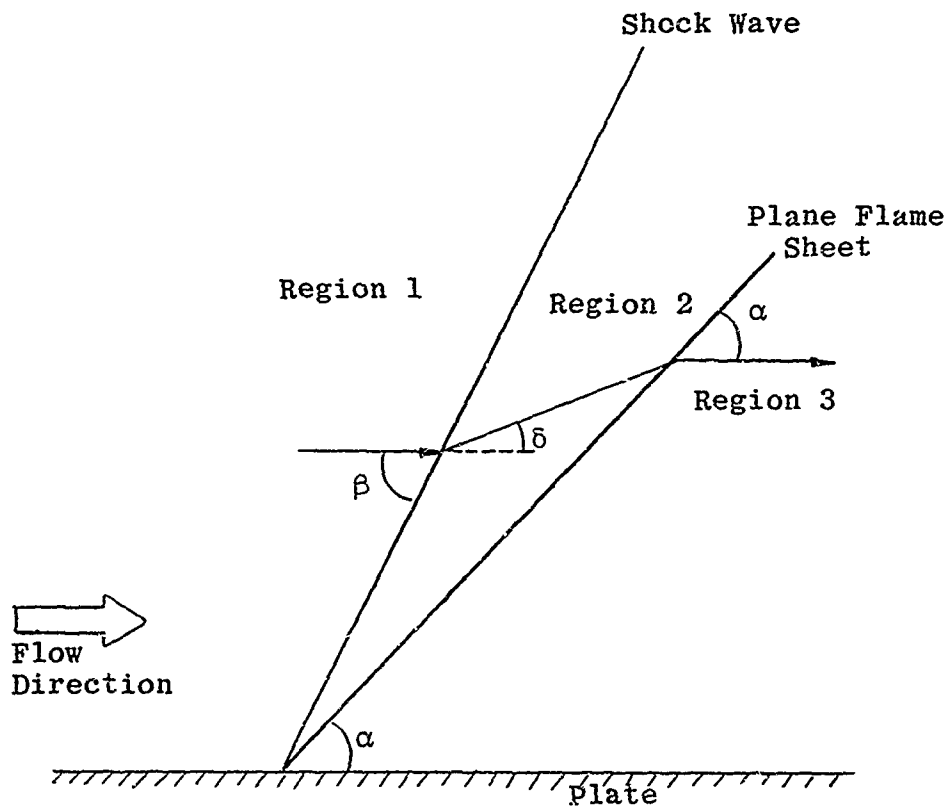


Figure 6. Schematic Drawing of Plane Flame and Shock Wave

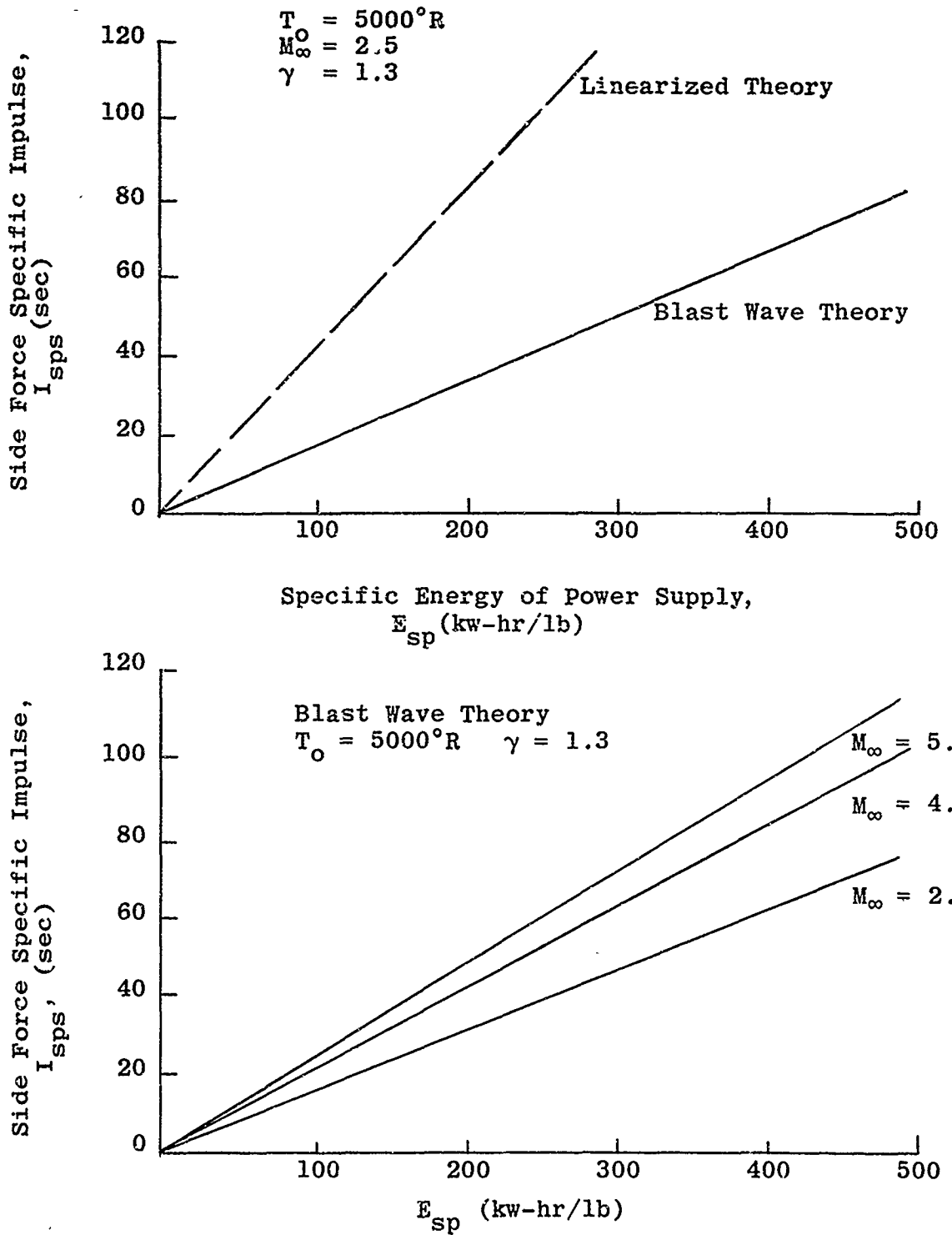


Figure 7. Theoretical Performance of Side Force Specific Impulse

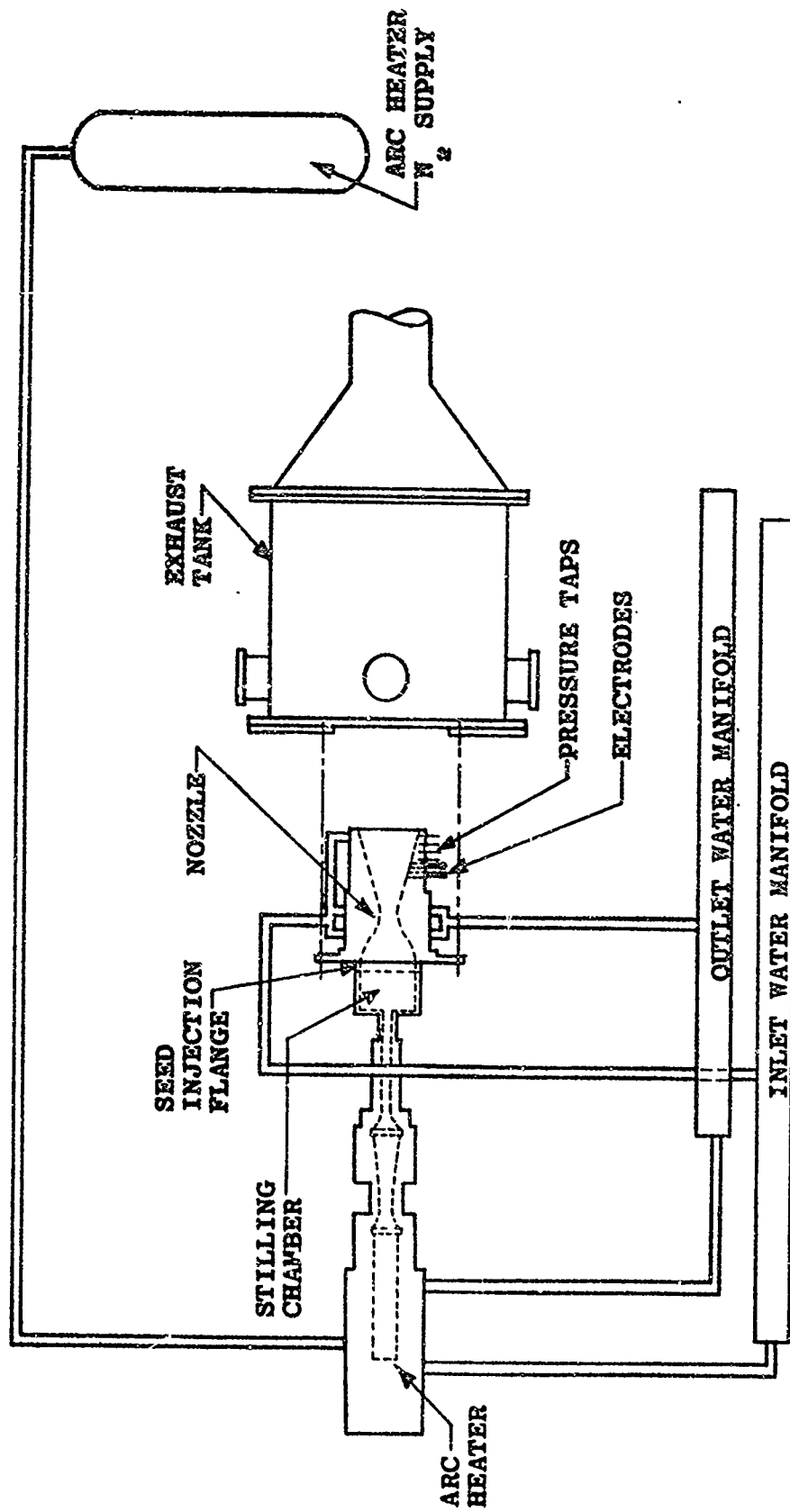


Figure 8 - Schematic Diagram of the Test Set-up

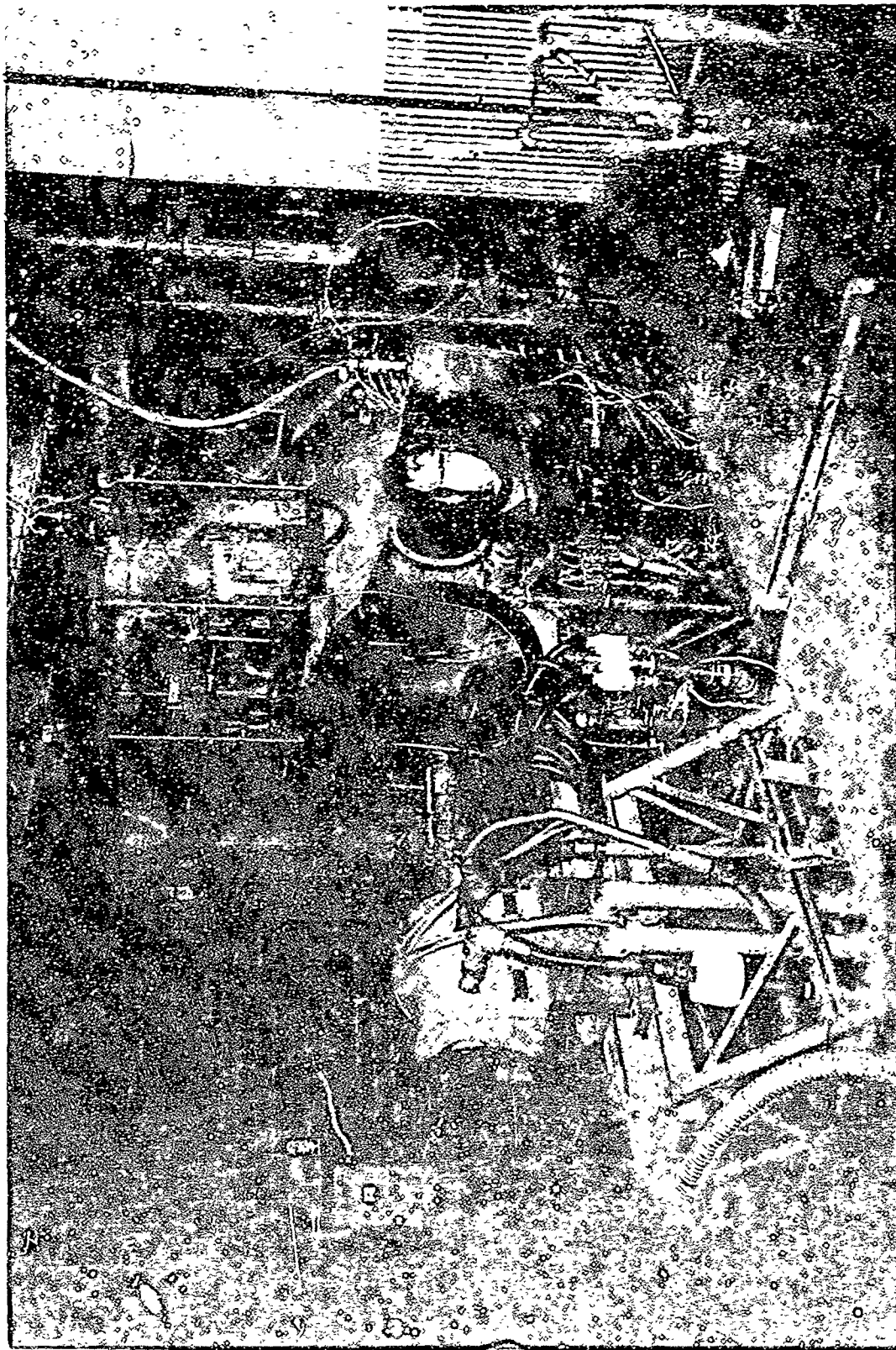
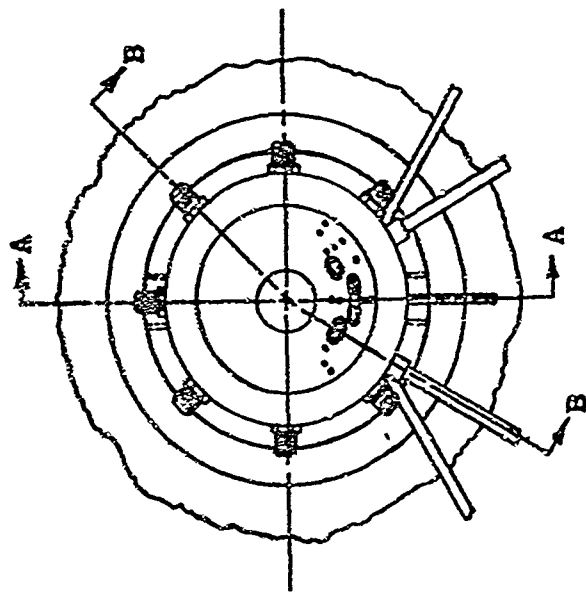
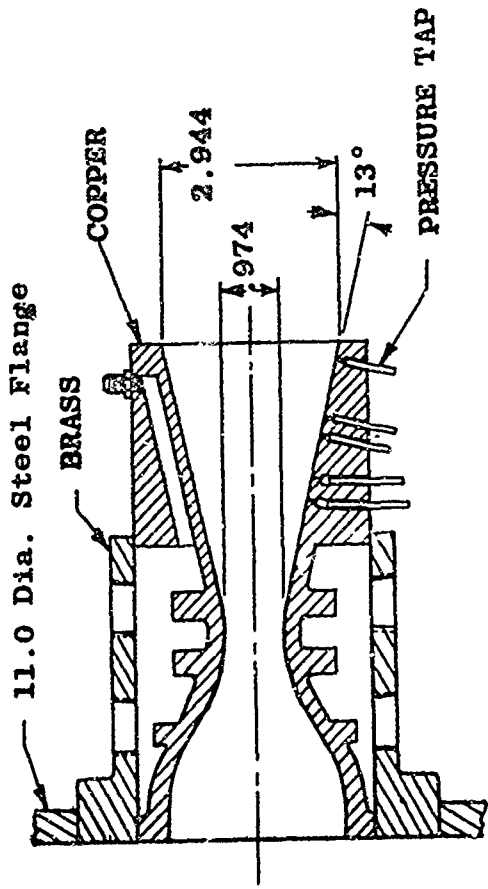


Figure 9 Photograph of the Test Facility

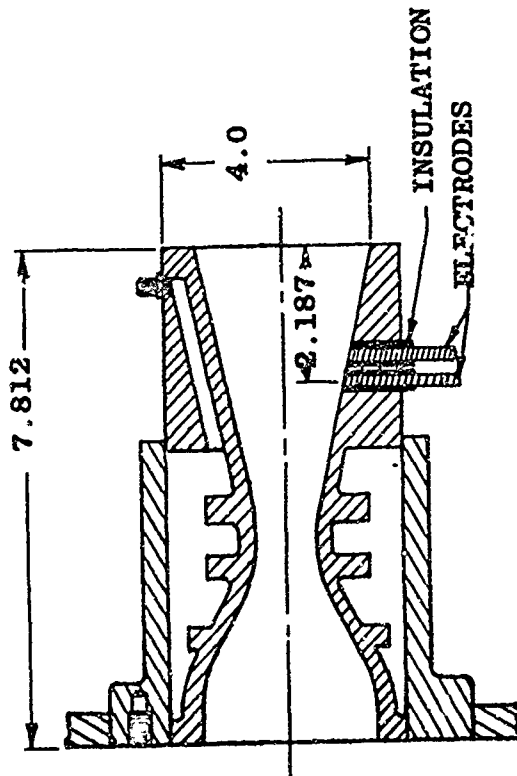


NOTE: All dimensions in inches

SCALE: 1" = 3"



SECTION A-A



SECTION B-B

Figure 10 - Axisymmetrical Water-Cooled Copper Nozzle

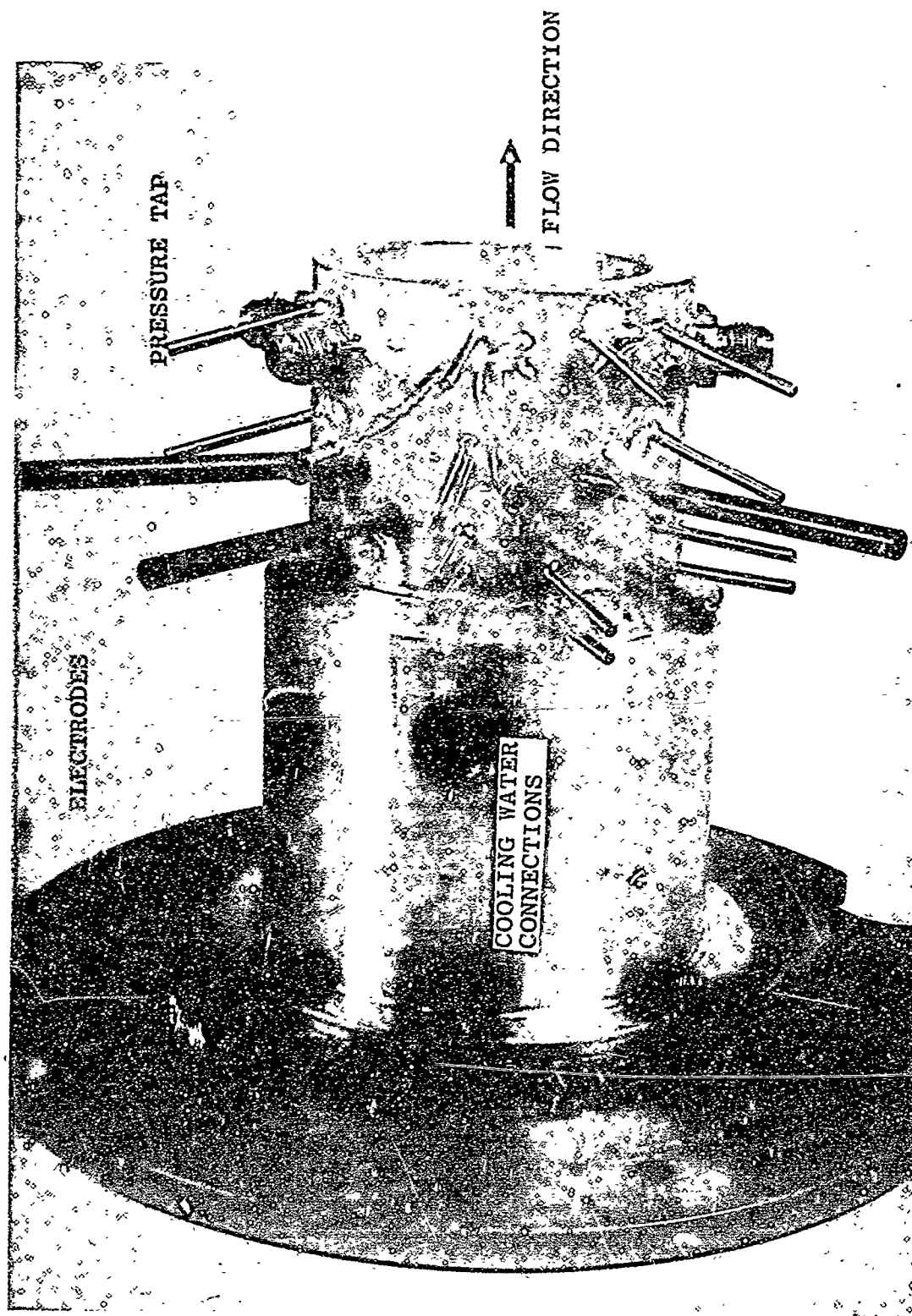


FIGURE 11. SIDE-VIEW OF THE AXISYMMETRIC WATER-COOLED COPPER NOZZLE

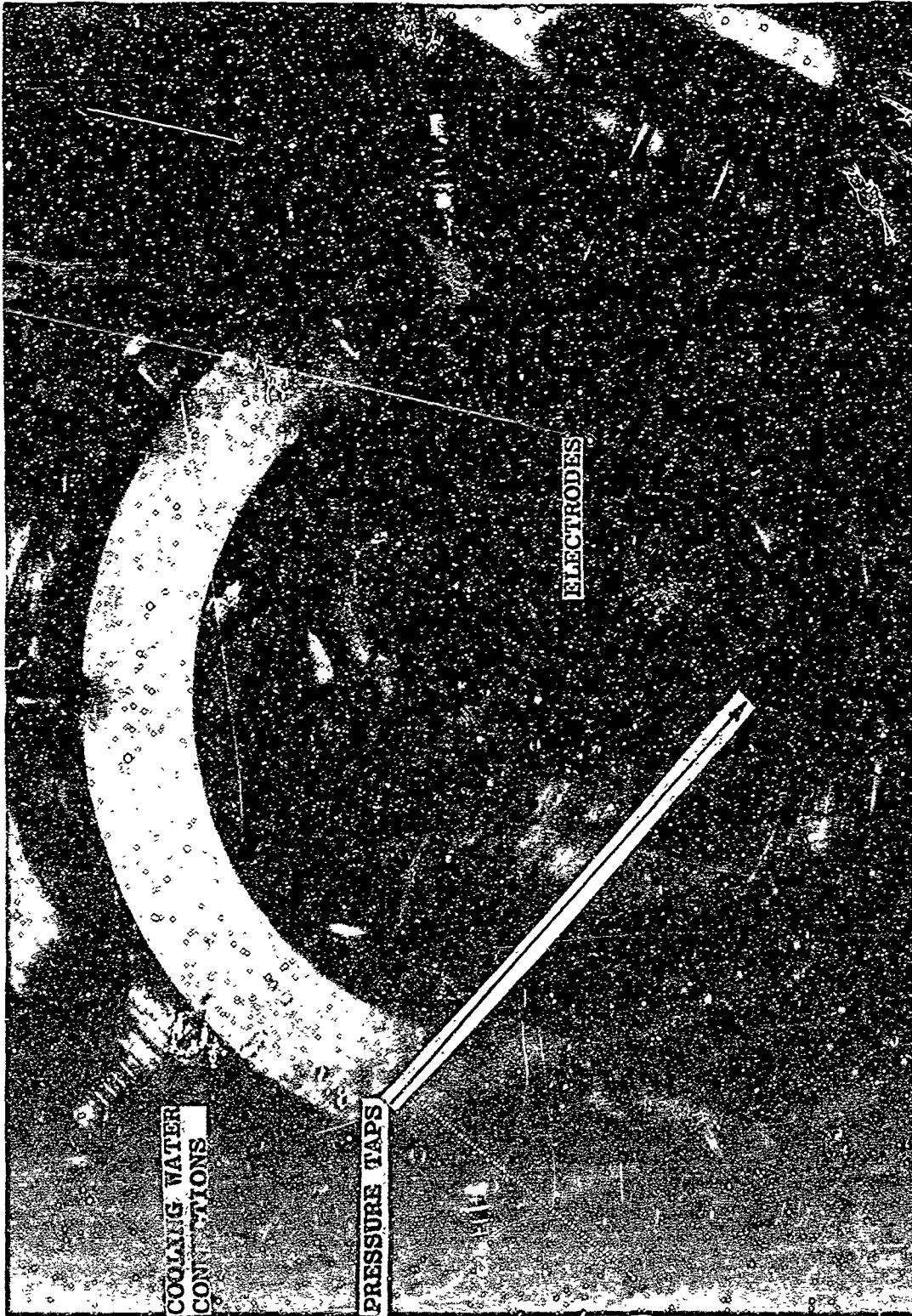


FIGURE 12. END-VIEW OF THE AXISYMMETRIC WATER-COOLED COPPER NOZZLE

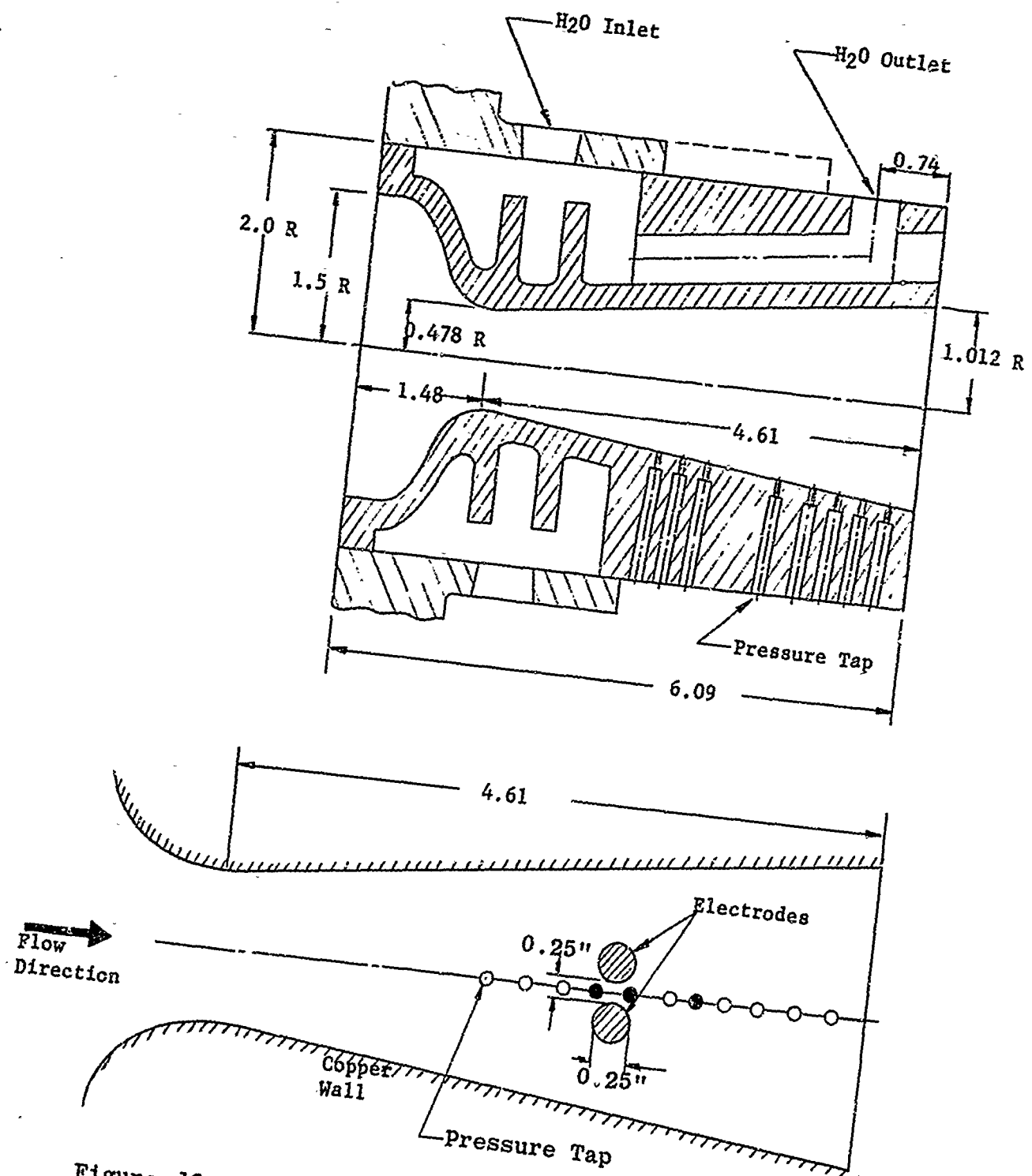


Figure 13. Modified Axisymmetric Water-Cooled Copper Nozzle

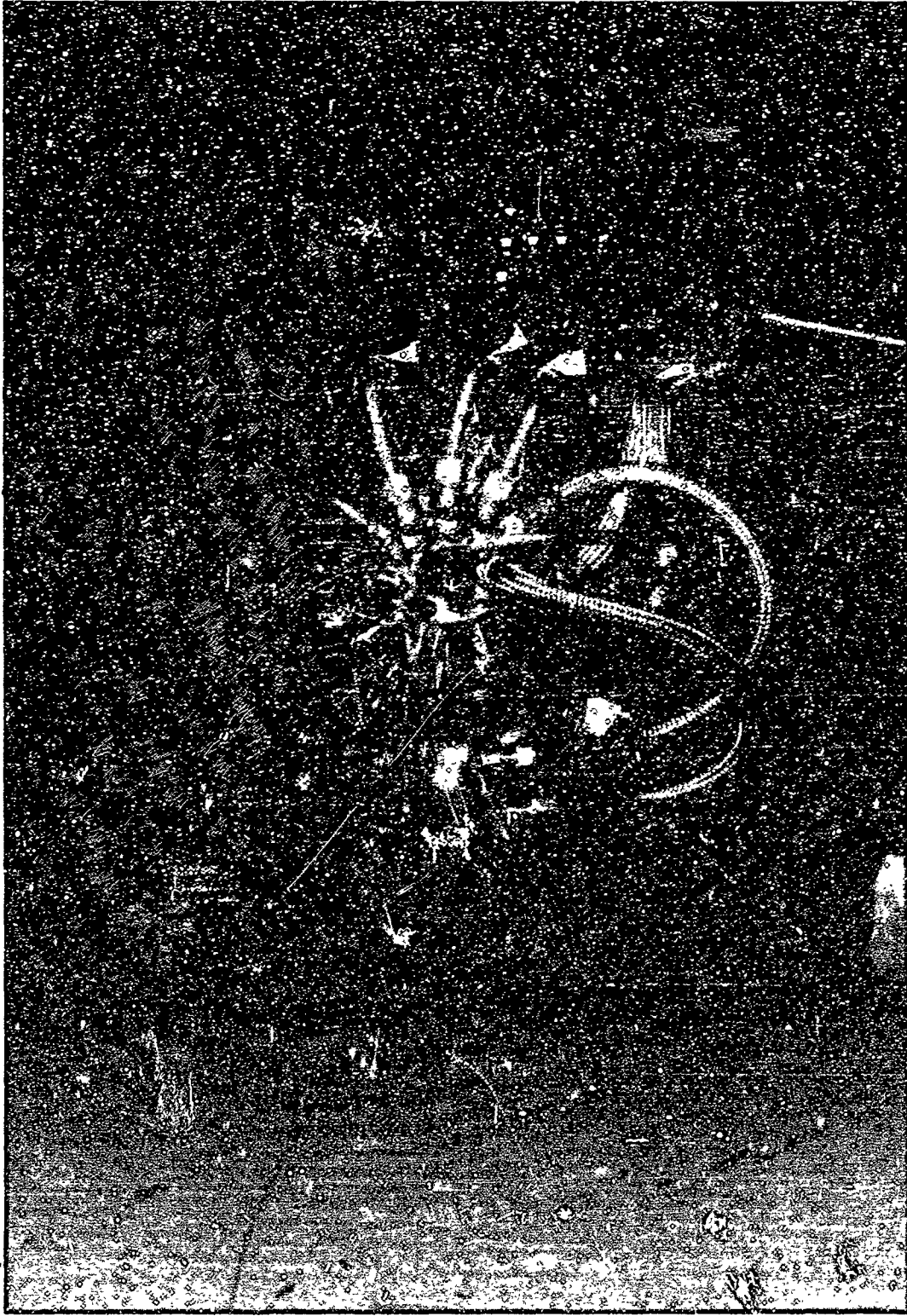


Fig. 14. Assembly of the Modified Axisymmetric Water-Cooled Copper Nozzle

Approved for Release by NSA on 05-08-2014 pursuant to E.O. 13526



Fig. 15. End-View of the Modified Axisymmetric Water-Cooled Copper Nozzle

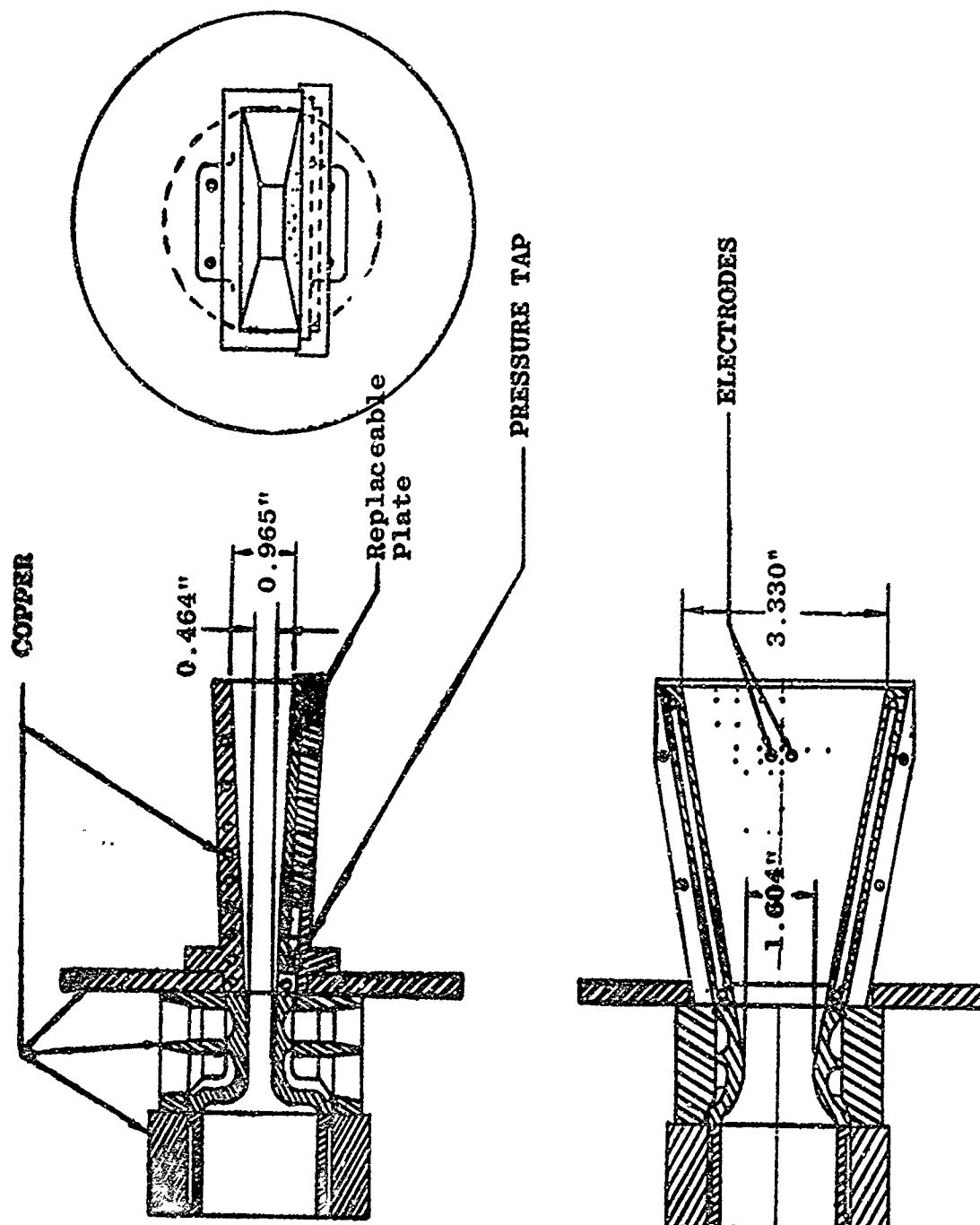


Figure 16. DRAWING OF RECTANGULAR TEST NOZZLE

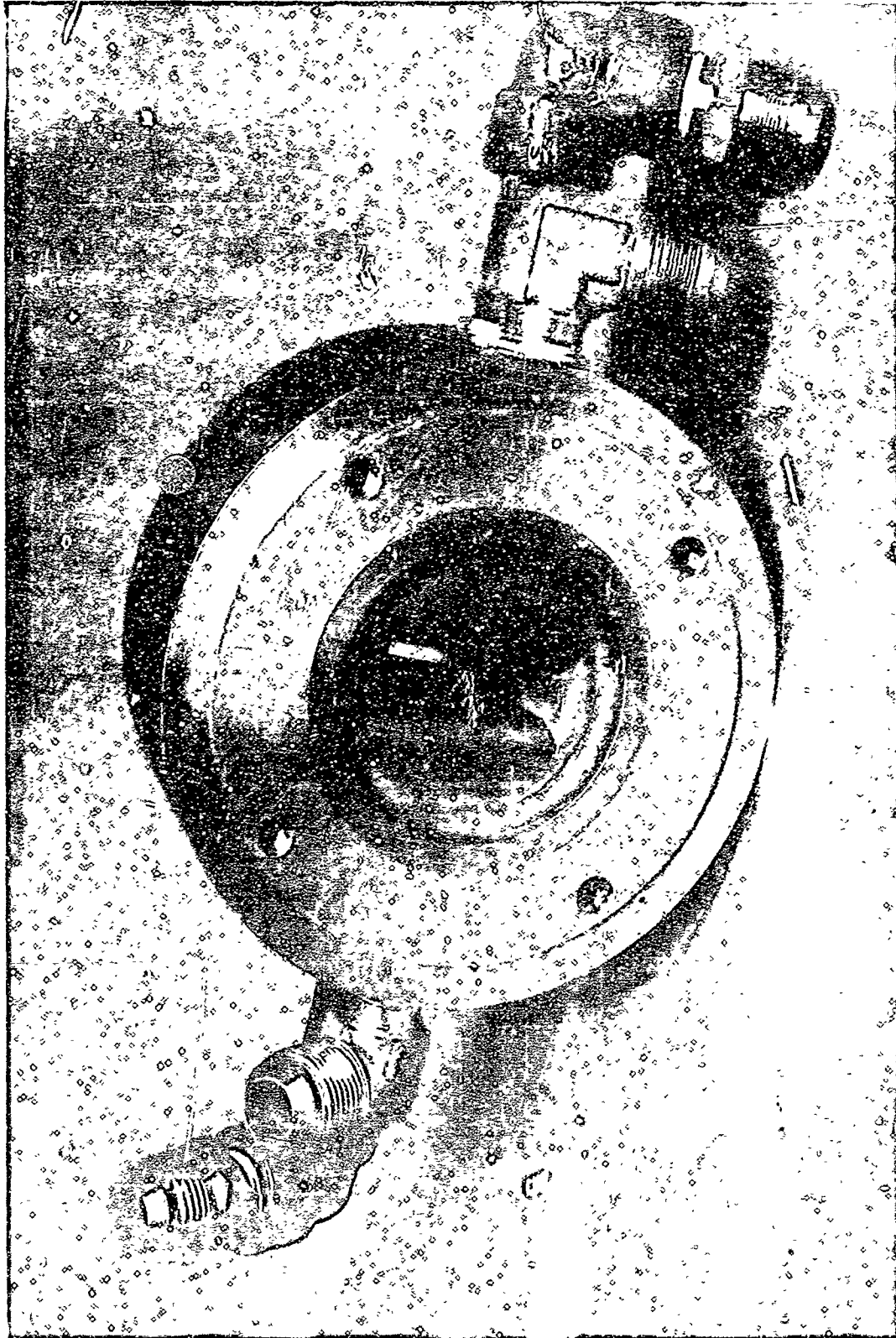


Figure 17. Photograph of the Rectangular Nozzle Throat
(looking downstream)

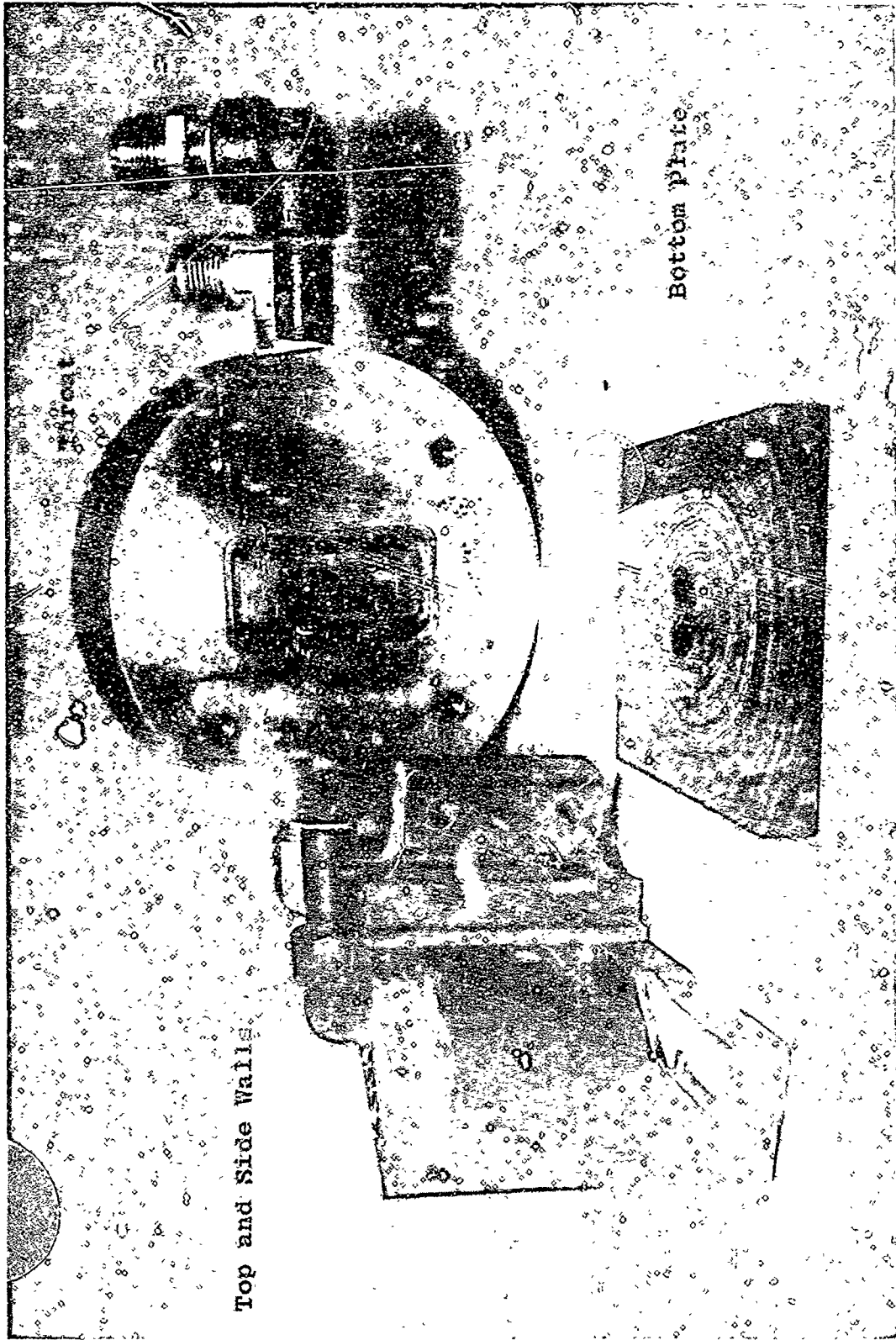


Fig. 18. Parts of the Rectangular Nozzle with Silicon Phenolic Plate
(looking upstream)

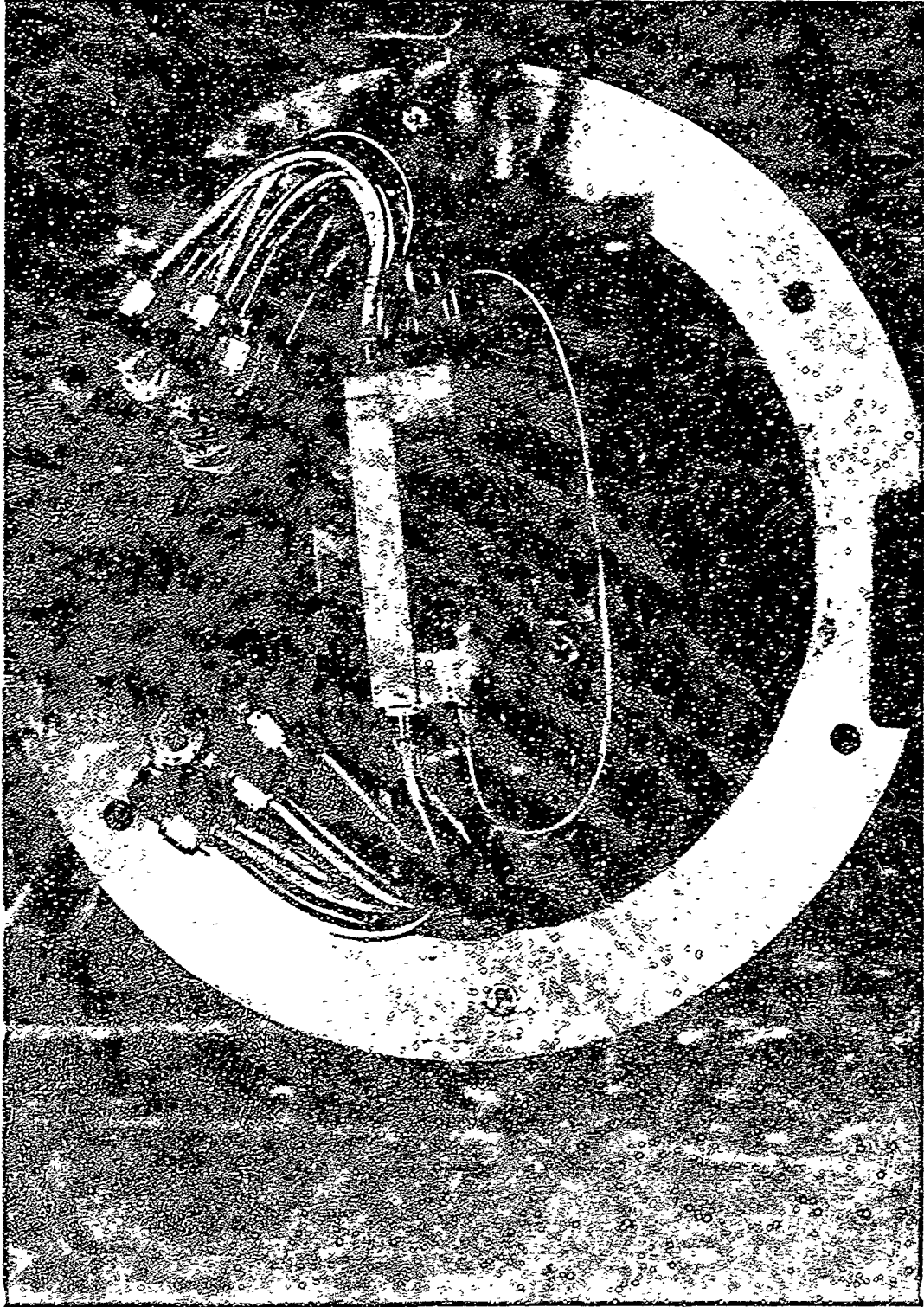


Fig. 19. End-View of the Rectangular Nozzle Assembly with Silicon Phenolic Plate



Fig. 20. Side-View of the Rectangular Nozzle Assembly with Silicon Phenolic Plate

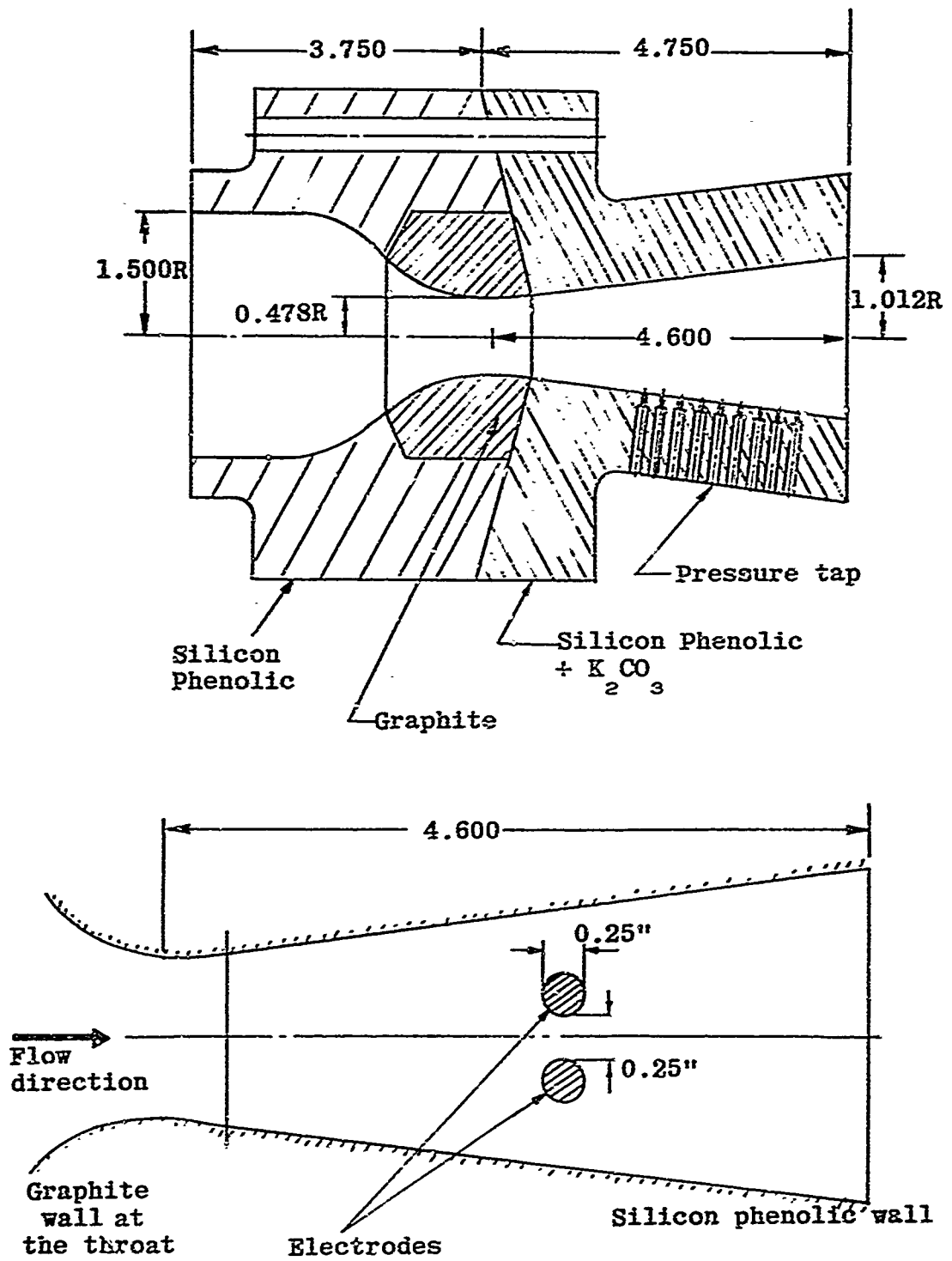


Figure 21. Drawing of Axisymmetric Silicon Phenolic Nozzle



Fig. 22. Side-View of the Axisymmetric Silicon Phenolic Nozzle

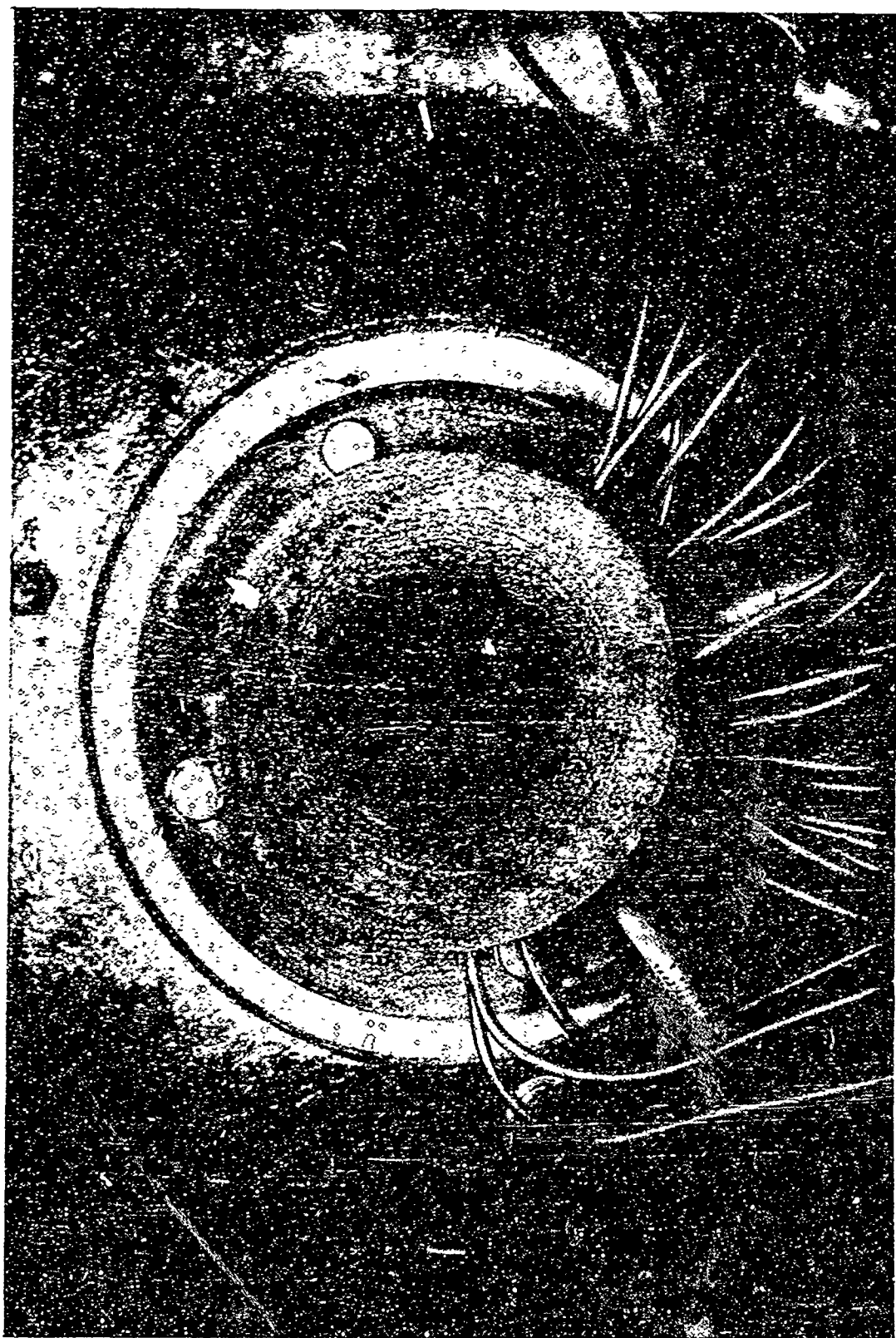


Fig. 23. End-View of the Axisymmetric Silicon Phenolic Nozzle

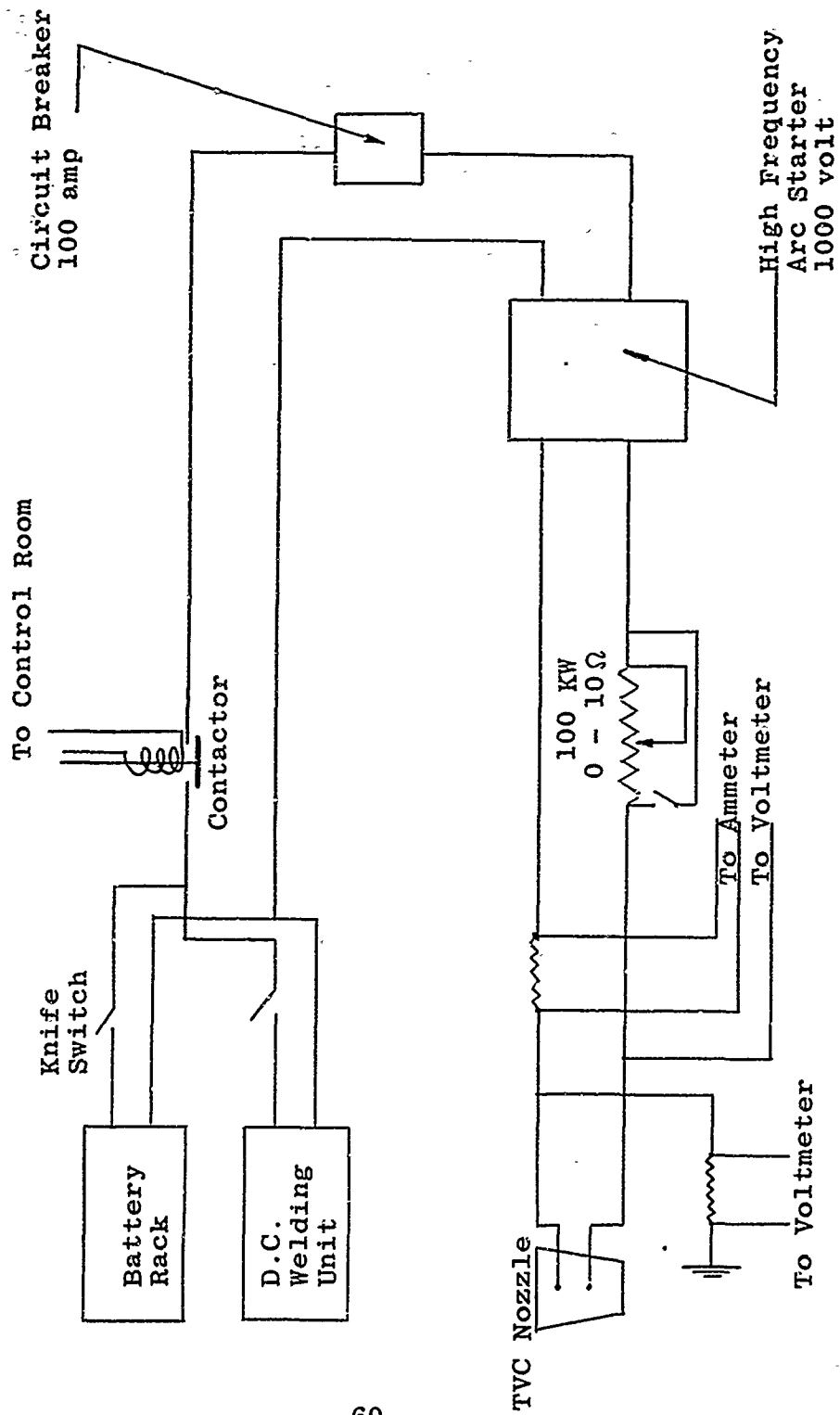


Figure 24. Electrode Electrical System Schematic

SYMBOLS

- = Axisymmetric water-cooled copper nozzle
- △ = Rectangular nozzle with copper plate
- = Modified axisymmetric water-cooled copper nozzle
- = Axisymmetric silicon phenolic nozzle
- ▲ = Rectangular nozzle with silicon phenolic plate

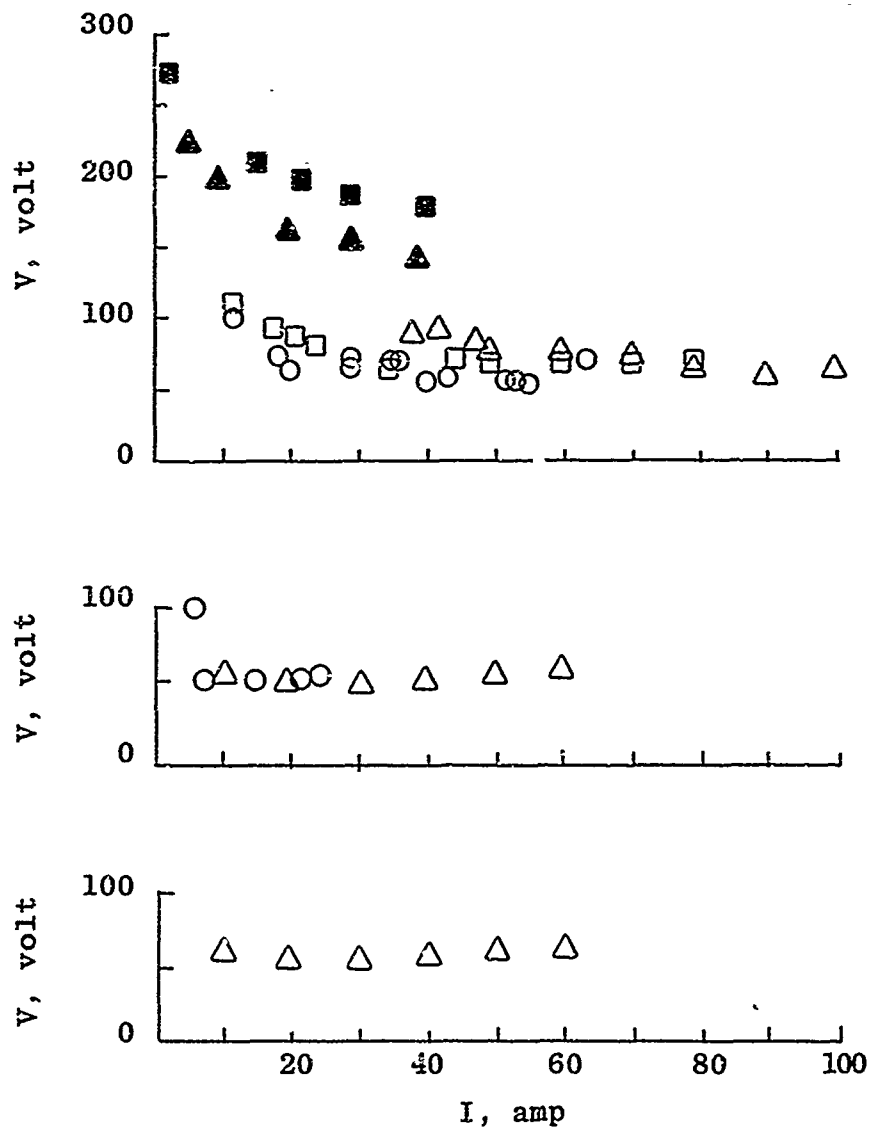


Figure 25. Measured Arc Characteristic

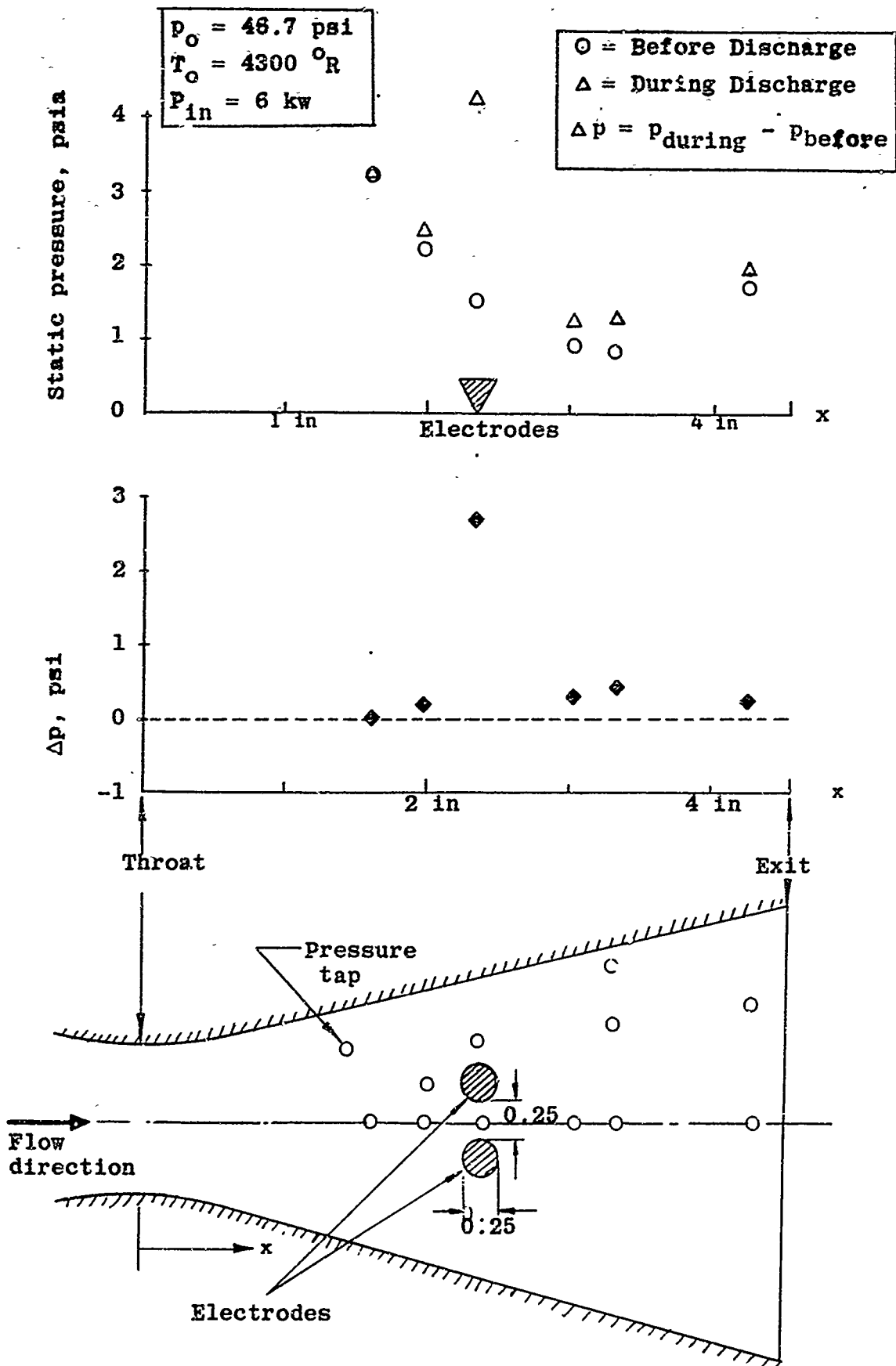


Figure 26. Pressure Distributions along Nozzle Center Line
 (Axisym. Copper Nozzle Cross-Flow Electrodes,
 0.25 in. apart)

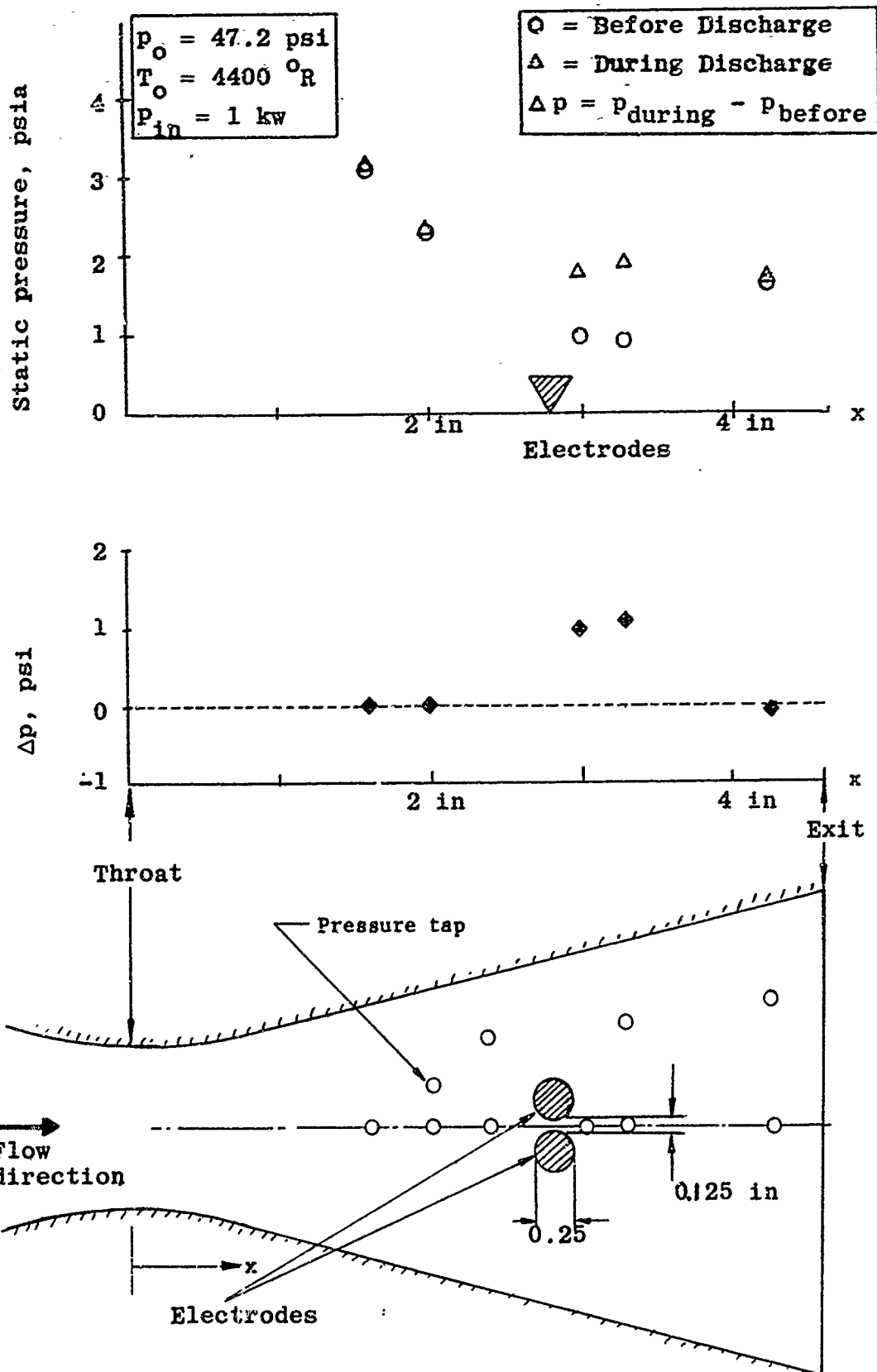


Figure 27. Pressure Distributions along Nozzle Center Line (Axisym. Copper Nozzle Cross-Flow Electrodes, 0.125 in. apart)

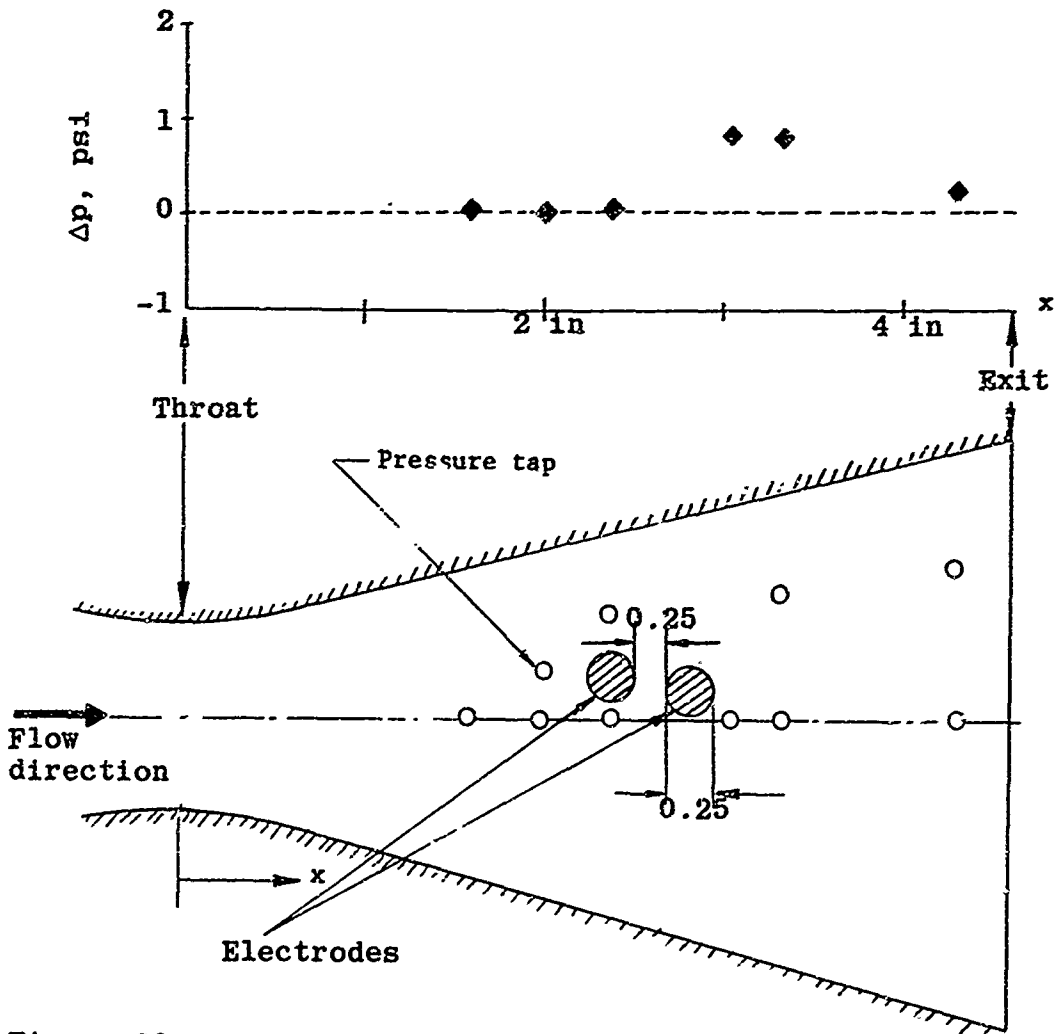
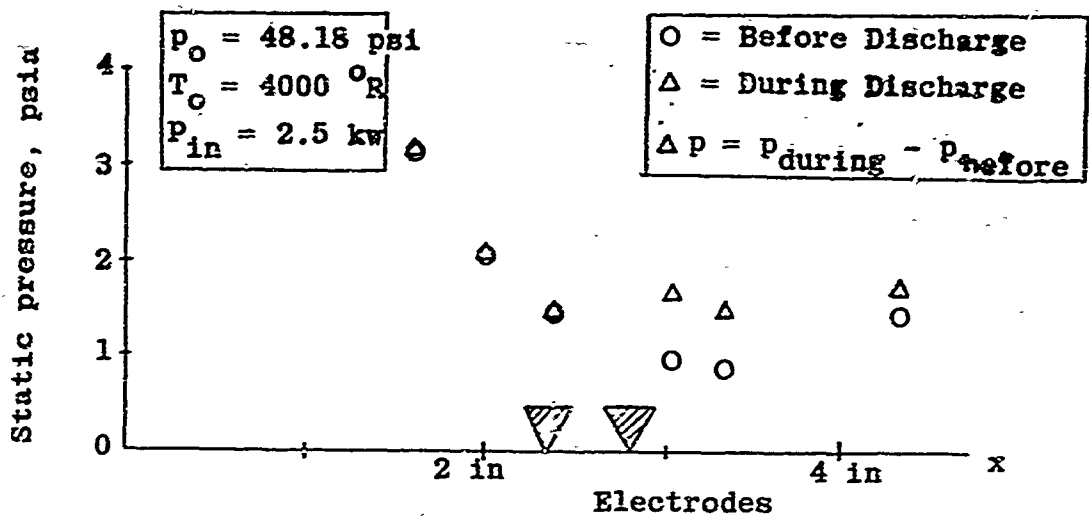


Figure 28. Pressure Distributions along Nozzle Center Line
 (Axisym. Copper Nozzle Parallel-Flow Electrodes,
 0.25 in. apart)



FIGURE 29. POST-DISCHARGE OF THE AXISYMMETRIC COPPER NOZZLE

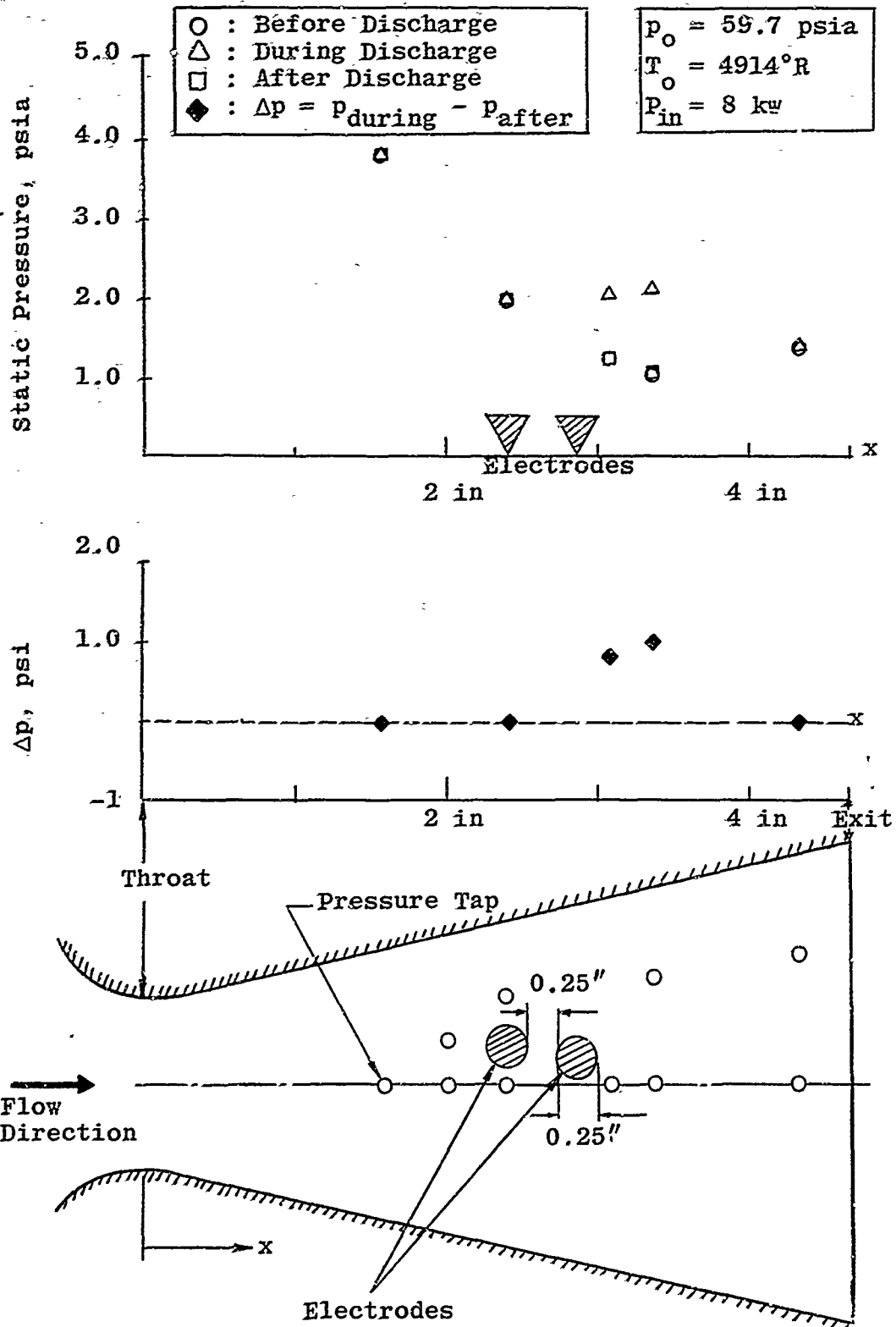


Figure 30. Pressure Distributions Along Nozzle Centerline (Axisymmetric Nozzle; 0.25 in. apart with K_2CO_3 Seedings and Boron Nitride Insulations)

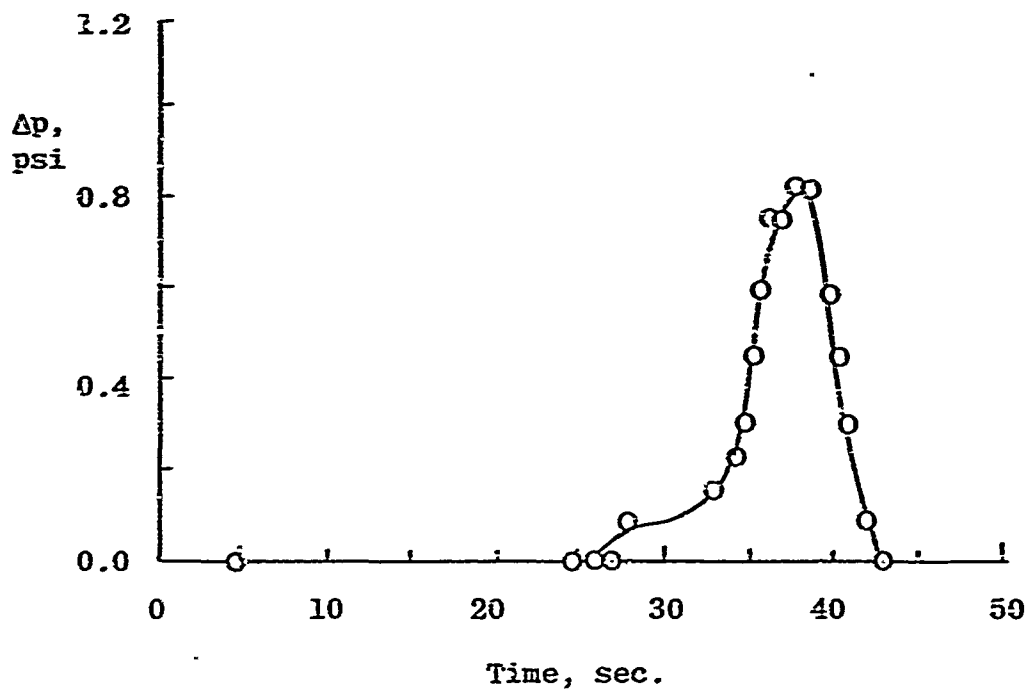
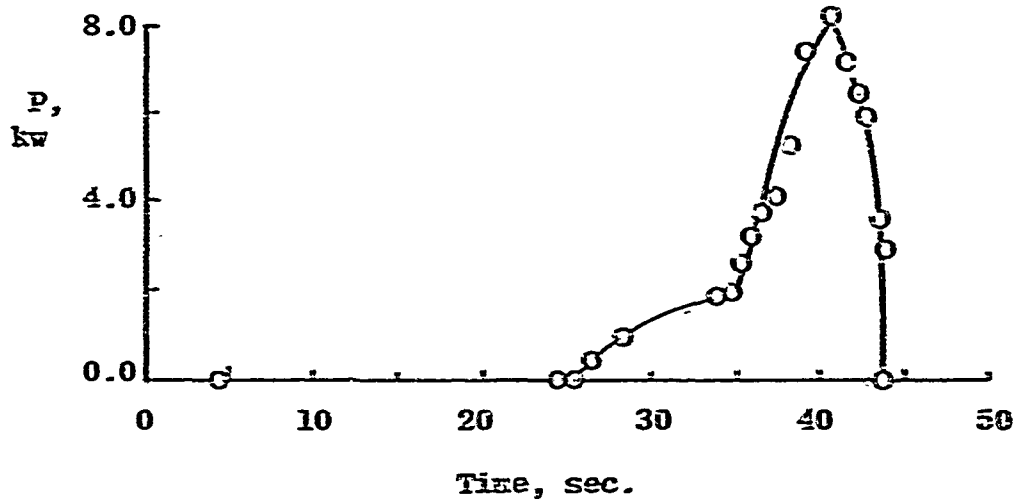


Figure 31. Variations of Pressure Rise and Power Input as a Function of Time

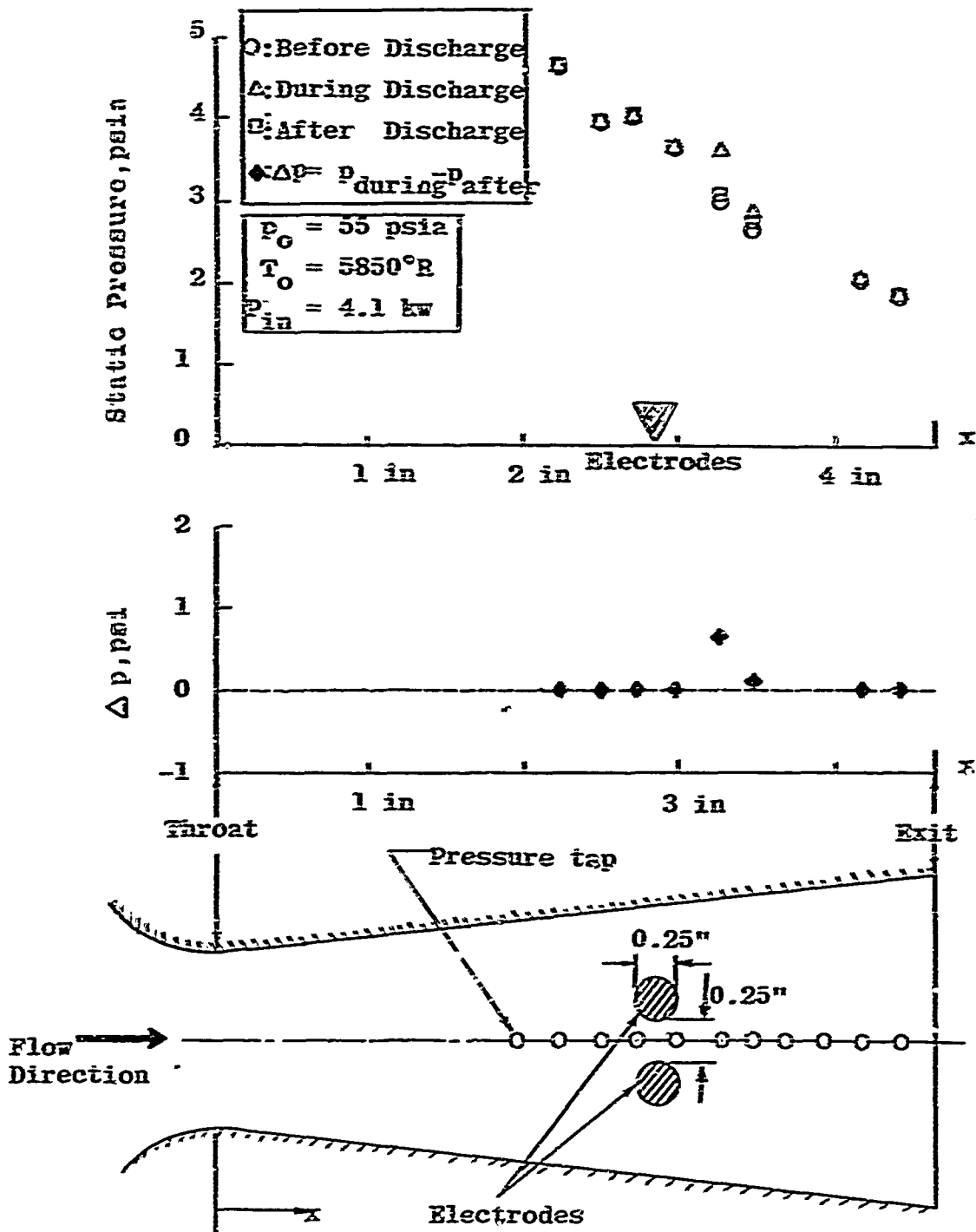


Figure 32. Pressure Distributions along Nozzle Center-line
 (Modified Axisymmetric Copper Nozzle, Cross-flow,
 0.25 inches apart) 68

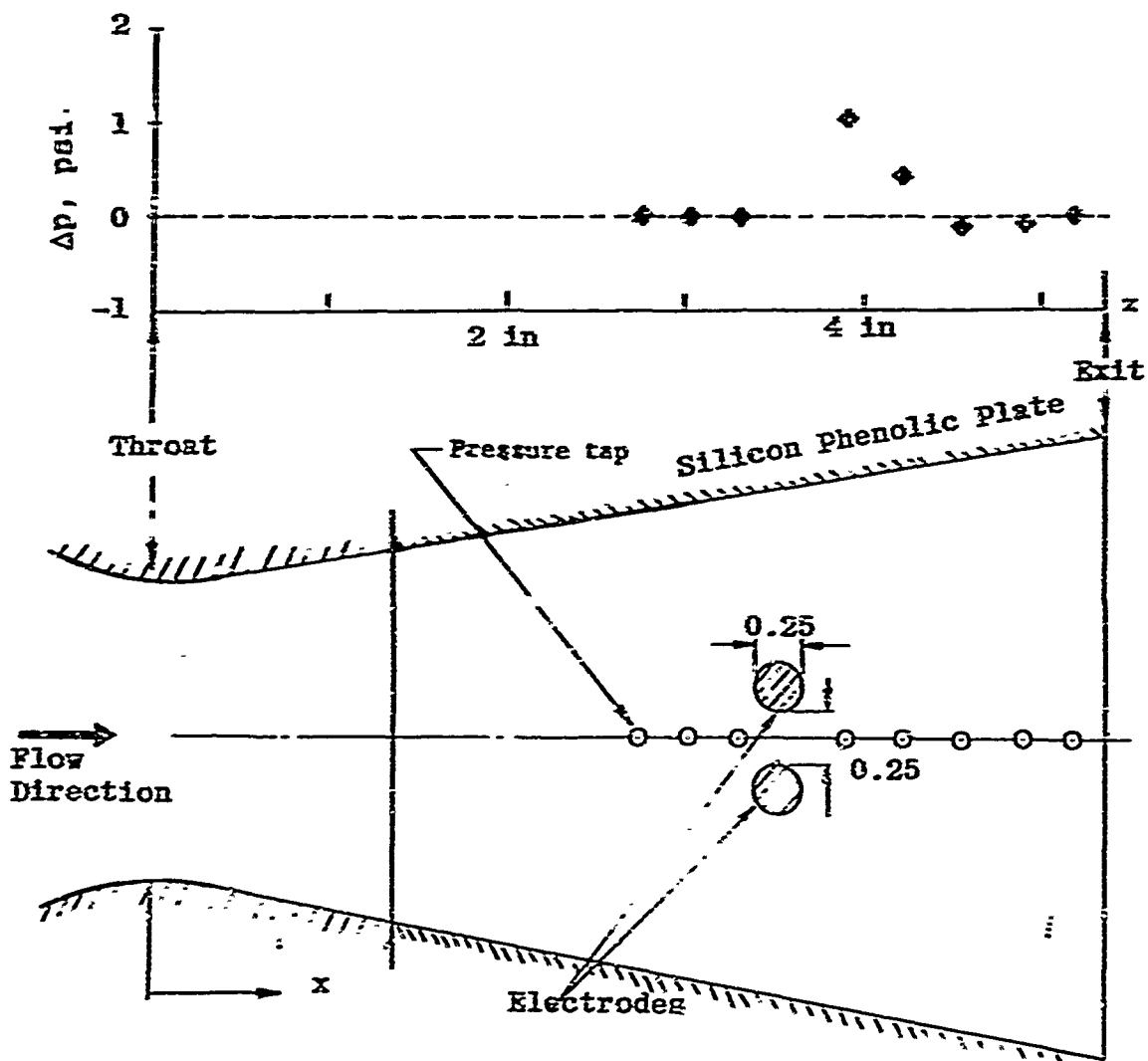
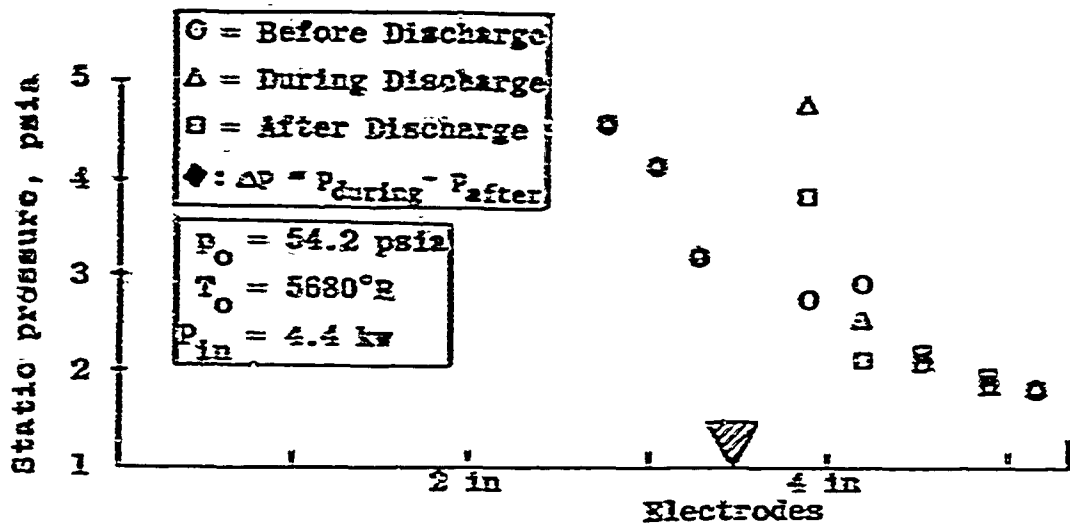
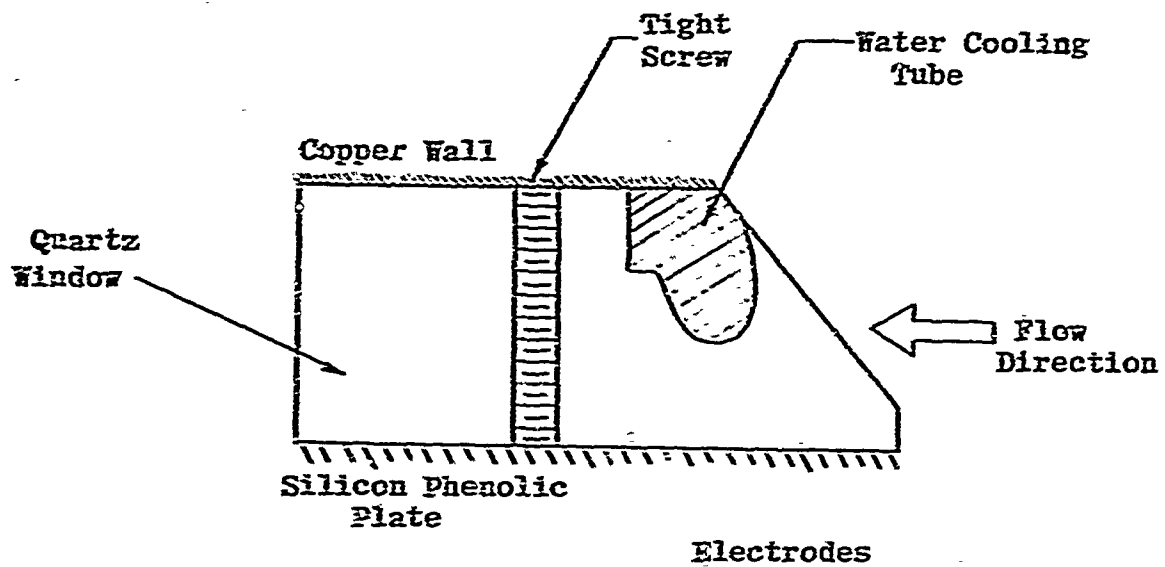
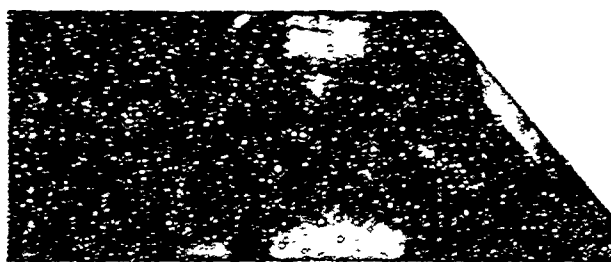


Figure 33. Pressure Distributions along Nozzle Center-Line (Rectangular Nozzle with Silicon Phenolic Plate, Cross-Flow, 0.25 in. apart)



Mach No. = 2.5, Nitrogen Flow Only



Electric Arc and Flow Field Interaction

Figure 34. Flow Field Disturbance Visualization



FIGURE 35 POST-DISCHARGE OF THE RECTANGULAR NOZZLE (CROSS-FLOW,
SILICON PHENOLIC PLATE)

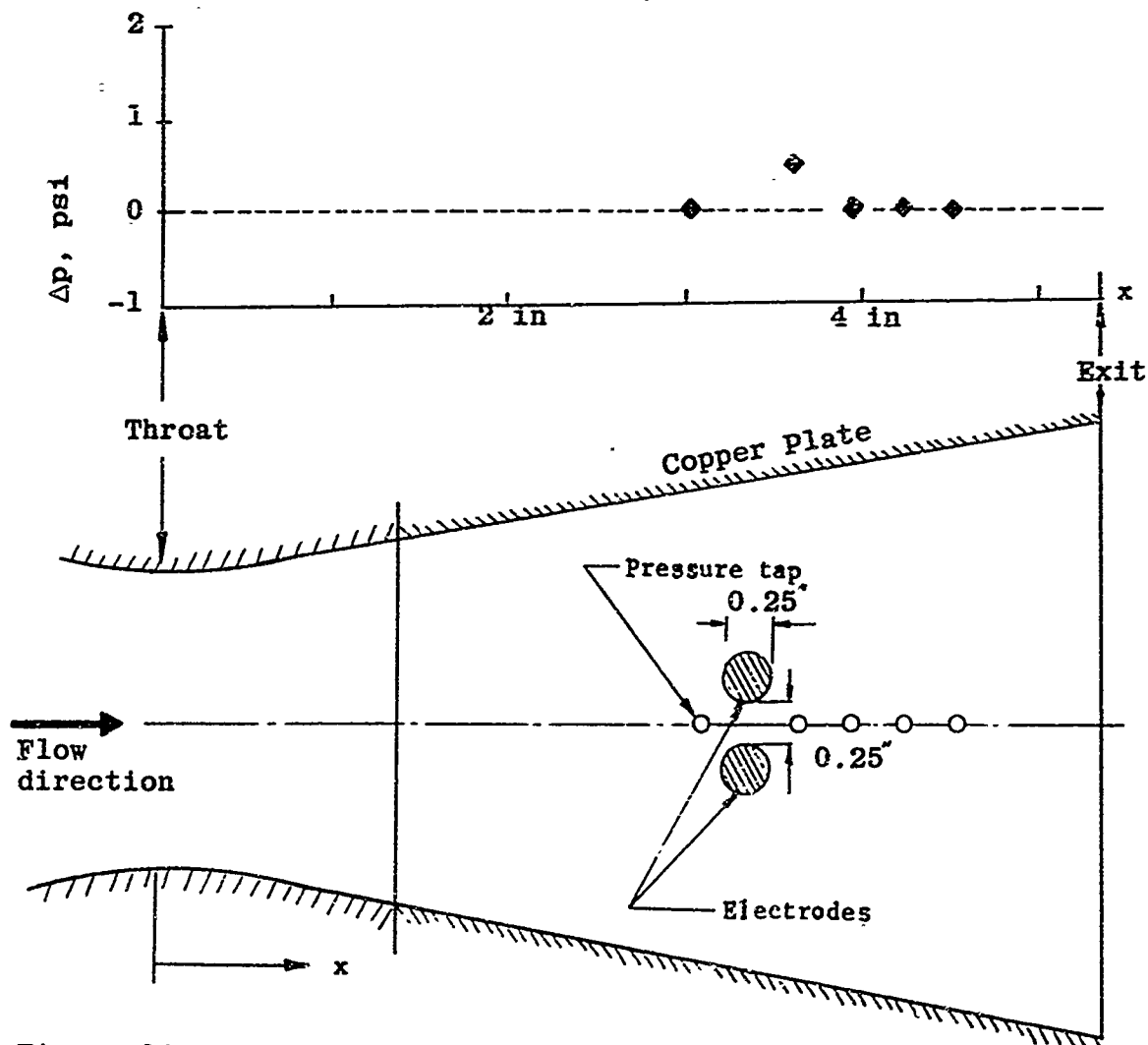
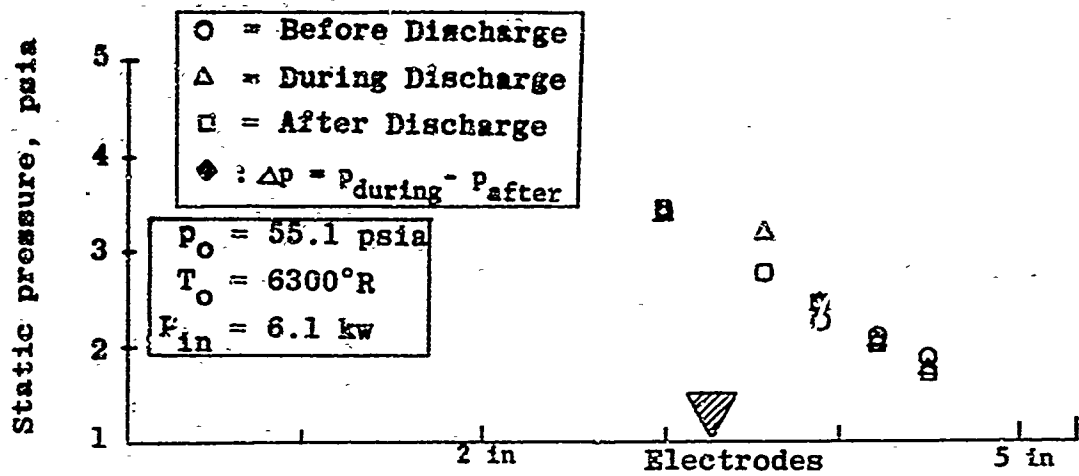


Figure 36. Pressure Distributions along Nozzle Center Line
 (Rectangular Nozzle with Copper Plate, Cross-Flow
 Electrodes, 0.25 in. apart)



FIGURE 37 POST-DISCHARGE OF THE RECTANGULAR NOZZLE (CROSS-FLOW,
COPPER PLATE)

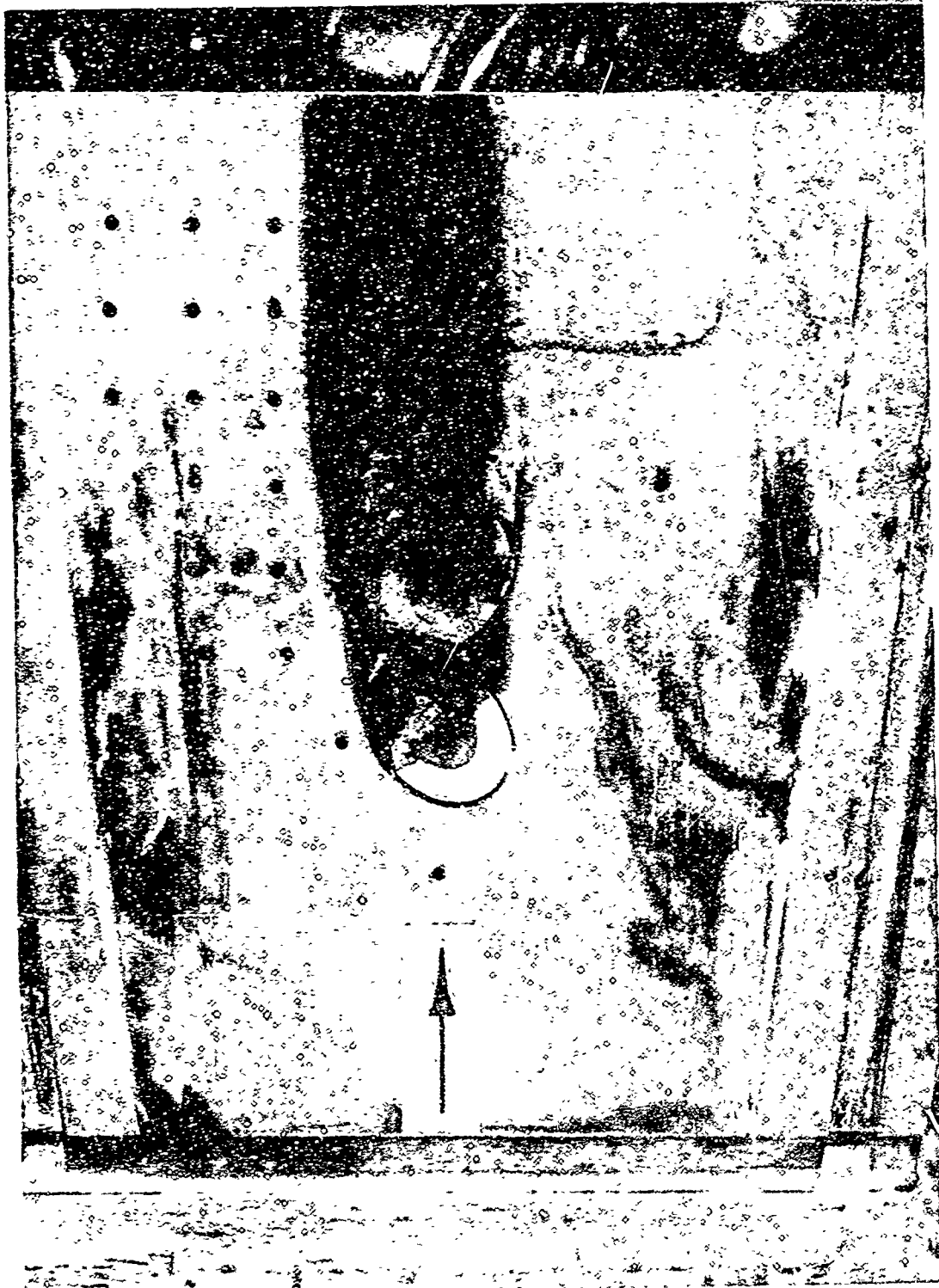


FIGURE 38 POST-DISCHARGE OF THE RECTANGULAR NOZZLE (PARALLEL-FLOW,
COPPER PLATE)

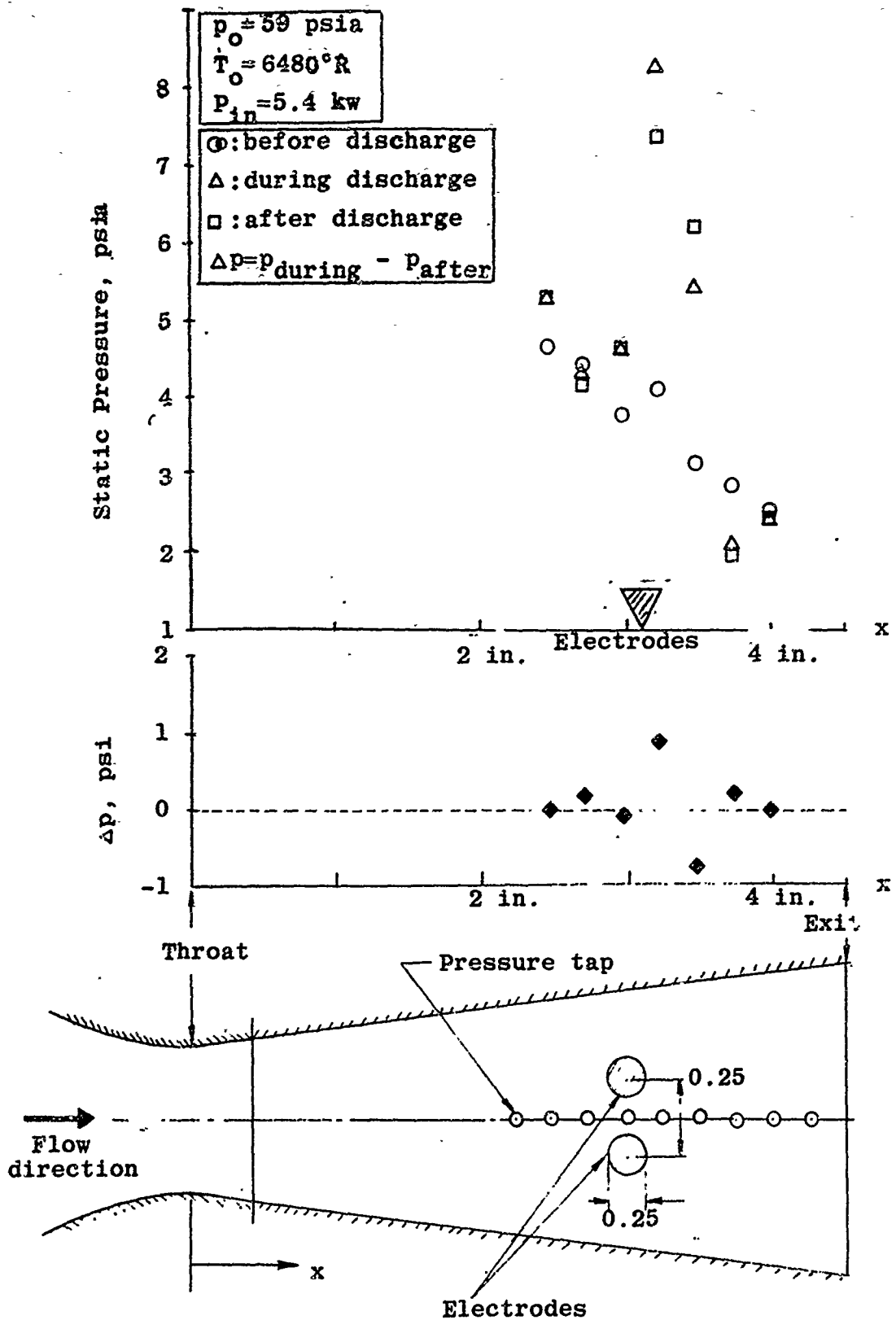
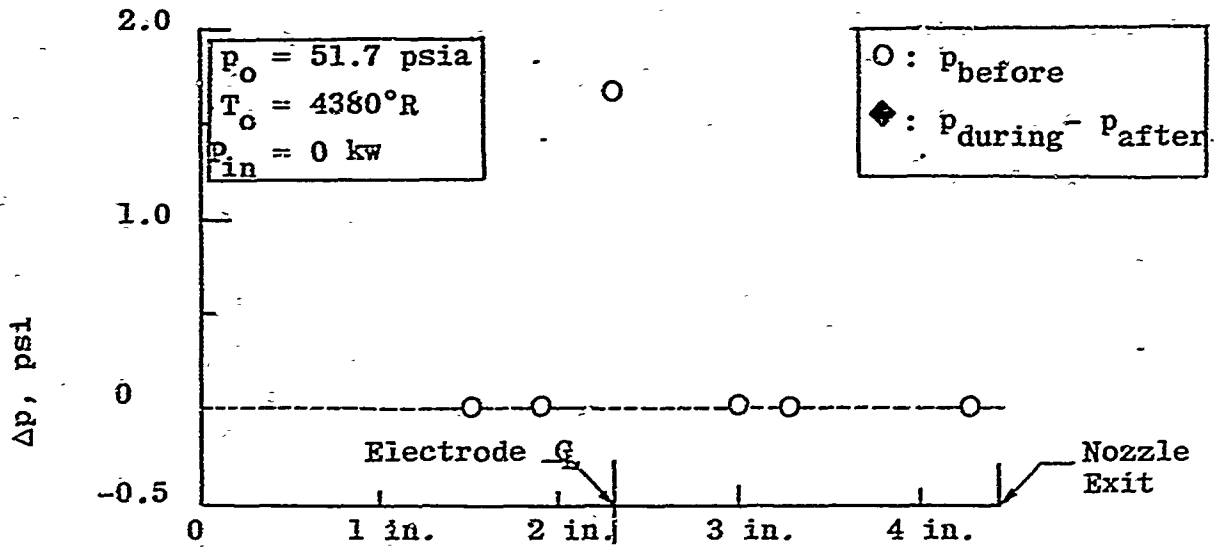


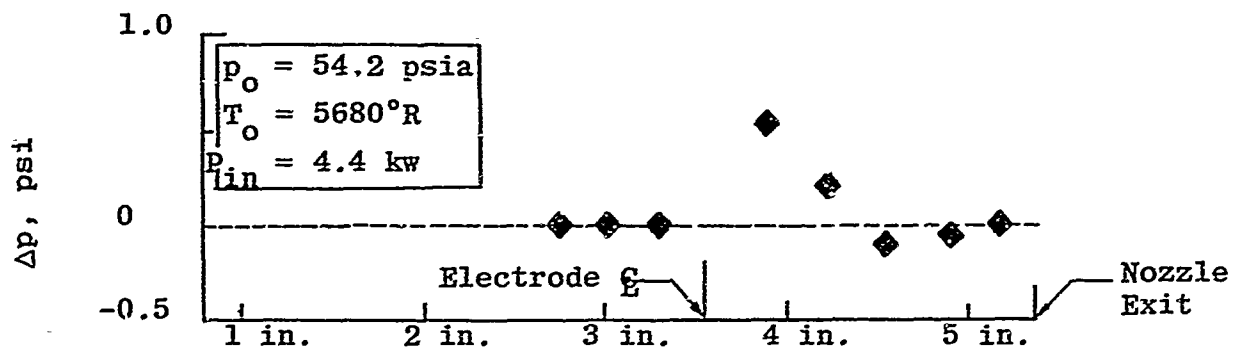
Figure 39. Pressure Distributions along Center Line of the Axisymmetric Silicon Phenolic Nozzle



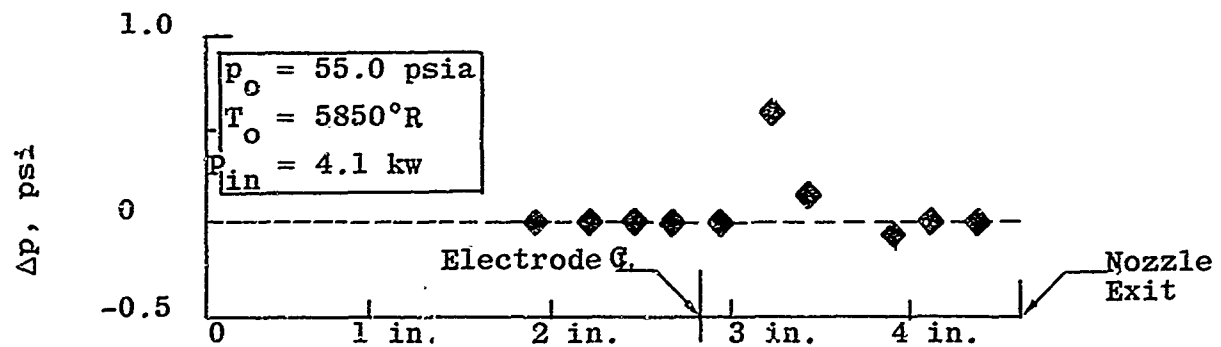
FIGURE 40. POST-DISCHARGE OF THE AXISYMMETRIC SILICON PHENOLIC NOZZLE



a. Axisymmetric Copper Nozzle with Electrodes Protruding 0.06 inches



b. Rectangular Nozzle with Silicon Phenolic Plate



c. Modified Axisymmetric Copper Nozzle

Figure 41. Pressure Rise due to Different Methods of Flow Disturbances

APPENDIX I

DISCUSSION ON "ANALYSIS OF THE FLUID MECHANICS OF
SECONDARY INJECTION FOR THRUST VECTOR CONTROL,"
BY BROADWELL

Broadwell (Ref. 4) demonstrated that the blast wave analogy can be employed in explaining and predicting the side force by the secondary mass injection thrust vector control. He successfully derived the side force expression by integrating the pressure differential, obtained by the blast wave theory, over the affected area and resulted in

$$F_s = \sigma(\gamma) E M_\infty \quad (1)$$

Obviously, to our study, the line energy source E is contributed by the rate of thermal energy addition Q or equivalent to the electrical power input P_{in} only. The relation of E to P_{in} has been discussed in detail in the main text. In case of secondary mass injection, Broadwell related E to the drag force caused by the secondary fluid injection which is analogous to the derivation originated in Lees' paper (Ref. 16). Lees argued that in order to hold a blunt-nosed body in a hypersonic stream, it is necessary to apply a drag force. This drag force then can be shown equivalent to the line energy source in the cylindrical blast wave case.

The linearized small disturbance theory was employed by Wu, Chapkis and Mager (Ref. 2) in determining the side force generated by the slot type secondary fluid injection. The theoretical prediction yields good agreement with experimental results. However, Broadwell (Ref. 4) stated that the linearized disturbance theory implicitly included the mass source entering the free stream with an x-component velocity of the same magnitude of the free stream. Then he argued that the initial x-velocity of injectant has to be zero, and added an additional term to the side force equation originally derived in Wu, et al, (Ref. 2). His result is as follows:

$$F_s = \frac{\dot{m}_i u_\infty}{\sqrt{M_\infty^2 - 1}} + \frac{M_\infty \dot{m}_i u_\infty}{\sqrt{M_\infty^2 - 1}} \quad (2)$$

As it may be seen, and also pointed out by himself, that the added second term could be order of magnitude larger than the original first term, since $M_\infty > 1$. Experimental results contradict with this order of magnitude large side force prediction. Furthermore, he claimed that when $M_\infty^2 \gg 1$ the linearized theory with the added term are comparable with the blast wave theory with a volume effect. These two theories are not comparable, because the linearized theory is valid only at moderate Mach number, while the blast wave theory is valid only at hypersonic conditions.

In fact, the mass enters the main stream with zero x-component of velocity relative to the surface. This mass injection disturbs the main flow. It is a false statement to assume the flow enters with x-component velocity of u_∞ , and then "make" the x-component to be zero. The small disturbance theory is derived under the assumption that the uniform velocity is much larger than the disturbance velocity. This is somewhat different from the blast wave theory, because the blast wave theory was originally derived from the case of a quiescent ambient atmosphere. Therefore, in order to use the blast wave theory in a steady flow stream, a superposition of the same magnitude of the free stream velocity to the disturbance source is required.

Therefore, it can be concluded that the second term of the right-hand side of Equation 2 should not be included.

APPENDIX II

WILLMARTH'S HEAT AND MASS ANALOGY

In this Appendix we are going to outline briefly Willmarth's analysis of the heat source, mass source and body force analogy in supersonic flow by small disturbance theory.

The governing equations of motion, including mass source, body force and heat addition, neglecting viscosity and heat conduction, can be written as follows:

$$\frac{\partial \rho}{\partial t} + \nabla \cdot (\rho \vec{W}) = \dot{n} (x, y, z, t) \quad (1)$$

$$\rho \frac{\partial \vec{W}}{\partial t} = - \nabla p + \vec{f} (x, y, z, t) \quad (2)$$

$$\frac{DS}{Dt} = \frac{C_v (\gamma - 1)}{p} \dot{q} (x, y, z, t) \quad (3)$$

where \vec{W} = velocity vector
S = entropy of the flow
 \dot{n} = fluid source strength, mass/sec/volume
f = body force/volume
 \dot{q} = heat source strength, ft-lb/sec/volume

And, in addition, we assume the equation of state

$$p = \rho RT \quad (4)$$

and the equation of entropy

$$S = C_v \ln \left(\frac{p}{\rho^{\gamma}} \right) + S_0 \quad (5)$$

If the disturbances are small, namely,

$$\vec{W} = u_0 \vec{i}_x + \vec{W}_1, \quad \frac{|\vec{W}_1|}{u_0} \ll 1$$

$$p = p_0 + p_1, \quad \frac{p_1}{p_0} \ll 1$$

$$\rho = \rho_0 + \rho_1, \quad \frac{\rho_1}{\rho_0} \ll 1$$

$$T = T_0 + T_1, \quad \frac{T_1}{T_0} \ll 1$$

$$S = S_0 + S_1, \quad \frac{S_1}{S_0} \ll 1$$

Where $\vec{W}_1 =$ disturbed velocity vector $= u_1 \vec{i}_x + v_1 \vec{i}_y + w_1 \vec{i}_z$. Therefore, the governing equations may be linearized. The results are:

$$u_0 \frac{\partial \rho_1}{\partial x} + \rho_0 \nabla \cdot \vec{W}_1 = \dot{n} \quad (6)$$

$$\rho_{\infty} u_{\infty} \frac{\partial \vec{H}_1}{\partial x} + \nabla p_1 = \vec{f} \quad (7)$$

$$u_{\infty} \frac{\partial S_1}{\partial x} = (\gamma-1) \frac{C_v \dot{q}}{\rho_{\infty}} \quad (8)$$

$$S_1 = \frac{C_v}{\rho_{\infty}} (\rho_1 - a_{\infty}^2 \rho_1) \quad (9)$$

Combining the above equations, the result in the x-component becomes:

$$(1 - u_{\infty}^2) \frac{\partial u}{\partial x} + \frac{\partial u}{\partial y} + \frac{\partial w}{\partial y} = \frac{\dot{m}}{\rho_{\infty}} + \frac{\gamma-1}{\rho_{\infty} a_{\infty}^2} \dot{q} - \frac{u_{\infty}}{\rho_{\infty} a_{\infty}^2} f_x \quad (10)$$

Which is the form, we cited in Section II of Equation 15.

It can be seen that a mass source per volume of strength \dot{m} will produce the same disturbance as an energy source of strength \dot{q} if $\dot{m} = (\gamma-1) \dot{q}/a_{\infty}^2$, or the same as a body force per volume f_x , if $\dot{m} = u_{\infty} f_x/a_{\infty}^2$. Therefore, there exists an analogy among the three disturbance sources. The equivalences for the total rate of mass addition \dot{m} , energy addition \dot{Q} and the total body force F_x are as follows:

$$\dot{m} = \frac{\gamma-1}{a_{\infty}^2} \dot{Q} = - \frac{u_{\infty}}{a_{\infty}^2} F_x \quad (11)$$

APPENDIX III

SURVEY ON CHEMICAL BATTERY POWER SOURCES

At present, the available chemical battery power sources are unsuited for use in rocket application. This is largely due to the fact that the available batteries are not designed for such purposes because of its weight and life duration.

The theoretical performances of the state of art of available chemical batteries are listed as follows (Ref. 25):

Type of Battery	Theoretical Maximum Performance, w-hr/lb
Lead-acid	75
Nickel-cadium	90
Mercury-zinc	100
Zinc-silver oxide	180

The actual performance of the above batteries are considerably less than the theoretical values. The extensive research now under way has substantially increased the battery performance, yet from the system point of view, it is still too heavy for the airborne type application.

Ray and Ross (Ref. 26) reported that a system producing as high as ~300 w-hr/lb specific energy battery is being developed. Its reactants are liquid lithium and gaseous chlorine, and the electrolyte is fused lithium chloride. Experimental data indicates a power density of about 15 w/sq. cm. They reported that the major uncertainty of this battery is lifetime. The short lifetime may not be suited for some other purpose but could be suited for the airborne short time application.

It is worthwhile to point out here that the airborne MHD power source, besides the chemical battery, may be also promising in the future. J. B. Dicks and Associates (Ref. 27) are now engaged in developing MHD generators by using superconducting magnet for airborne purposes. Using a liquid propellant motor with mass flow rate of 4 lb/sec, with the power generation unit located at the nozzle exit at a pressure of 5 atm, 1.5 kw/lb can be generated with a maximum voltage of 3000 volts. This weight includes the magnet, channel and magnet coolant.

In order to get some feeling of the required power source weight, a sample calculation for a main thrust of $F_0 = 10,000$ lb motor of chamber temperature of $T_t = 5000^\circ\text{R}$, has been made. Assuming that the deflection angle ϵ is 4° and the electrodes are embedded at $M_\infty = 4.0$ station inside the exhaust nozzle, then the required power source weight consumption rate \dot{w} can be calculated by the following equation:

$$\dot{w} = \left[\frac{F_0 \tan \epsilon \sqrt{\gamma R}}{\sigma(\gamma)} \right] \frac{\sqrt{T_t}}{E_{sp}}$$

where R = gas constant, $\sigma(\gamma)$ is a constant from blast wave theory and E_{sp} = specific energy of power source. From the above equation the total weight of power supply W is therefore directly proportional to the specific energy of power source E_{sp} and the duration of time applied. At present, the best battery available on market (Ref. 28) is about in the order of $E_{sp} \approx 30$ (w-hr)/lb. The corresponding battery consumption rate can be estimated as $\dot{w} \approx 110$ lb/sec. This is still under the assumption that a very short time battery is available. However, according to the manufacturer, the battery is designed for three minutes use. If the battery of specific energy of ~ 300 (w-hr)/lb may be available in the future as reported by Ray and Ross (Ref. 26), the weight consumption rate will be about $\dot{w} \approx 11$ lb/sec for this specific application.

APPENDIX IV

INFLUENCE PARAMETERS ON THE ARC DISCHARGE

In order to determine the arc voltage and the current under our specific conditions, an order of magnitude estimation has been conducted. The test conditions are as follows:

gas medium = nitrogen

arc length = $1.4 \text{ cm} > L > .6 \text{ cm}$ (cross flow configuration
an average arc length of 1 cm is used in the
calculation)

gas stream static pressure = $p \approx .07 \text{ atm} \approx 53 \text{ mm Hg}$

gas stream static temperature = $T \approx 1200^\circ\text{K}$

gas stream Mach number = $M_\infty \approx 2.5$

The literature survey reveals that in Ref. (29) the most similar case to our test conditions was investigated. The arc was discharged between a point cathode and a ring-shaped anode in coaxial arrangement and were 35 mm apart. The gas medium was argon with flow Mach number 3. The ambient pressure was 16 mm Hg. A minimum arc current of 150 amps and a maximum arc voltage of about 60 volts were observed.

PREDICTION OF MAINTENANCE VOLTAGE

In order to extend the above results to our experiment, several transformations have to be made corresponding to our test conditions.

Transformation of the Medium

The influence of the flow media on the arc discharge has been studied by John and Bade (Ref. 30). They investigated different flow media at a mass flow rate of about 0.5 gr/sec and at a static pressure of about 1 atm. The investigations, for a parallel flow configuration, showed that the smaller the molecular weight of the medium the higher the voltage required to maintain the arc. In the case of nitrogen and argon, the required voltage ratio is about 3 to 2 (nearly independent of the arc current). The maximum arc voltage given in Ref. (29) should be corrected accordingly to a nitrogen stream which gives $V_a \approx 90$ volts.

Transformation of the Mass Flow Rate

For air at a static pressure of about 1 atm, the influence of the mass flow rate has also been studied by John and Bade (Ref. 30). From the observation of a cross flow configuration, the necessary voltage to maintain the arc is increased if the mass flow rate is increased. More specifically, the voltage is increased by about 20% (independent of the arc current) if the mass flow rate is doubled.

In our case, a rough estimation of the mass flow rate passing through the arc gives $\dot{m} < 3.2$ gr/sec, where the arc radius has been assumed to be 0.1 cm. This is about 1/50 of our total mass flow rate of the nozzle. In view of this, the arc voltage should be corrected to $V_a \approx 200$ volts.

Transformation of the Arc Length

Busz and Finkelburg (Ref. 31) investigated the effect of the electrode gap for an argon arc at 200 amps. Their results showed that the larger the arc length the larger the required voltage to maintain the arc. If it is assumed that the same qualitative behavior exists for a nitrogen arc, then, according to Busz and Finkelburg (Ref. 31) the arc voltages compare like

$$\frac{V_{35\text{mm}}}{V_{6\text{mm}}} \approx 2$$

Hence, a corrected value for the arc voltage should be about 100 volts.

Transformation of the Ambient Pressure

In Ref. (32), the relation between arc voltage and ambient pressure is given in detail. It can be observed that the arc voltage decreases as the pressure decreases. However, it may be found that this decrease of the arc voltage for low pressure arcs is less substantial than in case of high pressure levels. In view of Ref. (32), it may be assumed that no transformation is needed.

The maintenance voltage of the arc in our case may then be said to be about 100 volts. It is known from experiments (Ref. 32) that in order to establish a stable arc it is required that

$$V_o \approx 2V_a$$

Therefore, the required power source voltage, V_o , is about 200 volts in our case, while the arc power supply should be 15KW approximately. Using the voltage balance of the circuit, the outer circuit resistance may be calculated to be about 0.7 ohms.

ESTIMATION OF BREAKDOWN VOLTAGE RANGE

Another property which has to be estimated is the breakdown voltage. The estimation is based on the results given in the classical work of Cobine (Ref. 18) for the following test parameters:

electrode gap: 0.6 cm

static pressure: 53 mm Hg

Figure IV-1 (reproduced from Ref. (18)) may be used to estimate the breakdown for the arc to 23,000 volts approximately.

As it is pointed out by Cobine (Ref. 18), this breakdown voltage may be decreased considerably if there is an insulator connecting the electrodes. This is due to the phenomenon of collection of surface charge. In addition, the presence of any gas layer, moisture or dust again may decrease the breakdown voltage. Under these conditions it is recommended (Ref. 18) to allow a factor of 3 in the gap length. Moreover, Howell (see the same reference), has found that at high pressures the breakdown voltage can be reduced by a factor of 4 if the surfaces of electrodes are rough. Therefore, the minimum breakdown voltage, assuming rough electrodes and surface charge, could be as low as approximately 400 volts.

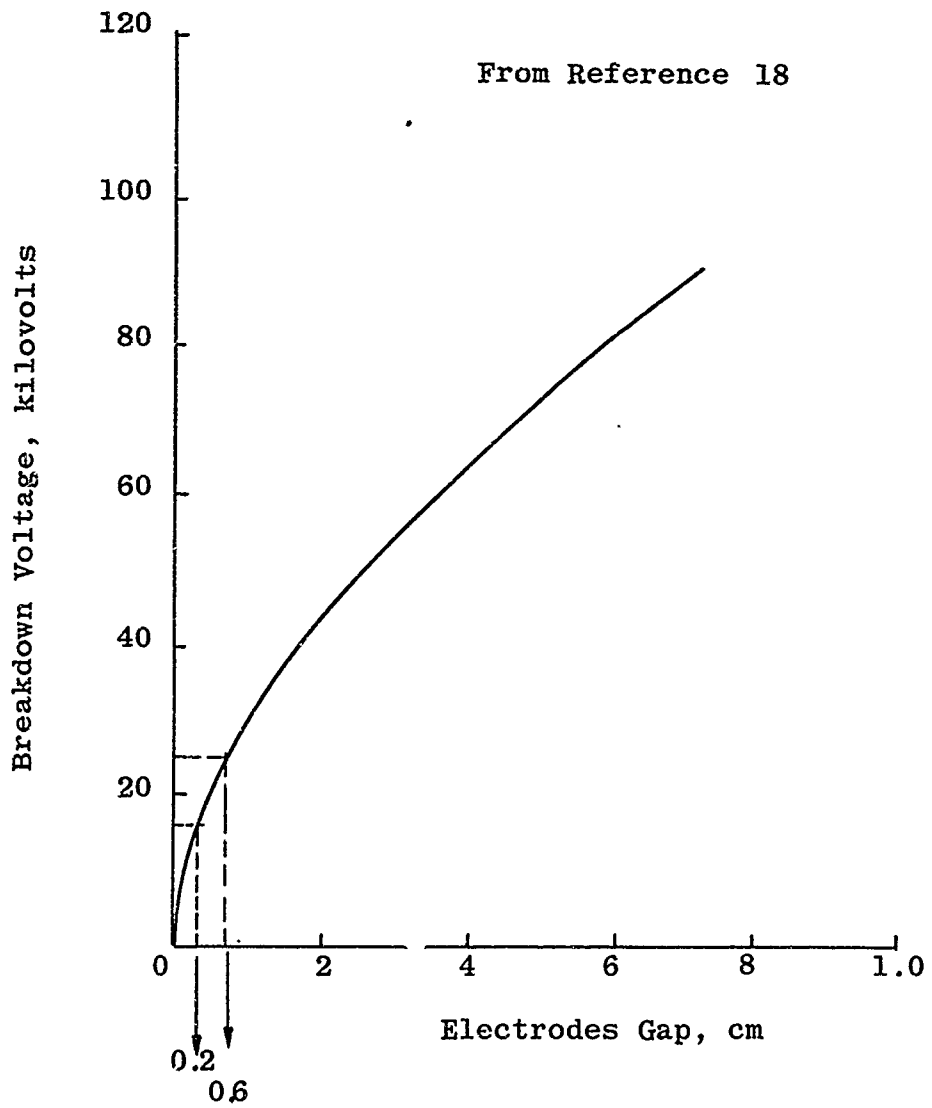


Figure IV-1. Breakdown Voltage between Cylindrical Rods at Atmospheric Pressure

APPENDIX V

ANALYTICAL DETERMINATION OF THE ARC CHARACTERISTIC

Employing the Ellenbaas Energy Equation, an approximate method to determine the operation parameter of an electric arc discharge has been established by Maecker (Ref. 19) using the Schmitz's approximation. The analysis given herein connects the characteristics of the electric discharge with the parameter of the outer circuit. It should be noted that Maecker's original analysis was derived for a contained cylindrical arc. Since no theory exists in predicting the arc characteristic corresponding to our case, it is felt that Maecker's theory may be used in order to obtain at least some qualitative information.

The voltage balance for the whole circuit is (Fig. V-1):

$$V_o - R_a I - R_c I = 0 \quad (1)$$

where

V_o = battery or power source voltage

R_a = resistance of the arc

R_c = resistance of the outer circuit

I = current of the circuit

Under the assumption of a cylindrical arc the electric field strength may be written as

$$E = \frac{V}{L}$$

where L stands for the arc length. Then, Equation (1) may be rewritten as:

$$\frac{V_o}{L'} - \frac{R_c I}{L'} = \frac{V_a}{L'} = E_a(I) \quad \left| \begin{array}{l} \text{at point of} \\ \text{operation} \end{array} \right. \quad (1a)$$

where $E_a(I)$ is the arc characteristic, or the current-voltage relationship of the arc.

Neglecting any mass flow as well as radiation, the Ellenbaas Energy Equation in cylindrical coordinates takes the following form:

$$\sigma(T)E_a^2 + \frac{1}{r} \frac{d}{dr} [rk(T) \frac{dT}{dr}] = 0 \quad (2)$$

where

r = arc radius

$\sigma(T)$ = electrical conductivity

k = thermal conductivity

T = temperature of the gas

Introducing the heat conduction function,

$$S = \int_0^T k(T) dT \quad (3)$$

then, the energy equation takes the form

$$\sigma(T)E_a^2 + \frac{1}{r} \frac{d}{dr} [r \frac{dS}{dr}] = 0 \quad (4)$$

In general, the electrical conductivity $\sigma(T)$ varies rather significantly with gas temperature, hence the material function is $\sigma = \sigma(S)$. Usually this is determined experimentally and given in graphs. In view of the substantial temperature differences between the core of the arc discharge and the boundary, the material function may be approximated by two linear segments dividing the arc into two regions, (Fig. V-2). Let σ^* be the electrical conductivity corresponding to a point of the approximating line segment (Fig. V-2) then $\sigma = \sigma(S)$ may be expressed as:

$$\begin{aligned}\sigma^* &= 0 && \text{for } 0 < S < S_a \\ \sigma^* &= \alpha(S - S_a) && \text{for } S_a < S < S_o\end{aligned}$$

where α is the slope of one of the line segments. As mentioned, the above approximation divides the arc into two regions, namely, the outer region without electrical conductivity and the inner region with electrical conductivity. These two regions can be considered separately as follows:

The Region with Electric Conductivity

In this region $\sigma^* = \alpha(S - S_a)$, defining $x \equiv rE_a\sqrt{\alpha}$, we find that Equation (4) may be reduced to

$$\sigma^*_{xx} + \frac{1}{x} \sigma^*_x + \sigma^* = 0 \quad (5)$$

where subscript x denotes the differentiation with respect to x . This equation is a zeroth order Bessel Equation. Since $\sigma^*(x)$ has to be finite for all x and $J_0(x=0) = 1$, we have

$$\sigma^*(x) = \sigma^*_o J_0(x) = \frac{S - S_a}{S_o - S_a} \quad (6)$$

The last term follows simply from the geometry of Fig. V-2. We note that for $x = x_o = 2.405$ the Bessel function reaches its first zero; in that case $\sigma^*(x = 2.405) = 0$ and $S = S_a$.

The Region without Electric Conductivity

In this region the energy equation, i.e., Equation (4) becomes $C_1 = x \, dS/dx$. In order to determine the integration constant C_1 , we require that the slopes dS/dx for the outer and inner regions to be matched at the intersection. From the solution of the inner region, we have

$$\left. \frac{dS}{dx} \right|_0 = (S_0 - S_a) \left. \frac{d(J_0[x])}{dx} \right|_0 = - (S_0 - S_a) J_1(x_0)$$

Multiplying this by $x_0 = 2.405$, we have

$$x_0 \left. \frac{dS}{dx} \right|_0 = - 1.248 (S_0 - S_a)$$

Matching this result with the outer region solution, we obtain

$$C_1 = x \frac{dS}{dx} = - 1.248 (S_0 - S_a)$$

Now a second integration of $dS = - 1.248 (S_0 - S_a) \frac{dx}{x}$ gives, using the boundary condition that for $x = x_0$, $S = S_a$.

$$\frac{S - S_a}{S_0 - S_a} = - 1.248 \ln \frac{x}{x_0} \quad (7)$$

Replacing x by its definition $x \equiv r E_a \sqrt{\alpha}$, and requiring that $r = r_a$ and $S = 0$ at the wall the following relation is obtained:

$$\frac{S_a}{S_0 - S_a} = 1.248 \ln \left| \frac{r_a}{2.405} \right| E_a \sqrt{\alpha} \quad (8)$$

where r_a is the arc tube radius in Maecker's original text.
The electrical field strength is

$$E_a = 2.405 \cdot \frac{1}{r_a \sqrt{\alpha}} \cdot e^{\frac{S_a}{1.248(S_o - S_a)}} \quad (9)$$

Writing Equation (7) for $x = r$ and $x_o = r_a$, the following equation is obtained:

$$S = - 1.248(S_o - S_a) \ln \frac{r}{r_a} \quad (10)$$

The power conducted through the face of the assumed cylindrical arc may be expressed by

$$\begin{aligned} P_a &= I \cdot E_a = - 2\pi r k(T) \frac{dT}{dr} \\ &= - 2\pi r \frac{dS(T)}{dr} \end{aligned} \quad (12)$$

or in view of Equation (10),

$$\begin{aligned} P_a &= (2\pi)(1.248)(S_o - S_a) \\ &= 7.84(S_o - S_a) \end{aligned} \quad (13)$$

On the other hand, Equation (8) after some manipulation, can be rewritten as

$$E_a = \frac{1.08}{r_a \sqrt{\alpha}} \cdot \exp.\left[\frac{S_o}{1.248(S_o - S_a)}\right] \quad (14)$$

so that,

$$\frac{P_a}{E_a} = \bar{i} = 7.27 r_a \frac{\sigma_o^*}{\sqrt{\alpha}} \exp.\left[-\frac{S_o}{1.248(S_o - S_a)}\right] \quad (15)$$

It can be observed that for constant arc power and a given gas, the values of S_o and T_c are independent of the arc tube radius. On the other hand, it is evident that the arc current varies proportionally and the electric field varies inverse proportionally with the arc radius.

To approximate the material function $\sigma(S)$ with the line segment of Fig. V-2, two filling factors f and f_1 were defined by Maecker (Ref. 19) such that:

$$f = \frac{1}{\sigma_o S_o} \int_0^{S_o} \sigma dS \quad ; \quad f_1 = \frac{S}{S_o} \frac{\int_0^{S_o} \sigma dS}{\int_0^S \sigma dS} \quad (16)$$

Now the Equations (13), (14) and (15) may be rewritten to obtain:

$$P_a = 6\pi z f_1(T) S_o(T) \quad , \quad [\text{kw/cm}] \quad (17)$$

$$E_a = \frac{3.24}{r_a} f_1(T) \sqrt{\frac{S_o(T)}{2f(T)\sigma_o(T)}} \exp.\left[\frac{1}{3zf_1(T)}\right], \quad [\text{volt/cm}] \quad (18)$$

$$I = 7.27 r_a \sqrt{2f(T)S_o(T)\sigma_o(T)} \exp.\left[-\frac{1}{3zf_1(T)}\right], \quad [\text{amp}] \quad (19)$$

where $z = 1.248$. These equations enable us to find the arc characteristics provided $S_o(T)$, $\sigma_o(T)$, $f(T)$ and $f_1(T)$ are known as functions of the arc center temperature. In addition it is also necessary to know the arc tube radius.

To demonstrate the method of determining the arc characteristics from measured values of arc current and arc voltage, the following test data will be considered:

Arc Current I [amps]	Arc Voltage V _a [volts]	Arc Power P _a [kw]
26	115	2.99
64	25	1.60
104	57.5	5.98
94	60	5.64
102	47.5	4.84
148	40	5.92
78	0	0

These data are given in Fig. V-3 assuming that the average arc length is 1 cm. As it has been mentioned the arc characteristic may be determined with the aid of the Equations (17), (18) and (19). The unknown properties $S(T_c)$, $\sigma(T_c)$, $f_1(T_c)$ and $f(T_c)$ are given in Ref. (19) for nitrogen as functions of the axis temperature of the arc. The temperature at the arc axis are not known a priori. However, they may be estimated as follows.

Assuming a linear decrease of the arc temperature from its axis value T_c to its edge value T_a (here the edge is the boundary between the arc and the external flow field). The average value for the arc temperature may be defined as

$$\bar{T} = \frac{T_c + T_a}{2} \quad (20)$$

So that the axis temperature may be written as

$$T_c = 2\bar{T} - T_a \quad (21)$$

The average plasma temperatures are given as functions of the arc power in Ref.(33). It should be noted that even though the temperature values given in Ref. (33) are corresponding to an argon plasma, the graphs as shown in Fig. V-4 should still give qualitative representation of the temperature, at least within the limits of our approximation. The effect of the mass flow rate upon the average temperature may be neglected (Ref. 34).

Now the edge temperature of the arc has been assumed to be the static temperature of the free stream ($T \approx 1200^\circ\text{K}$). It should be noted however, that this temperature may be somewhat low as compared to the actual case. In Fig. V-3 the calculated power line corresponding to that edge temperature of the arc is shown with the measured data. The agreement is fair. The discrepancy can be explained simply by the assumption made concerning the temperature at the arc boundary being the static temperature of the free stream. Obviously the assumed value was too low; this possibility has already been mentioned. In view of the Equations (17) and (21), it might be observed that it is possible - using an iterative procedure - to determine the correct value of the edge temperatures. Fig. V-4 shows the calculated arc characteristics for different arc radii as well as the measured data. Again, the correct arc radius may be obtained by an iterative procedure.

It should be pointed out here that Maecker's method was derived for a contained cylindrical arc, hence, the results cannot be safely claimed to be directly applicable to our case in a strict manner. However, since we are interested mainly in obtaining some qualitative data concerning arc center and arc boundary temperature as well as the arc radius, the way of obtaining these quantities as stated above seems justifiable. One may observe that the measured arc characteristic is most closely represented by the arc characteristic of an arc operating in a tube of approximately 0.1 cm.

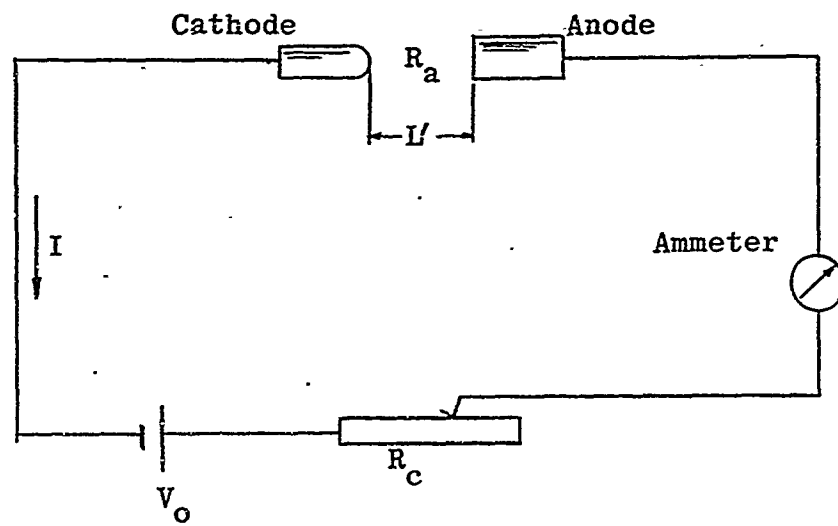


Figure V-1. Principal Circuit Diagram

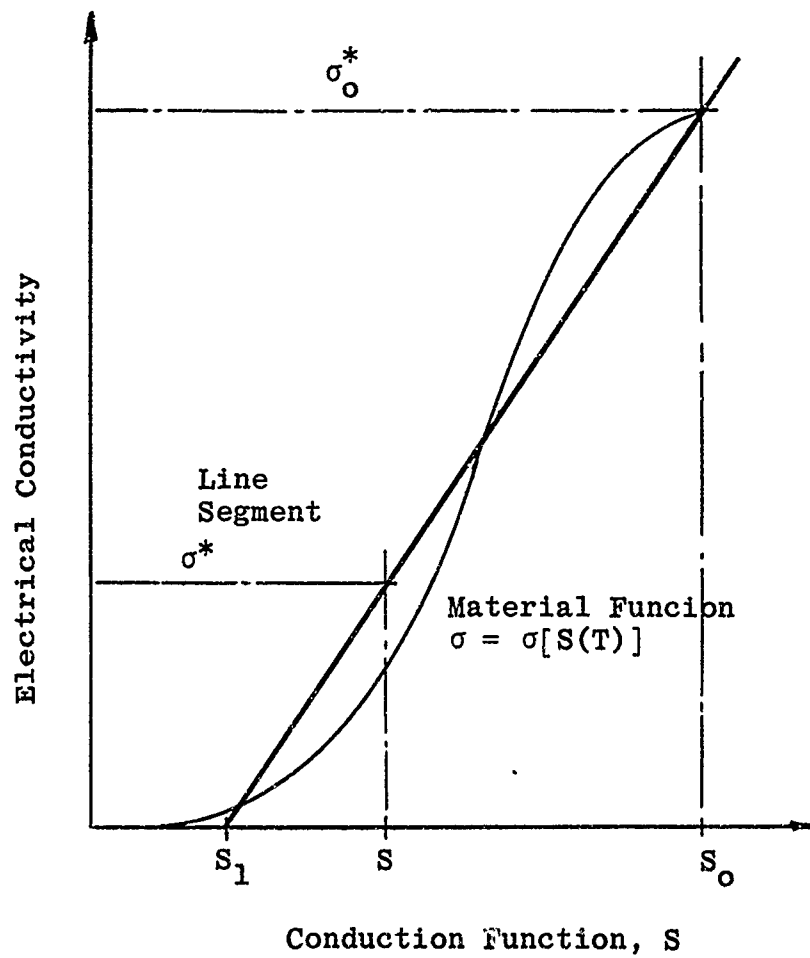


Figure V-2. Graphical Approximation of Material Function

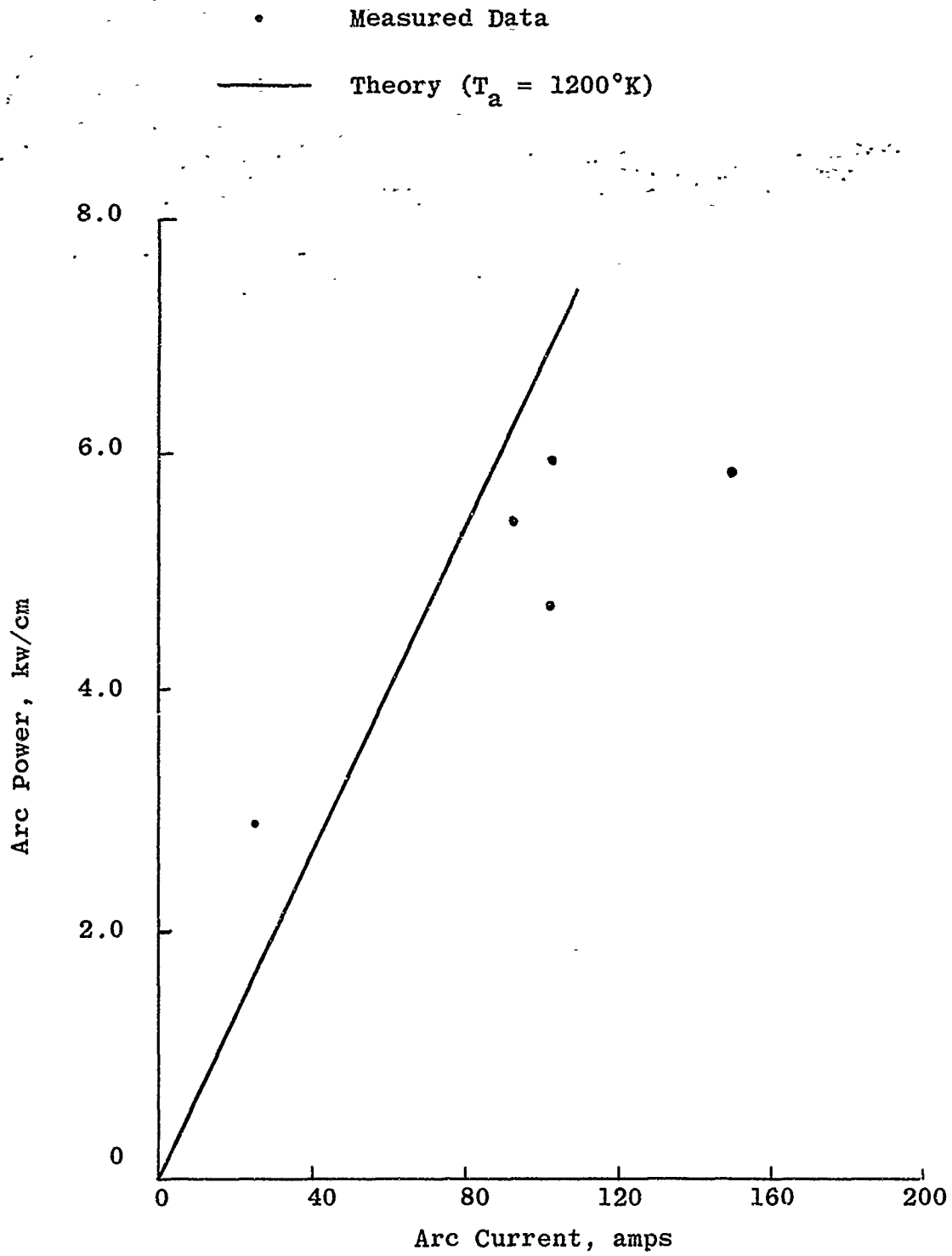


Figure V-3. Predicted and Measured Arc Power

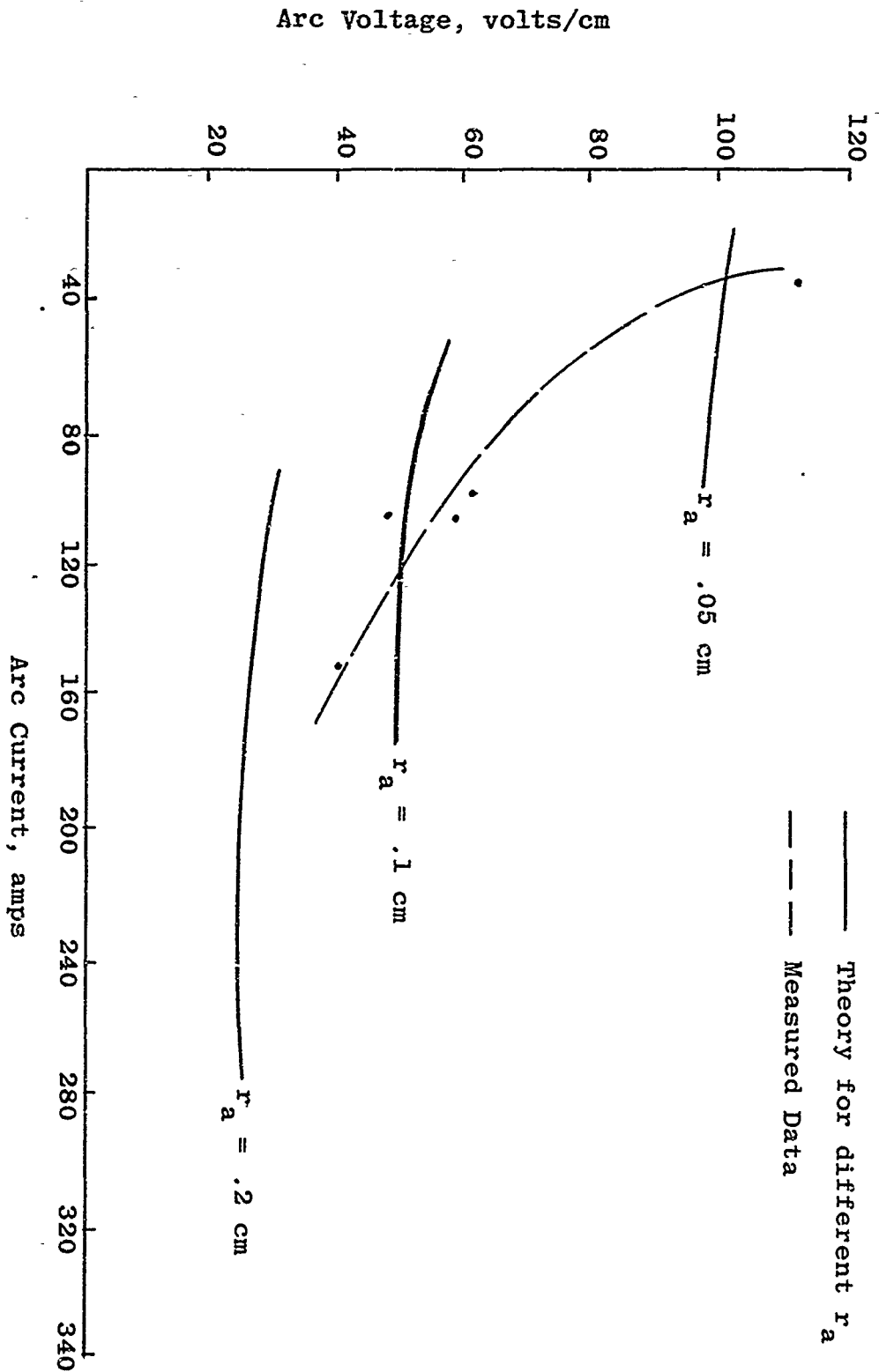


Figure V-4. Calculated and Measured Arc Characteristic

APPENDIX VI

DIFFICULTIES OF THE EXPERIMENT

Information on pressure distribution in a flow field disturbed by electric discharge is not available in the literature. The magnitudes of the pressures and their affected areas could only be evaluated by using the simplified theories established for thrust vector control by secondary injections. Different opinions in theoretical considerations, as discussed in Appendix I, made it necessary to conduct an experimental investigation. However, the mechanism of creating the flow field disturbance by an electric arc discharge was not well-understood; for example, the breakdown voltage of an electric arc could not be analytically determined in a supersonic flow field (Appendix IV). The additional material problems for both the nozzle section and the electrode insulations also needed to be explored. In order to solve all these major problems, a water-cooled axisymmetric copper nozzle was built (Fig.10) for preliminary investigation in order to determine the design criteria.

PRELIMINARY TEST

The first test was successfully completed with the following information confirmed:

- 1) The water-cooled copper nozzle designed at a marginal strength by considering steady state heat transfer of conduction and convection sustained the high temperature environment for ten to thirty seconds without problem.
- 2) The arc can be established between a pair of cross-flow electrodes of 0.25 inch apart at a breakdown voltage of 375 volts for a nitrogen stream of Mach number 2.8 with static pressure of 2 psia and stagnation temperature of 4000°R.
- 3) The electrode configurations affected the breakdown voltage as well as the effective area. Since the highest breakdown voltage was considered within the practical range, it was felt that the largest affected area should be more useful for thrust vector control applications. The largest effective area was obtained for the configuration that the two electrodes were perpendicular to the flow direction.

- 4) An electric arc can cause the static pressure rise in a supersonic flow field. The arc can be maintained without the confinement of a magnetic field.

The difficulties encountered in the test for the preliminary investigations were as follows:

Flow Separations

The nozzle was designed for a back pressure of 1 psia which was originally expected from the test facility. Leakage problems in the vacuum system were not able to be solved during the time allocated for this test. Thus the pressure distributions (Figs. 26, 27 and 28) at the nozzle exit should not be considered relevant to the purpose of this test. A back pressure of 2 psia must be used as the design parameter of the future test nozzles.

Material Problems

The insulation material between the electrodes and the copper was severely damaged as shown in Fig. 29. Micarta, silicon phenolic, and boron nitride were used. Micarta was melting and running with the flow almost instantly. Silicon phenolic became a good electric conductor at high temperature. Boron nitride was ablated at a comparatively slow rate and was considered the best insulation material for this purpose.

The method of electrode protrusion for protecting the insulation was tested by extending the electrodes approximately one-half of the boundary layer displacement thickness into the free stream. The insulation was comparatively better protected but the flow field was also disturbed substantially. Fig. IV-1 shows the pressure distributions caused by electrode protrusion with and without discharge. It was thus felt that the electrode protrusion did not have any advantage and should not be used for further testing.

Pressure Response Rate

Transducers and manometers were used for pressure measurements. Due to the distance between the apparatus and the instrumentation panel, a finite time period was required to reach a steady state reading. The pressure response history was recorded and is shown in Fig. VI-1 for both transducers and manometers. It can be seen that the transducers required 0.8 seconds and the manometers required 3.0 seconds to reach the true pressure values of the flow field.

Data Uncertainty

The material problem required the discharge time to be as short as possible in order to produce minimum damage which influenced the flow field pressure readings. On the other hand, the pressure response rate requires longer time in order to register the steady state readings. Since these two demands could not be satisfied simultaneously, a compromised time interval had to be selected. Three seconds for electric discharge was decided for the future test with pressure data taken after the discharge for comparing with that before discharge. If any disagreement occurred between the after and before discharge values, the pressure differences obtained by subtracting the after discharge value from the during discharge value should be used in order to give a more conservative result for side force evaluation.

Practice of Side Force Evaluation

With the static pressure data from the preliminary test, it was possible to evaluate the generated side force for both practice and curiosity. The practice was to determine the actual difficulty which might be involved. The curiosity was to check the different opinions of Appendix I, since an order of magnitude difference of the generated side force was in question.

It was felt that the pressure measurements were not as comprehensive as needed in order to give a quantitative side force evaluation. However, since the preliminary investigation had to provide the various combinations for electrode configurations, the limited pressure data were used for the order of magnitude comparison to verify the different opinions of the analytical considerations.

The procedure of Appendix VII was used for the side force evaluation. With very limited numbers of data points on pressure distributions, only the order of magnitude of the side force was able to be evaluated and agreed well in the order of magnitude with Broadwell's modified linearized theory (Appendix I). This information was exciting because it could bring the thrust vector control by electric discharge comparable with the secondary injection scheme even with present technology on power sources, namely chemical batteries. The determining factor of the success of this new concept, however, lies on a detailed verification of the pressure measurements in the entire flow field especially in the vicinity downstream of the electrodes.

DETAILED EXPERIMENT

From the experience of the preliminary test, a rectangular nozzle was designed in order to satisfy the following purposes:

- 1) Detailed pressure measurements
- 2) Visualization of the flow field caused by the electric discharge
- 3) Hot and cold boundary layer effects at the discharge
- 4) Electrode configuration effect on the high pressure areas.

The nozzle consisted of three parts as shown in Fig. 18. The bottom plate could be replaced easily for boundary layer and electrode configuration investigations. Three different materials were used for the bottom plate:

Boron Nitride

From the insulation material experience, the boron nitride appeared to be the most attractive choice because of its high thermal shock resistance. A plate was built with heavy concentration of pressure taps in the vicinity of the electrodes. Pressure checks indicated very serious leakage problems for all pressure taps. Several methods were tried for preventing the leakage, only the metallic coated boron nitride plate appeared to be possible. However, the cost and time needed for this process made it impractical because the number of pressure taps and different configurations required.

Silicon Phenolic

Silicon phenolic appeared to be the second to the best choice, if the electrodes were insulated with boron nitride. This plate was made and tested. The flow field disturbance by electric discharge was clearly observed through quartz windows downstream of the electrodes. The only problem was the deformation of the plate at high temperature. Severe ablation of the phenolic material occurred in the vicinity of the electrodes. The static pressure after discharge did not return to the values before discharge as shown in Fig. 33. Nevertheless, the pressure distribution is different from the interpolated results of the axisymmetric copper nozzle where the sharp pressure drop right behind the pressure peak could not be determined. Side force evaluation was made by using the pressure difference during and after discharge. The evaluated side force, however, was an order of magnitude smaller than that obtained from the preliminary

test and agreed well with the theoretical results of Section II. It was felt that the only way to confirm the magnitude of the side force should be achieved from the test results where the pressure measurements after discharge returned to that of before discharge.

Water-cooled Copper

Water-cooled copper appeared to be free from deformation and was used for the bottom plate with boron nitride as electrode insulators. The discharge was established from the cathode to copper then to the anode. This process transformed a large quantity of the supplied electric energy to the cooling water. Ceramic spray of the copper plate was used and proved to be the best method for this purpose. Pressure distributions were measured as shown in Fig. 36. The pressure readings after and before discharge were identical, but the area with pressure rise during discharge was small. Due to the need of the boron nitride insulators, no pressure tap was available between the electrodes. Nevertheless, it is obvious, the peak pressure rise dropped sharply along the flow direction. The side force evaluation confirmed the theory of Section II.

Silicon Phenolic Axisymmetric Nozzle

A silicon phenolic axisymmetric nozzle was also tested for the purpose of confirming the rectangular nozzle results and comparing the cold boundary layer effect. The pressure distribution is shown in Fig. 39. The evaluated side force again confirmed the theoretical results of Section II.

CONCLUDING REMARKS

It was felt that an additional test should be conducted by using the rectangular nozzle with ceramic sprayed copper plate. However, more pressure measurements with faster responses would be desired. A modification was needed by re-fabricating a new copper plate and re-installing the pressure transducers closer to the test nozzle.

The project was terminated for the following reasons:

- 1) Additional time and funds would be required for further testing which appeared to conflict with the higher priority projects scheduled for the test facility in the near future.
- 2) The material problem is very severe from the system applications point of view. This could not be solved even with more precise test data available.

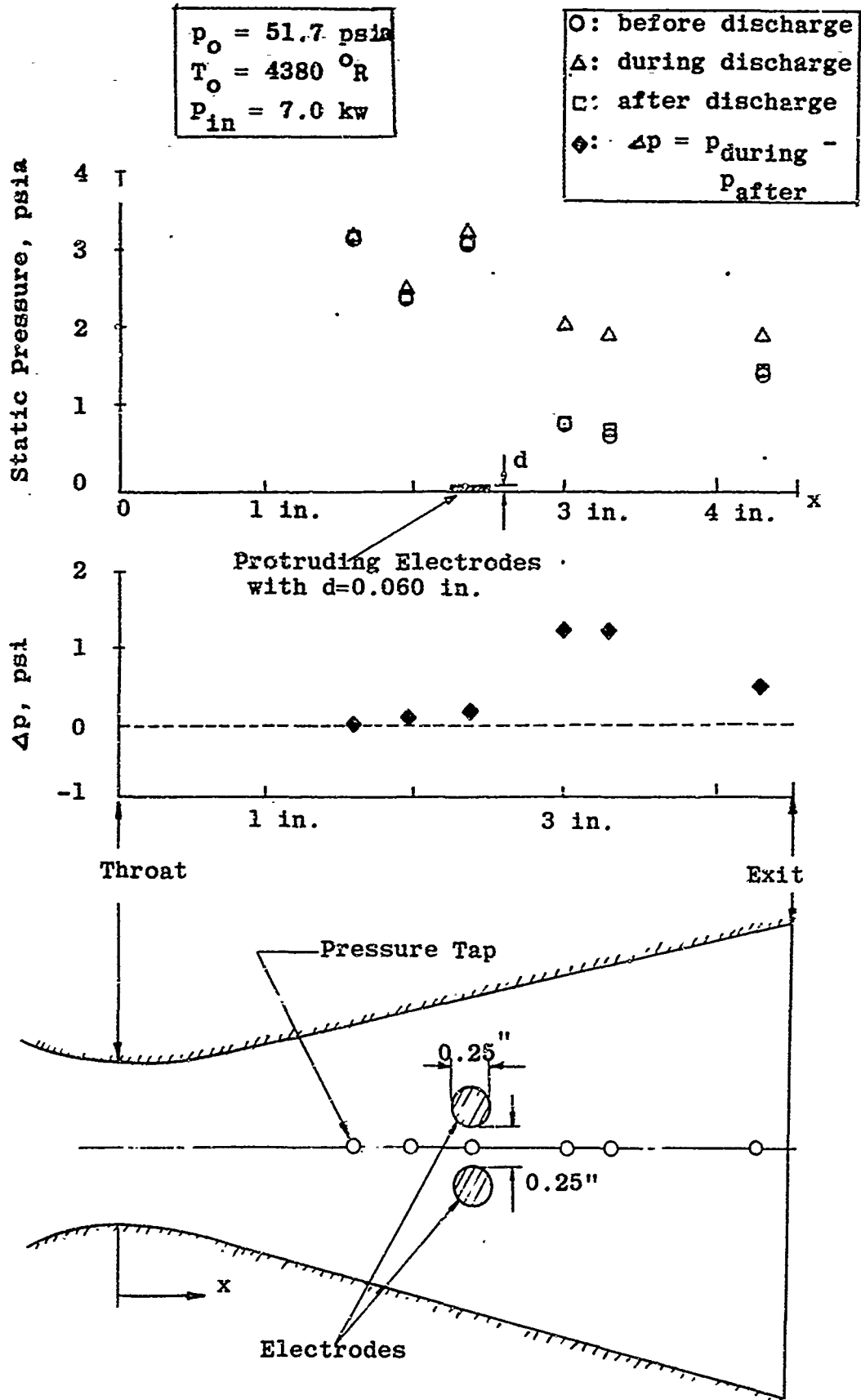


Figure VI-1. Pressure Distributions Affected by Electrode protrusion

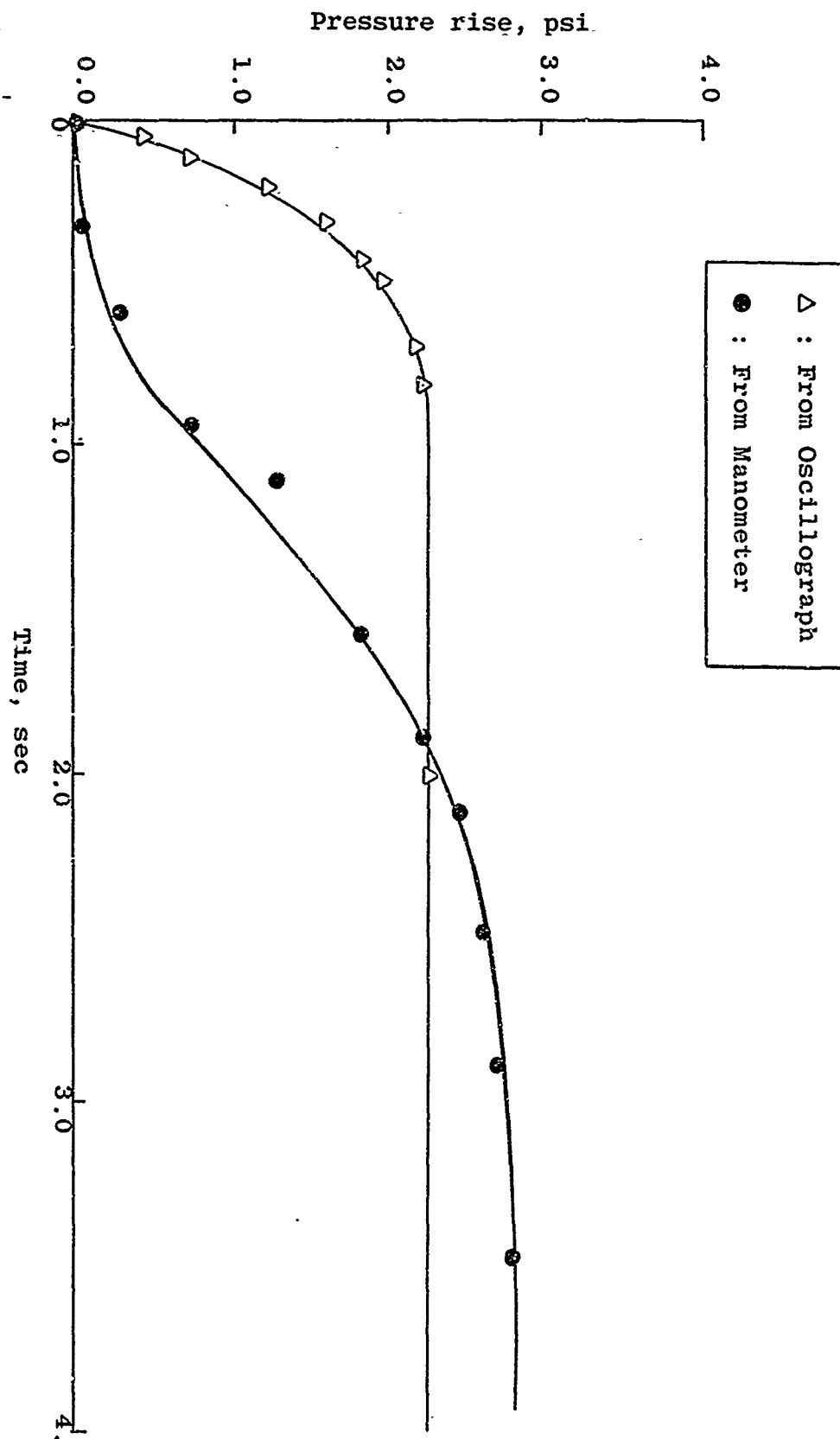


Figure VI-2. Pressure Response History

APPENDIX VII

AN EXAMPLE OF THE SIDE FORCE CALCULATION

An example to illustrate the side force evaluation is presented here for the purpose of indicating the attainable accuracy in the calculation. The test results obtained from the axisymmetric silicon phenolic nozzle are used for the numerical calculation. The pressure tap distributions onto the projected area are shown in Fig. VII-1. The x-axis is along the flow direction and the y-axis normal to the flow direction. Since the electrodes are symmetric to the nozzle centerline, the pressure distributions are also assumed to be symmetric to the same centerline.

Pressure readings before, during and after discharge have been all recorded. Fig. VII-2 shows the reading along nozzle centerline (y_0 -section). Figure VII-3 and Figure VII-4 show the readings along x_1 -section and x_2 -section, respectively. Similarly, readings in sections x_3 , x_4 , x_5 , y_1 , and y_2 can be obtained. Due to the material deformation under high temperature environment, it is noted that the pressure readings before and after discharges are not consistent. In order to be able to study the feasibility of this concept, the pressure rise caused by electric discharge is assumed to be the pressure difference between, during (P_{during}) and after (P_{after}) discharges. The side force is then evaluated as

$$F_s = 2 \int_A (P_{\text{during}} - P_{\text{after}}) dA$$

where A is one-half of the affected area or the area behind the shock. Dividing the affected area A into some reasonably small subdivisions, ΔA_i , and since these subdivisions are sufficiently small, we can assume that the pressure change is constant within each subdivision. In some high pressure gradient regions a finer partition is used. The mean value of the pressures is chosen at each subdivision. Those mean values are obtained from Figures VII-2, VII-3, and VII-4. Let,

$$\Delta A_i = \text{the area of each subdivision,}$$

then

$$(P_{\text{during}} - P_{\text{after}})_i \Delta A_i = \text{the side force produced in } \Delta A_i.$$

Summing up all the affected areas, ΔA_i , we obtain

$$F_s = 2 \sum_i (P_{\text{during}} - P_{\text{after}})_i \Delta A_i = \text{total side force.}$$

The procedure of the side force calculation for the silicon phenolic nozzle is as follows:

1. Choose $\Delta A_i = \frac{1}{64} \text{ in}^2$ as shown in Fig. VII-5.
2. Find all the pressure rises

$$\Delta P_i = (P_{\text{during}} - P_{\text{after}})_i$$

3. Trace out the isobaric area. Namely, to determine the number of small blocks, N_i , with same values of pressure rise ΔP_i .
4. Then, we can write

$$\begin{aligned} F_s &= 2 \sum_i (P_{\text{during}} - P_{\text{after}})_i \Delta A_i \\ &= 2 \sum_i \Delta P_i (N_i \Delta A_i) \\ &= 2(\Delta A_i) \sum_i (\Delta P_i)(N_i) \end{aligned}$$

which gives

$$\begin{aligned} F_s &= 2 \times \left(\frac{1}{64}\right) [(0.1)(18.5) + (0.2)(15.5) \\ &\quad + (0.25)(3) + (0.3)(9) + (0.8)(0.5) \\ &\quad + (-0.2)(1) + (-0.5)(1.5) + (-0.8)(0.5)] \\ &= 0.26 \text{ lbs.} \end{aligned}$$

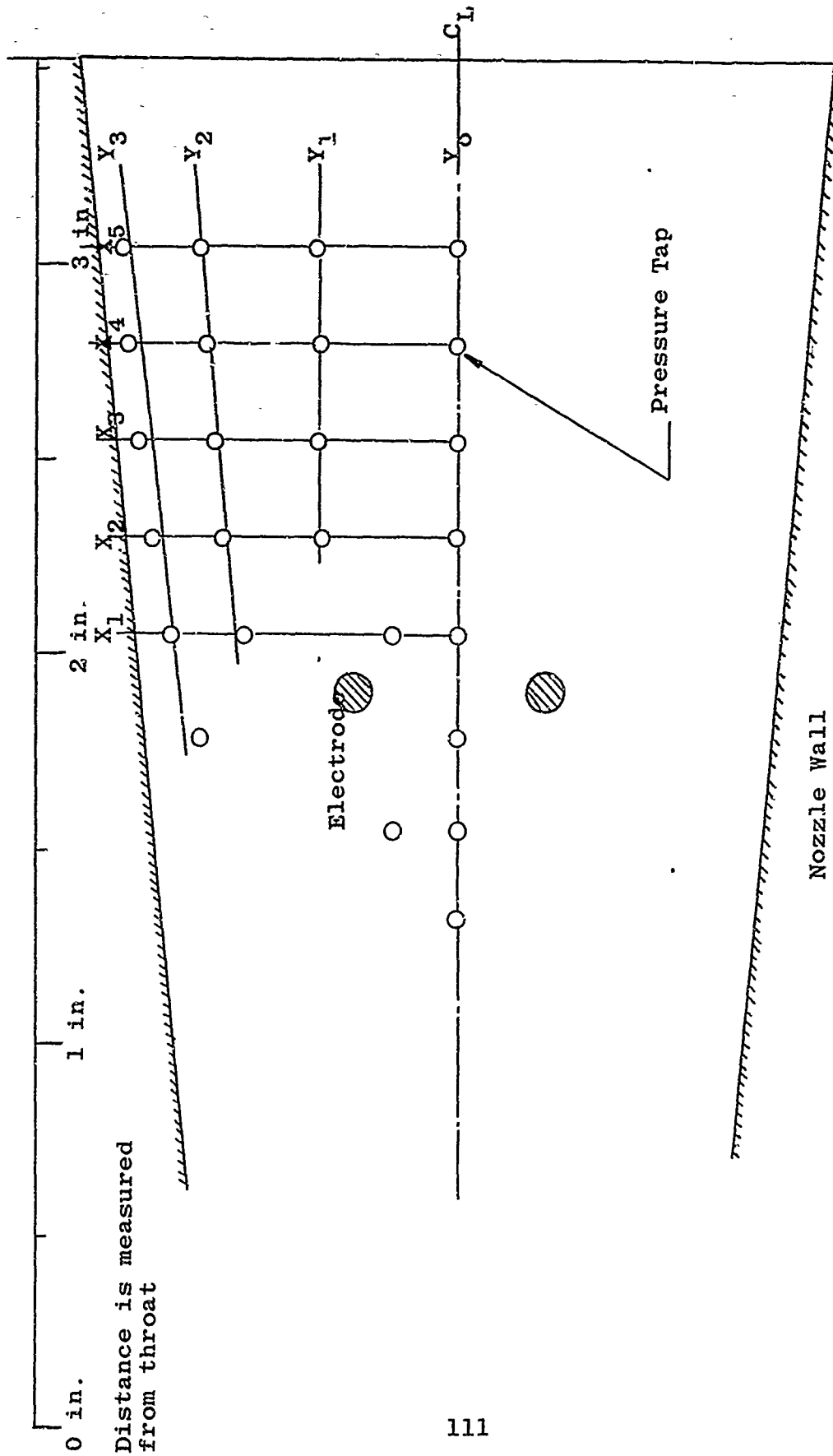


Figure VII-1. The Axisymmetric Silicon Phenolic Nozzle with 0.5 in. Electrode Distance in Cross-Flow

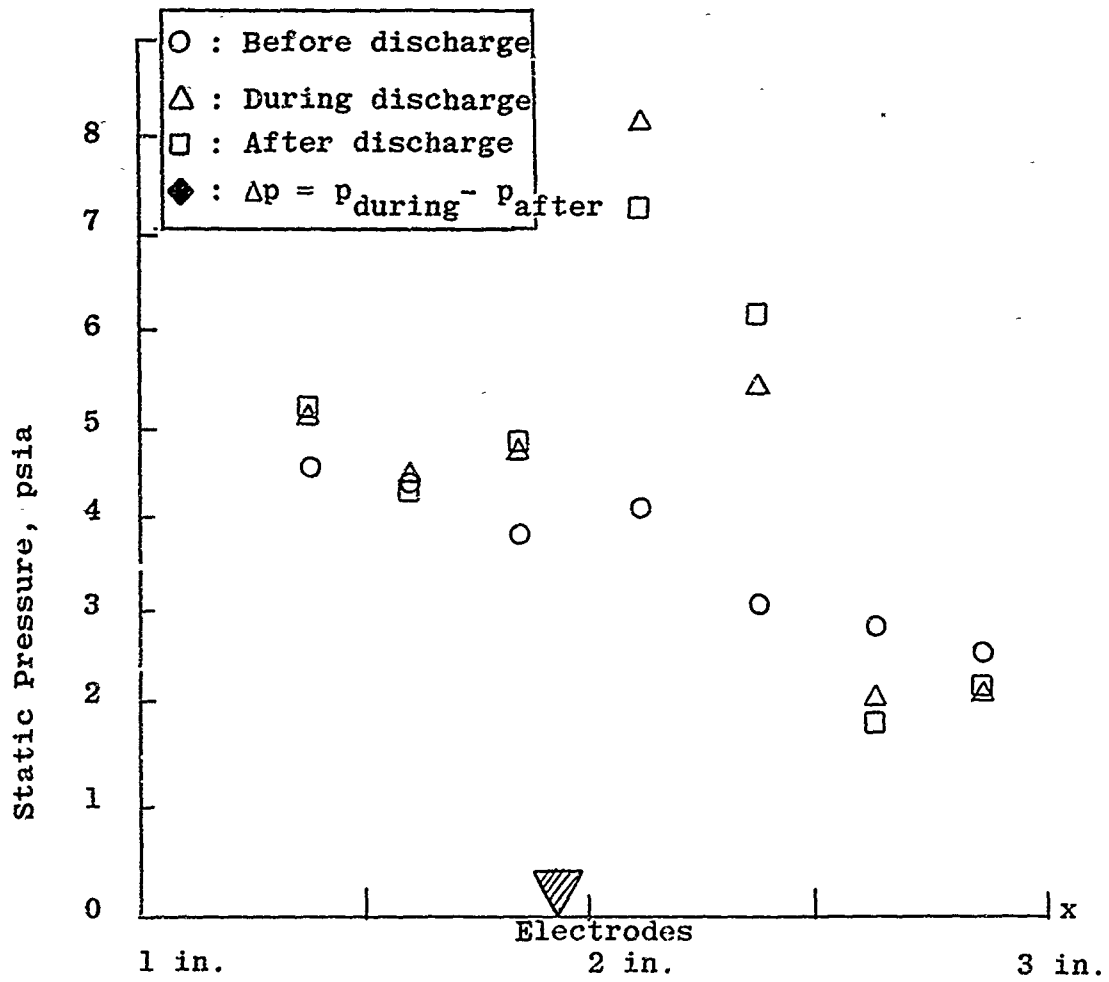


Figure VII-2. Pressure Readings along Center-Line of the Axisymmetric Silicon Phenolic Nozzle.

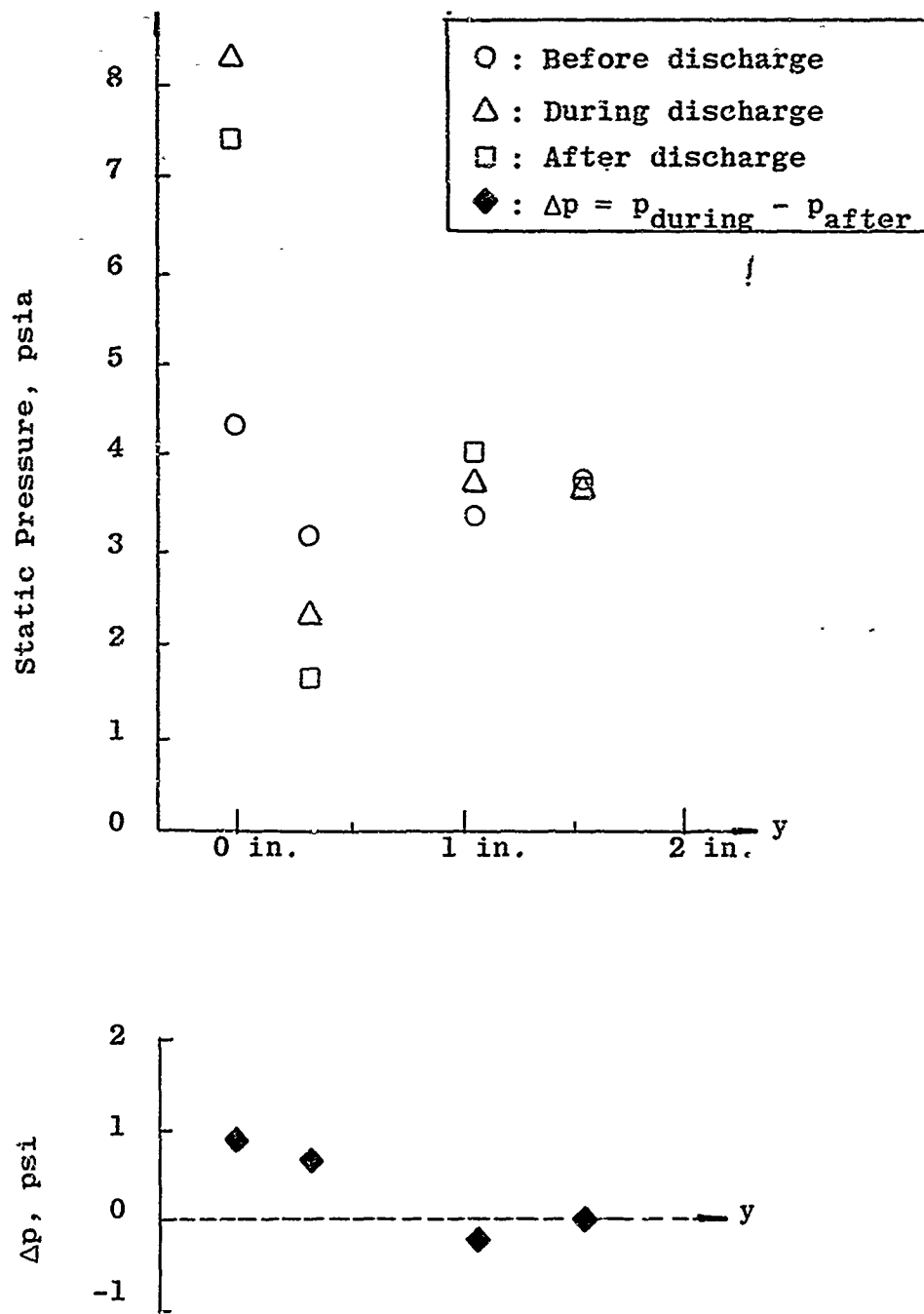


Figure VII-3. Pressure Readings along X_1 -Section
 ($y = 0$ is the projection of Y_0 -Section)

○ : Before Discharge
 △ : During Discharge
 □ : After Discharge
 ◆ : $\Delta p = p_{\text{during}} - p_{\text{after}}$

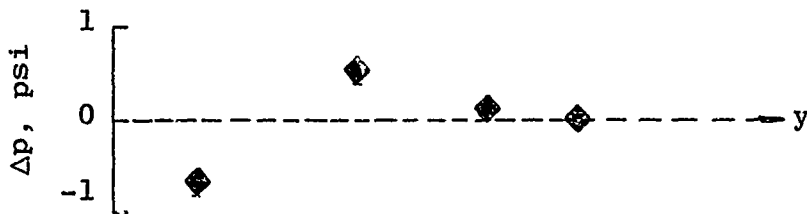
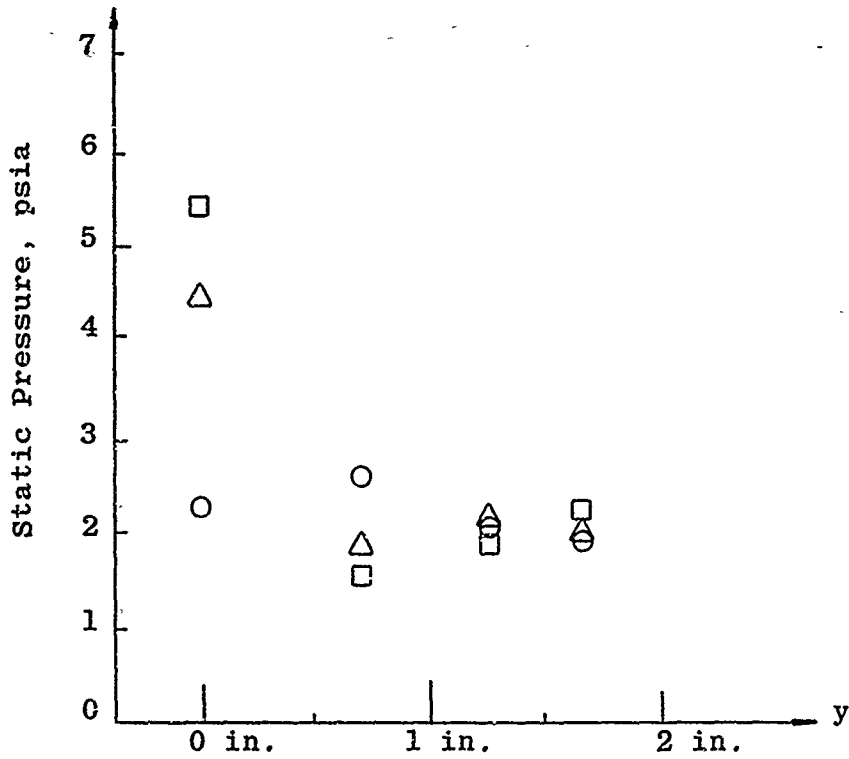
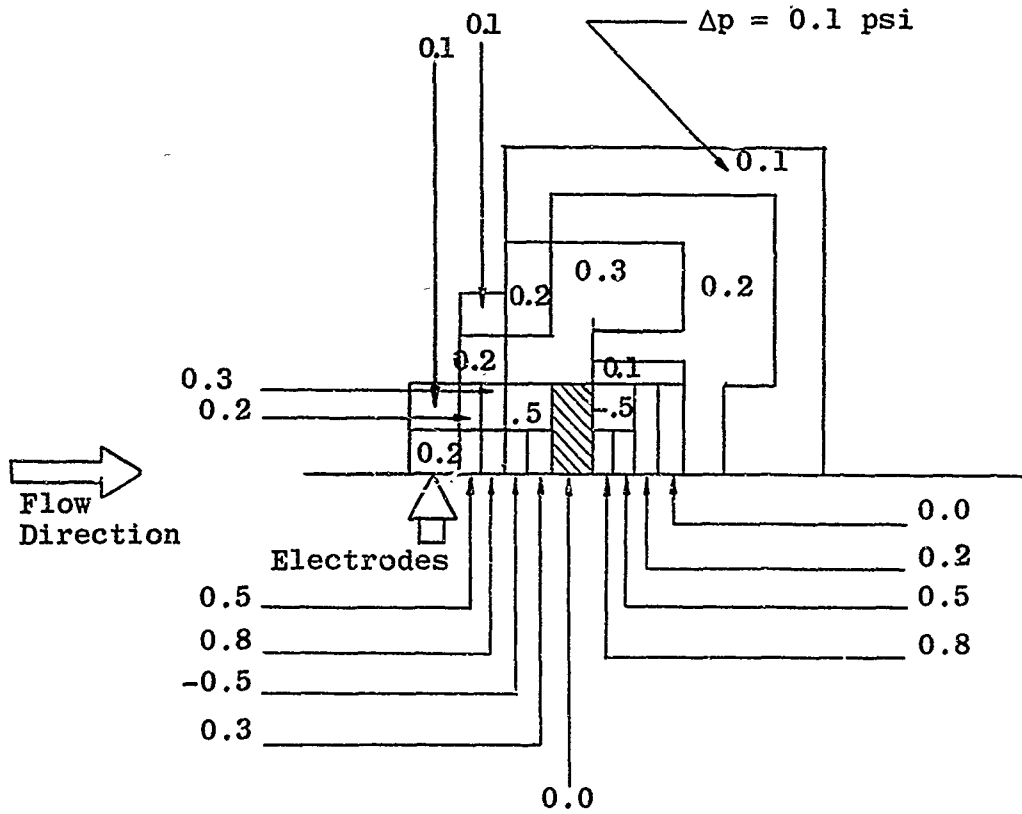


Figure VII-4. Pressure Readings along X_2 -Section

$$A_i = \square = 1/64 \text{ in}^2$$



NOTE: Those indicated values represent the pressure changes in that area

Figure VII-5. Pressure Change over all the Affected Area

REFERENCES

1. Hausmann, G. F., "Thrust Axis Control of Supersonic Nozzles by Airjet Shock Interference," United Aircraft Corp. Dept. Rep. R-63143-24, May 2, 1952.
2. Wu, J. M., Chapkis, R. L., and Mager, A., "Approximate Analysis of Thrust Vector Control by Fluid Injection," J. of ARS, Vol. 31, pp. 1677-1685, Dec., 1961.
3. Sehgal, R., and Wu, J. M., "Thrust Vector Control by Liquid Injection into Rocket Nozzles," J. Spacecraft, Vol. 1, pp. 545-551, Sept-Oct., 1964.
4. Broadwell, J. E., "Analysis of the Fluid Mechanics of Secondary Injection for Thrust Vector Control," STL Rept. 6120-7744-MU-000, March 1962, Also, AIAA J., May, 1963.
5. Kaufman, L. G., "Hypersonic Flow Past Transverse Jets," paper presented at AIAA Fifth Aerospace High Speed Mach No. - Application Science Meeting, Jan., 1967.
6. Hicks, B. L., "An Extension of the Theory of Diabatic Flow," Phys. Rev., Vol. 77, No. 2, p. 286, Jan., 1950.
7. Chu, B. T., "Pressure Waves Generated by Addition of Heat in a Gaseous Medium," NACA TN 3411, June, 1955.
8. Willmarth, W. W., "The Production of Aerodynamic Forces by Heat Addition on External Surfaces of Aircraft," Rand Corp., Research Memo RM-2078, December 30, 1957.
9. Marlotte, G. L., "An Experimental Investigation of the Effect of a Transverse Hypersonic Flow Velocity upon a Low-Density D. C. Electric Discharge in Air," Hypersonic Res. Proj. Memo No. 66, GALCIT, Caltech, Pasadena, Calif., 1962.
10. Schoeck, P. A. and Maisenhaelder, F., "Experimental Investigations of the Energy Balance of Electric Arcs with Superimposed Gas Flow," International Conf. on Phenomena in Ionized Gases, Belgrad, Aug. 1965, North Holland Publishing Comp., Amsterdam, 1965.

11. Schoeck, P. A., "An Investigation of the Anode Energy Balance of High Intensity Arcs in Argon," pp. 353-400, Modern Devel. in Heat Transfer, Academic Press Inc., New York, 1963.
12. Taylor, G. I., "The Formation of a Blast Wave by a Very Intense Explosion I, Theoretical Discussion," Proc. Roy. Soc. (a), Vol. 201, No. 1065, pp. 159-174, 1950.
13. Sakurai, A., "On the Propagation and Structure of the Blast Wave I and II," J. of Phy. Soc. of Japan, Vol. 8, No. 5, Sept-Oct., 1953.
14. Sedov, L. I., "Similarity and Dimensional Methods in Mechanics," Academic Press, New York & London, Chapter IV, 1959.
15. Lin, S. C., "Cylindrical Shock Waves Produced by Instantaneous Energy Release," J. Appl. Phys., Vol. 25, No. 1, pp. 54-57, Jan., 1954.
16. Lees, L., "Inviscid Hypersonic Flow Over Blunt-Nosed Slender Bodies," GALCIT Rept. Hypersonic Research Project Memo. No. 31, Caltech, Feb., 1956.
17. Roman, W. C. and Myers, T. W., "Experimental Investigation of an Electric Arc in Transverse Aerodynamic and Magnetic Fields," AIAA, Paper No. 67-98, Fifth Aerospace Science Meeting, New York, Jan., 1967.
18. Cobine, J. D., "Gaseous Conductors," Dover Publications, New York, Chap. VII, 1958.
19. Maecker, H., "Ueber die Charakteristiken zylindrischer Boegen," Zeitschrift fuer Physik 157, 1-29, 1959.
20. Cambel, A. B., "Plasma Physics and Magnetofluidmechanics," McGraw-Hill, 1963.
21. Cheng, S. I., "Unpublished report", Aero. Dept., Princeton University, New Jersey, 1967.
22. Test Facilities Handbook, (Fifth Ed.), Arnold Engineering Development Center, Arnold Air Force Station, Tenn., July, 1963.

23. Newton, J. F., Jr. and Spaid, F. W., "Experiment on the Interaction of Secondary Injectants and Rocket Exhaust for Thrust Vector Control," Technical Report No. 32-203, Jet Propulsion Laboratory, California Institute of Technology, Pasadena, California, Feb., 1962.
24. Vas, I. E. and Bogdonoff, S. M., "Interaction of a Turbulent Boundary Layer with a Step at $M = 3.85$," Princeton Univ. Rept. No. 295, April 1955.
25. Stuhlinger, E. and Mesner, G., "Space Science and Engineering," pp. 421-422, McGraw-Hill Book Co., 1965.
26. Ray, E. and Ross, D. P., "Power Systems-Advances and Levels," Astr. & Aero., pp. 36-42 (especially p. 42), Vol. 1, Jan., 1965.
27. Dicks, J. B., Under Research for Aero Propulsion Laboratory, Contract No. F33615-67-C-1919, Wright-Patterson AFB, Ohio, J. B. Dicks and Associates, Tullahoma, Tenn., 1967.
28. Manufacture Specifications No. 495, Eagle-Picher Co., Joplin, Missouri, 1967.
29. Peters, Th., "Lichtbogenentladungen in Ueberschallstroemungen," Astronautica Acta, Vol. II, No. 4, 1965
30. John, R.R., and Bade, W. L., "Recent Advances in Electric Arc Plasma Generation Technology," ARS J., Jan., 1961.
31. Busz, G., and Finkelburg, W., "Thermische Lichtboegen hoher Temperatur und niedriger Brennspannung," Zeitschrift fuer Physik, Vol. 138, 1954.
32. Finkelburg, W., and Maecker, H., "Elektrische Boegen u. Thermisches Plasma," Handbuch der Physik, Vol. XXII, Springer Verlag Berlin, 1956.
33. Stokes, C. S., "Heat Transfer Rates of an Argon Plasma Jet," Journal of the Electrochemical Society, Vol. 107, Jan., 1960.
34. Cremers, C. J., "Temperature Field in an Arc with Transpiration-cooled Anode," AIAA Journal, Vol. 3, No. 10, 1965.

UNCLASSIFIED

Security Classification

DOCUMENT CONTROL DATA - R&D

(Security classification of title, body of abstract and indexing annotation must be entered when the overall report is classified)

1. ORIGINATING ACTIVITY (Corporate author) The University of Tennessee Space Institute Tullahoma, Tennessee 37388		2a. REPORT SECURITY CLASSIFICATION Unclassified	
		2b. GROUP	
3. REPORT TITLE Electric Arc Discharge in Supersonic Flow for Thrust Vector Control			
4. DESCRIPTIVE NOTES (Type of report and inclusive dates) Final Report - Feb. 15, 1966 - May 31, 1967			
5. AUTHOR(S) (Last name, first name, initial) Wu, Jain-Ming and Lee, Shen C.			
6. REPORT DATE September 30, 1967		7a. TOTAL NO. OF PAGES 140	7b. NO. OF REFS 34
8a. CONTRACT OR GRANT NO. AF 04(611)-11388		9a. ORIGINATOR'S REPORT NUMBER(S)	
b. PROJECT NO.			
c.		9b. OTHER REPORT NO(S) (Any other numbers that may be assigned this report)	
d.		AFRPL-TR-67-202	
10. AVAILABILITY/LIMITATION NOTICES "This document is subject to special export controls and each transmittal to foreign governments or foreign nationals may be made only with prior approval of AFRPL (RPPR/STINFO), Edwards, California 93523"			
11. SUPPLEMENTARY NOTES		12. SPONSORING MILITARY ACTIVITY Air Force Rocket Propulsion Laboratory Research and Technology Division Air Force Systems Command, USAF Edwards Air Force Base, California	
13. ABSTRACT The phenomenon of disturbances caused by electric arc discharge in a supersonic flow was studied both analytically and experimentally. The purpose was to study the feasibility of using this concept for attitude control of space vehicles. A possible application for rocket propelled vehicles was selected for the test condition of an experimental program. Fair agreement was obtained between the test results and the analytical solutions. It was found that: <ol style="list-style-type: none">1. A local static pressure rise can be created by the electric discharge in a supersonic stream.2. The electric field to initiate discharge was about 2×10^3 volts/in for nitrogen stream at Mach number 2.5 with static pressure of 2 psia and stagnation temperature of 4000°R.3. The arc discharge, without a magnetic field, in a supersonic flow of Mach number 2.5 can be maintained and is stable.4. The affected area is small which resulted in small side force.5. The generated side force per unit electric power input is small in view of the available electric power supply. The use of an electric discharge for practical thrust vector control of rocket motors is only feasible if the power supply can be improved.			

DD FORM 1473
1 JAN 64

UNCLASSIFIED

Security Classification

UNCLASSIFIED

Security Classification

12. KEY WORDS	LINK A		LINK B		LINK C	
	ROLE	WT	ROLE	WT	ROLE	WT
Thrust Vector Control Space Vehicle Attitude Control Arc Discharge in Supersonic Flow Interaction of Arc and Gaseous Flow Arc Ignition and Characteristic High Speed Flow Disturbance Aerodynamic Force						

INSTRUCTIONS

1. ORIGINATING ACTIVITY: Enter the name and address of the contractor, subcontractor, grantee, Department of Defense activity or other organization (corporate author) issuing the report.

2a. REPORT SECURITY CLASSIFICATION: Enter the overall security classification of the report. Indicate whether "Restricted Data" is included. Marking is to be in accordance with appropriate security regulations.

2b. GROUP: Automatic downgrading is specified in DoD Directive 5200.10 and Armed Forces Industrial Manual. Enter the group number. Also, when applicable, show that optional markings have been used for Group 3 and Group 4 as authorized.

3. REPORT TITLE: Enter the complete report title in all capital letters. Titles in all cases should be unclassified. If a meaningful title cannot be selected without classification, show title classification in all capitals in parenthesis immediately following the title.

4. DESCRIPTIVE NOTES: If appropriate, enter the type of report, e.g., interim, progress, summary, annual, or final. Give the inclusive dates when a specific reporting period is covered.

5. AUTHOR(S): Enter the name(s) of author(s) as shown on or in the report. Enter last name, first name, middle initial. If military, show rank and branch of service. The name of the principal author is an absolute minimum requirement.

6. REPORT DATE: Enter the date of the report as day, month, year, or month, year. If more than one date appears on the report, use date of publication.

7a. TOTAL NUMBER OF PAGES: The total page count should follow normal pagination procedures, i.e., enter the number of pages containing information.

7b. NUMBER OF REFERENCES: Enter the total number of references cited in the report.

8a. CONTRACT OR GRANT NUMBER: If appropriate, enter the applicable number of the contract or grant under which the report was written.

8b, 8c, & 8d. PROJECT NUMBER: Enter the appropriate military department identification, such as project number, subproject number, system numbers, task number, etc.

9a. ORIGINATOR'S REPORT NUMBER(S): Enter the official report number by which the document will be identified and controlled by the originating activity. This number must be unique to this report.

9b. OTHER REPORT NUMBER(S): If the report has been assigned any other report numbers (either by the originator or by the sponsor), also enter this number(s).

10. AVAILABILITY/LIMITATION NOTICES: Enter any limitations on further dissemination of the report, other than those

imposed by security classification, using standard statements such as:

- (1) "Qualified requesters may obtain copies of this report from DDC."
- (2) "Foreign announcement and dissemination of this report by DDC is not authorized."
- (3) "U. S. Government agencies may obtain copies of this report directly from DDC. Other qualified DDC users shall request through _____."
- (4) "U. S. military agencies may obtain copies of this report directly from DDC. Other qualified users shall request through _____."
- (5) "All distribution of this report is controlled. Qualified DDC users shall request through _____."

If the report has been furnished to the Office of Technical Services, Department of Commerce, for sale to the public, indicate this fact and enter the price, if known.

11. SUPPLEMENTARY NOTES: Use for additional explanatory notes.

12. SPONSORING MILITARY ACTIVITY: Enter the name of the departmental project office or laboratory sponsoring (paying for) the research and development. Include address.

13. ABSTRACT: Enter an abstract giving a brief and factual summary of the document indicative of the report, even though it may also appear elsewhere in the body of the technical report. If additional space is required, a continuation sheet shall be attached.

It is highly desirable that the abstract of classified reports be unclassified. Each paragraph of the abstract shall end with an indication of the military security classification of the information in the paragraph, represented as (TS), (S), (C), or (U).

There is no limitation on the length of the abstract. However, the suggested length is from 150 to 225 words.

14 KEY WORDS: Key words are technically meaningful terms or short phrases that characterize a report and may be used as index entries for cataloging the report. Key words must be selected so that no security classification is required. Identifiers, such as equipment model designation, trade name, military project code name, geographic location, may be used as key words but will be followed by an indication of technical context. The assignment of links, rules, and weights is optional.